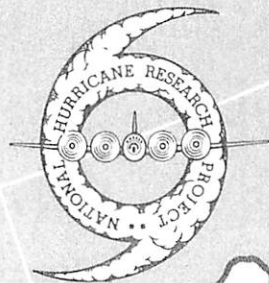


NATIONAL HURRICANE RESEARCH PROJECT

REPORT NO. 57

On the Dynamics of Disturbed Circulation
in the Lower Mesosphere



U. S. DEPARTMENT OF COMMERCE
Luther H. Hodges, Secretary
WEATHER BUREAU
F. W. Reichelderfer, Chief

NATIONAL HURRICANE RESEARCH PROJECT

REPORT NO. 57

On the Dynamics of Disturbed Circulation
in the Lower Mesosphere

by

R. H. Simpson

U. S. Weather Bureau, Washington, D. C.

A dissertation submitted to the Faculty of the Department of Geophysical Sciences at The University of Chicago
in partial fulfillment of requirements for the degree of Doctor of Philosophy.



Washington, D. C.
August 1962

NATIONAL HURRICANE RESEARCH PROJECT REPORTS

Reports by Weather Bureau units, contractors, and cooperators working on the hurricane problem are preprinted in this series to facilitate immediate distribution of the information among the workers and other interested units. As this limited reproduction and distribution in this form do not constitute formal scientific publication, reference to a paper in the series should identify it as a preprinted report.

- No. 1. Objectives and basic design of the NHRP. March 1956.
- No. 2. Numerical weather prediction of hurricane motion. July 1956.
Supplement: Error analysis of prognostic 500-mb. maps made for numerical weather prediction of hurricane motion. March 1957.
- No. 3. Rainfall associated with hurricanes. July 1956.
- No. 4. Some problems involved in the study of storm surges. December 1956.
- No. 5. Survey of meteorological factors pertinent to reduction of loss of life and property in hurricane situations. March 1957.
- No. 6. A mean atmosphere for the West Indies area. May 1957.
- No. 7. An index of tide gages and tide gage records for the Atlantic and Gulf coasts of the United States. May 1957.
- No. 8. Part I. Hurricanes and the sea surface temperature field. Part II. The exchange of energy between the sea and the atmosphere in relation to hurricane behavior. June 1957.
- No. 9. Seasonal variations in the frequency of North Atlantic tropical cyclones related to the general circulation. July 1957.
- No. 10. Estimating central pressure of tropical cyclones from aircraft data. August 1957.
- No. 11. Instrumentation of National Hurricane Research Project aircraft. August 1957.
- No. 12. Studies of hurricane spiral bands as observed on radar. September 1957.
- No. 13. Mean soundings for the hurricane eye. September 1957.
- No. 14. On the maximum intensity of hurricanes. December 1957.
- No. 15. The three-dimensional wind structure around a tropical cyclone. January 1958.
- No. 16. Modification of hurricanes through cloud seeding. May 1958.
- No. 17. Analysis of tropical storm Frieda 1957. A preliminary report. June 1958.
- No. 18. The use of mean layer winds as a hurricane steering mechanism. June 1958.
- No. 19. Further examination of the balance of angular momentum in the mature hurricane. July 1958.
- No. 20. On the energetics of the mature hurricane and other rotating wind systems. July 1958.
- No. 21. Formation of tropical storms related to anomalies of the long-period mean circulation. September 1958.
- No. 22. On production of kinetic energy from condensation heating. October 1958.
- No. 23. Hurricane Audrey storm tide. October 1958.
- No. 24. Details of circulation in the high energy core of hurricane Carrie. November 1958.
- No. 25. Distribution of surface friction in hurricanes. November 1958.
- No. 26. A note on the origin of hurricane radar spiral bands and the echoes which form them. February 1959.
- No. 27. Proceedings of the Board of Review and Conference on Research Progress. March 1959.
- No. 28. A model hurricane plan for a coastal community. March 1959.
- No. 29. Exchange of heat, moisture, and momentum between hurricane Ella (1958) and its environment. April 1959.
- No. 30. Mean soundings for the Gulf of Mexico area. April 1959.
- No. 31. On the dynamics and energy transformations in steady-state hurricanes. August 1959.
- No. 32. An interim hurricane storm surge forecasting guide. August 1959.
- No. 33. Meteorological considerations pertinent to standard project hurricane, Atlantic and Gulf coasts of the United States. November 1959.
- No. 34. Filling and intensity changes in hurricanes over land. November 1959.
- No. 35. Wind and pressure fields in the stratosphere over the West Indies region in August 1958. December 1959.
- No. 36. Climatological aspects of intensity of typhoons. February 1960.
- No. 37. Unrest in the upper stratosphere over the Caribbean Sea during January 1960. April 1960.
- No. 38. On quantitative precipitation forecasting. August 1960.
- No. 39. Surface winds near the center of hurricanes (and other cyclones). September 1960.
- No. 40. On initiation of tropical depressions and convection in a conditionally unstable atmosphere. October 1960.
- No. 41. On the heat balance of the troposphere and water body of the Caribbean Sea. December 1960.
- No. 42. Climatology of 24-hour North Atlantic tropical cyclone movements. January 1961.
- No. 43. Prediction of movements and surface pressures of typhoon centers in the Far East by statistical methods. May 1961.
- No. 44. Marked changes in the characteristics of the eye of intense typhoons between the deepening and filling states. May 1961.
- No. 45. The occurrence of anomalous winds and their significance. June 1961.
- No. 46. Some aspects of hurricane Daisy, 1958. July 1961.
- No. 47. Concerning the mechanics and thermodynamics of the inflow layer of the mature hurricane. September 1961.
- No. 48. On the structure of hurricane Daisy (1958). October 1961.
- No. 49. Some properties of hurricane wind fields as deduced from trajectories. November 1961.
- No. 50. Proceedings of the Second Technical Conference on Hurricanes, June 27-30, 1961, Miami Beach, Fla. March 1962.
- No. 51. Concerning the general vertically averaged hydrodynamic equations with respect to basic storm surge equations. April 1962.
- No. 52. Inventory, use, and availability of NHRP meteorological data gathered by aircraft. April 1962.
- No. 53. On the momentum and energy balance of hurricane Helene (1958). April 1962.
- No. 54. On the balance of forces and radial accelerations in hurricanes. June 1962.
- No. 55. Vertical wind profiles in hurricanes. June 1962.
- No. 56. A theoretical analysis of the field of motion in the hurricane boundary layer. June 1962.

CONTENTS

	Page
ABSTRACT	1
SYMBOLS AND NOTATIONS	3
CHAPTER 1. INTRODUCTION	5
Background	5
CHAPTER 2. ANALYSIS PROCEDURES	10
Re-evaluation of Rawinsonde Observations	10
Compositing Methods	14
CHAPTER 3. CIRCULATION IN THE LOWER MESOSPHERE	
DURING JANUARY 1960	17
General Characteristics	17
Characteristics of the Shear Line	21
CHAPTER 4. DYNAMICS OF THE SHEAR LINE	32
Trajectories	32
Balance of Forces	35
Viscosity	36
Vertical Motion	39
Effect of radiation	42
Particle Dynamics	45
Conservation of Potential Vorticity	47
Comparison with Equatorial Shear Lines of the	
Troposphere	54
CHAPTER 5. RELEASE OF ENERGY	56
CHAPTER 6. TRANSPORT OF HEAT	60
CHAPTER 7. TRANSPORT OF ANGULAR MOMENTUM	63
Transport of Relative Angular Momentum	63
CHAPTER 8. SUMMARY AND CONCLUSIONS	66
ACKNOWLEDGMENTS	69
REFERENCES	69

ON THE DYNAMICS OF DISTURBED CIRCULATION
IN THE LOWER MESOSPHERE

R. H. Simpson
U. S. Weather Bureau, Washington, D. C.

ABSTRACT

Rawinsonde data from the West Indies, obtained during a winter period when most sounding balloons rose above 100,000 ft. were used to investigate the structure and dynamics of a large-scale disturbance in the lower mesosphere. The disturbance consisted of a shearing surface which sloped poleward and moved toward higher latitude at 12 kt. Its circulations increased with height and were most intense above 30 km. In many respects it resembled the equatorial shear line of the troposphere.

For the period of investigation, January 15 to February 3, 1960, temperatures in the lower mesosphere decreased equatorward from maximum values located near the Tropic of Cancer. East winds, increasing with height, extended poleward as far as the 35th parallel, with strong west winds farther north. The appearance of the shear line system in this setting led to a shortlived reversal of the mean meridional temperature gradient.

Particle trajectories computed relative to the moving system show that air which entered the system on the poleward side was overtaken by the shear line after about two days. However, air entering from the equatorward side never overtook the shear line, and in this sector the exchange of air with the environment occurred at less than half the rate indicated for the poleward sector.

Both the geostrophic and the frictionless equations of motion were found to be inadequate to describe the circulations of the shear line system. Computations indicate that friction plays a much more important role at these altitudes than it does in the troposphere. For example, balance of forces computations indicate that vertical shearing stresses contribute to acceleration with the same order of magnitude as pressure gradient forces. In some instances continuous deceleration was observed along trajectories which moved steadily toward lower pressure.

Vertical motions were computed by the adiabatic method. The largest vertical motion occurred several hundred kilometers north of the shearing surface where a large area of rising motion had peak values of 0.5 cm. sec.⁻¹. The shearing surface itself was associated mainly with sinking motion. On the equatorward side vertical motions were at a minimum.

The shear line system carried large gradients of potential vorticity. The mean profile of ξ_0 components normal to the shear line was similar to that of the subtropical jet stream. Neither the vorticity maximum, located

just north of the shear line, nor the minimum, 800 km. south of the shear line and comprising a broad area of negative values, can be attributed to horizontal advection. The indications are that some process in situ is responsible for these large peak values and unique distributions. The importance of eddy diffusion of heat in the vertical is discussed and it is shown that in the mesosphere substantial changes of potential vorticity may occur through this means. While this process cannot account for the negative values observed, it is shown that frictional torques may do so.

The poleward transport of heat by the asymmetric part of the circulation was found to be relatively small and insufficient to account for the spectacular, rapid warming of polar regions during winter which has been observed on some occasions.

The poleward transport of angular momentum by the asymmetric part of the circulation is of the order of 10^{24} gm. cm.²sec.⁻². This is sufficient to sustain or intensify such prominent regional circulations as the polar night jet stream.

SYMBOLS AND NOTATIONS

x, y, z	Cartesian coordinate axes directed east, north, and vertically upward
s, n, p	coordinate axes directed downward, to the right of the wind, and vertically along an axis of diminishing pressure
ϕ	latitude
a	radius of the earth
R	radius of curvature of a trajectory
t	time
u, v, w	zonal, meridional, and vertical wind components
ω	vertical wind speed with pressure as the vertical coordinate $\equiv \frac{dp}{dt}$
V	wind speed along a streamline
c	rate of movement of the shear line system
u_g, v_g	zonal and meridional components of the geostrophic wind
u_a, v_a	zonal and meridional components of the ageostrophic wind
Ω	angular velocity of the earth
f	Coriolis parameter
g	acceleration of gravity
∇	operator nabla $\equiv i \frac{\partial}{\partial x} + j \frac{\partial}{\partial y}$
F	external or frictional forces
$\overline{\tau}$	eddy stress tensor
ν	coefficient of eddy viscosity
p	pressure
h	geometric height of pressure surfaces
Φ	geopotential $\equiv gh$
T	temperature
θ	potential temperature

4

Γ_a	vertical variation of temperature due to dry adiabatic processes, using pressure as the vertical coordinate
Γ	vertical variation of environmental temperature using pressure as vertical coordinate
ρ	density
α	specific volume
H	heat content per unit mass
c_p	specific heat of air at constant pressure
L	latent heat of condensation
ξ	vertical component of the relative vorticity
Q	vertical component of the absolute vorticity
ξ_θ	potential vorticity
K	kinetic energy per unit volume
M	angular momentum

CHAPTER 1. INTRODUCTION

The nature of atmospheric circulation in the lower mesosphere has been difficult to investigate in the past because of instrument limitations and the relatively low altitudes achieved during regular rawinsonde flights. During the last decade, however, wind and temperature data obtained from rockets and other sources have suggested a number of improvements for stratospheric circulation models. Among these, the model proposed by Dobson [7] and his collaborator Brewer [3], that of Libby and Palmer [17], of Feely and Spar [10], and more recently one by Murgatroyd and Singleton [20] are especially noteworthy. Some models, derived from analyses of radioactive debris dispersion, emphasize the importance of inter-hemispheric exchanges and transports. In general, radioactive tracer studies have yielded major contributions to the knowledge of general circulations in the stratosphere and lower mesosphere (e.g., Machta [18] and Angell [1]). Nevertheless, no general agreement has been reached on a pole-to-pole model of circulations in these layers.

Early in 1960 an unusual opportunity arose to examine circulations in the lower mesosphere of the West Indies. High altitude meteorological observations required by the Navy's Skyhook 60 operation, and the cosmic ray research of the late Dr. Marcel Schein, were made at stations in the Caribbean and Bahama region during the period January 15 to February 3, 1960. Each station used plasticized 1,200 gm. balloons on regular rawinsonde flights, and they were able to obtain wind and temperature observations to altitudes generally above 100,000 ft. during this period. Thus, for the first time, it was possible to make synoptic-scale daily analyses of circulation in the lower mesosphere for tropical areas. A preliminary analysis of these data by Riehl and Higgs [30] revealed several unexpected circulation features, including a pronounced shear line. A similar shear line identified from less copious data of January 1959 is shown in figure 1. The discovery of this disturbance while plans were being formulated for the Skyhook operation established the need for high-altitude observations to predict the trajectory of the Skyhook balloon and to assist in planning the over-water launch and recovery of the instrument package.

The present study draws primarily upon these high-altitude observations to examine the structure of the shear line which crossed the West Indies during Skyhook 60, to analyze the balance of forces, and to compare this disturbance with its counterpart in the troposphere.

Background

The discussion here will be concerned with the layer extending downward from the mesopeak near 55 km. to the tropopause. Since in the Tropics the meso-incline ordinarily extends directly to the tropopause both summer and winter, the entire layer will be referred to as the lower mesosphere. This layer contains the bulk of atmospheric ozone. Therefore, the general circulation, being fundamentally geared to the temperature gradient, is necessarily influenced by the amount of ozone present and the planetary gradients of solar radiation absorbed. Since ozone is probably the principal heat absorber in the lower mesosphere (e.g., Penndorf [24] and Ohring [21]), it is not surprising that in the summer hemisphere, temperature above the tropopause characteristically increases upward to the top of the ozone layer. In winter at least

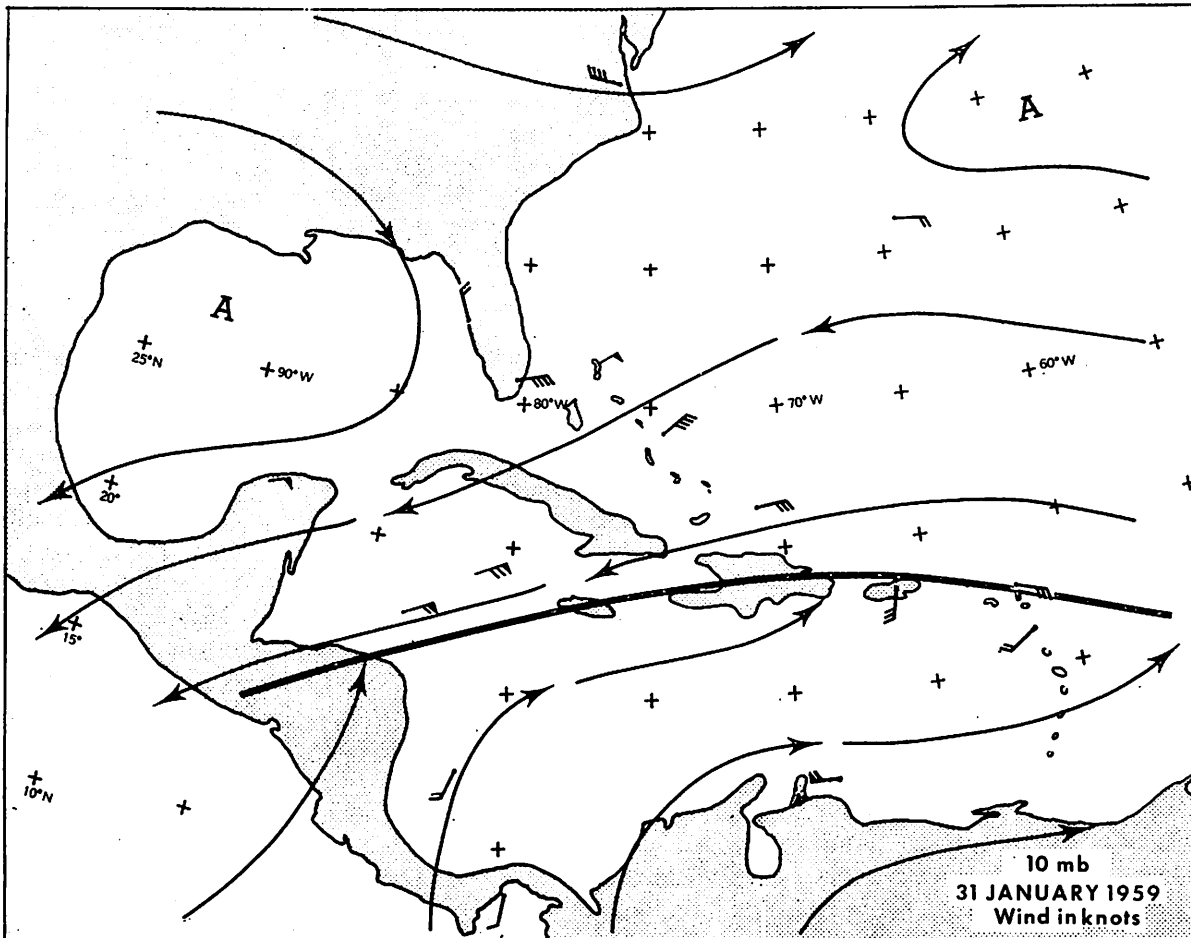


Figure 1. - Example of a West Indies shear line at 10 mb., January 31, 1959.

at those latitudes where ozone is in shadow, temperature may be nearly constant or may decrease with height throughout the mesosphere, an observation which led Palmén [22] in 1934 to suggest that winter circulations in the stratosphere comprise a broad belt of strong circumpolar westerlies. Court [4] reported that the Antarctic stratosphere in winter (based upon observations obtained during Operation Highjump) is essentially isothermal. In recent years this large contrast between summer and winter temperatures in the mesosphere has been verified observationally and has been discussed by Wexler [35,36].

If it is clear that ozone plays a dominant role in determining seasonal changes in temperature gradients in the mesosphere, it is less easy to understand why warmest temperatures in summer occur at high latitudes, or why greatest ozone amounts are observed at subpolar stations and lowest amounts near the equator. An even greater complication comes from the observed fact that all stations, regardless of latitude, have maximum ozone amounts in spring and minimum amounts in fall, whereas temperature extremes are reached near the solstices.

For such variations in space and time one must look to the general circulation for explanation. Until recently, interest in circulations of the lower

mesosphere has consisted primarily of explaining the distribution of ozone, and justifying the radiation budget for the layer. Little attention has been given to the dynamics of circulations, and with the exception of a study by Wexler and Moreland [37], which discusses the influence of planetary wave motion on sudden temperature changes in the stratosphere, there has been essentially no consideration given to the structure and role of disturbances.

There are three complete theories for the seasonal and latitudinal distribution of ozone, and several less complete circulation models. Concerning the distribution of ozone, Wulf [38] and later Craig [5] postulated an ozone source in equatorial regions with steady subsidence in the stratosphere bringing the ozone down. From these lower levels it spreads poleward along the tropopause and either finds its way into the troposphere or rises and returns equatorward. Craig argues that the depletion of ozone at the equator by subsidence and divergence is continually made up by photochemical processes in the upper portion of the layer. The tendency to accumulate large amounts of ozone at higher latitudes is attributed mainly to the fact that the tropopause lowers with latitude, providing a deeper stratosphere for storage. The meridional circulation required for this process is considered by Craig to be frictionally driven by the (thermally) direct cells in the troposphere. Since the tropospheric circulation is more vigorous in winter than in summer, the accumulation of ozone reaches a maximum in late winter due to the high frequency of winter storms.

Dütsch [8] argues that there is net cooling and contraction of the stratosphere in winter, net warming and expansion in summer. The expansion begins in late winter and spring at the top of the ozone layer, causing higher pressures at the top and lower densities at the base. With this as a model, and assuming no meridional motion, he computed the vertical displacement required for redistribution of density, as well as the photochemical contribution to changes in ozone amounts. This computation provided theoretical ozone values which varied with latitude and season in the same manner but with smaller magnitude than those from observational data.

The third theory, by Reed [26], accounts for ozone variations primarily in terms of synoptic-scale disturbances which affect deep layers of the atmosphere, including the lower mesosphere. He reasoned that an air column approaching a trough line converges horizontally and subsides with vertical divergence, while a column leaving a trough line experiences a like amount of horizontal divergence with rising motion, converging vertically. From this model he demonstrated that this process causes ozone amounts to increase in lower levels and to be depleted at upper levels where photochemical processes enter to replenish the supply and thus increase the total amount in the column. Reed argues that this accounts for the rapid increase of ozone during winter in middle and higher latitudes.

Of these three theories, that of Dütsch is especially attractive primarily because it is independent of meridional circulations, the existence of which is postulated on tenuous dynamical reasoning. Craig's hypothesis of descending motion over the equator is necessary to bring the ozone down to lower layers which are shielded from radiation which characteristically destroys ozone. However, the only dynamical reason which supports this hypothesis is the further assumption that the meridional cell in the lower

stratosphere is frictionally driven by tropospheric circulations. Since an assumption of descending motion at the equator tends to complicate the radiation budget of the stratosphere, most stratosphere circulation models have postulated rising motions over the equator. Reed's model suffers through the assumption that vorticity advection fields of a trough line in the troposphere extend their influence to sufficient depth in the mesosphere to cause systematic vertical motion patterns throughout the ozone-bearing columns. If this indeed happens, Reed's reasoning is perhaps better applied to the day-to-day changes in ozone associated with synoptic disturbances. For example, Haurwitz [11] used this same reasoning to show that maximum daily ozone amounts should be found to the rear of surface cyclones upstream from the upper-level trough line. Similarly Palmén [23] pointed out that maximum daily ozone amounts tend to be found at the point where the tropopause is lowest. Difficulties in using day-to-day variations in total ozone amounts as circulation tracers were indicated as early as 1930 by Dobson [6] who showed that at any given station the ozone amount recorded on any one day may well exceed the mean monthly amount for any station in the hemisphere.

All of the models thus far have assumed that the circulation in one hemisphere is essentially a mirror image of that in the other, and little or no consideration has been given to exchanges of mass, heat, and momentum between hemispheres. The earliest model which proposed and discussed a continuous pole-to-pole circulation in the mesosphere is that of Kellogg and Schilling [13]. It proposes rising motion over the summer pole, sinking over the winter pole, and net mass transport from the summer to the winter hemisphere. In this model, easterlies predominate in the summer hemisphere, westerlies in the winter, and the authors suggest a rapid, almost abrupt transition at equinoctial periods between the characteristic circulations of summer and winter. While observations accumulated during the past 10 years have tended to support it, this model requires modification in equatorial regions where observations during the IGY showed that easterlies in the summer hemisphere extend across the equator well into the winter hemisphere. Also, studies of the movement of atomic debris in low latitudes have shown little evidence of decided meridional transport. Rather, the debris tends to remain trapped near the equator for extended periods. However, Ohring [21], from a study of the radiation budget of the stratosphere, concluded that there must be net export of heat from the summer to the winter hemisphere in accordance with the Kellogg-Schilling model. Teweles et al. [33] presented analyses of 10-mb. data obtained during the IGY which supported the contention of Kellogg and Schilling that there must be an abrupt change in circulation between winter and summer regimes. In recent years, several investigators have reported evidence of a biennial reversal of zonal winds (Viezee [34], Ebdon [9], Reed et al. [27] and Angell and Korshover [2]) in which equatorial easterlies alternate with westerlies, a non-seasonal influence which is new to meteorological experience.

Three other models of more limited scope have been advanced which bear upon the general circulation problem in the stratosphere or lower mesosphere. The oldest, that of Dobson [9] and Brewer [3], came into being as a result of the authors' interest in explaining the dryness of the polar stratosphere. Their model calls for tropospheric air near the equator to rise and penetrate the tropopause, then spread poleward in the stratosphere, returning to the troposphere at middle and high latitudes. The second model, advanced recently by Libby and Palmer [17], proposes rising motion over the equator through a

deep stratospheric layer. The middle and upper portions of the air column move slowly poleward, while a return current, completely within the stratosphere, develops near the tropopause. The latter model has proved less durable than the former, primarily due to difficulty in satisfying the angular momentum budget and also because the return flow must face the braking action of circulations in the upper troposphere. Neither model has withstood the observational evidence from tracer studies of atomic debris.

The only model substantially in accord with observed movements of atomic debris is that of Feely and Spar [10] who propose that meridional transport in the stratosphere occurs by means of turbulent eddies. This model calls for a coefficient of horizontal eddy diffusion of the order $10^9 \text{ cm}^2 \text{ sec}^{-1}$, and a vertical coefficient of the order $10^3 \text{ cm}^2 \text{ sec}^{-1}$ in the Tropics, and $10^4 \text{ cm}^2 \text{ sec}^{-1}$ in higher latitudes.

From this collection of circulation models expressing widely divergent points of view, it is a refreshing and useful experience to acquire data which permit synoptic-scale analyses of circulations throughout the major portion of the ozone layer. Fortunately, data from the Skyhook 60 operation permit a quantitative examination to be made of the structure and dynamics of circulations in the West Indies, and the transports of heat and momentum along at least one avenue connecting the summer and winter hemispheres. While these data cover a relatively limited period of the year, they were obtained at a time when synoptic-scale disturbances were present, the analysis of which provides fuller insight into the dynamics of circulations in the mesosphere or even into the general circulation problem itself. While it cannot be assumed that the results apply uniformly to all equatorial regions, they will serve as a useful starting point for more objective examination of data from other equatorial areas; where reports are more widely separated in space and time.

CHAPTER 2. ANALYSIS PROCEDURES

Re-evaluation of Rawinsonde Observations

One of the principal difficulties encountered with high-altitude soundings made with standard rawinsonde instruments is due to the limitation of the baroswitch. At pressures lower than about 20 mb., this device becomes increasingly less accurate. While this may not influence the computation of pressure heights as much as temperature errors do, it may lead to very erroneous computations and positioning of winds. Also, in the West Indies network (fig. 2), not all stations used instruments of the same manufacture. Therefore it was considered necessary to obtain the original sounding records and re-evaluate pressure heights and winds for the period of investigation, January 15 to February 3, 1960. Both wind and temperature records were replotted for each station. For each sounding, mean temperatures were computed for the layers 200 to 150, 150 to 100, 100 to 50, 50 to 25, 25 to 10, 10 to 7, and 7 to 4 mb. A West Indies mean temperature for this period was obtained for each

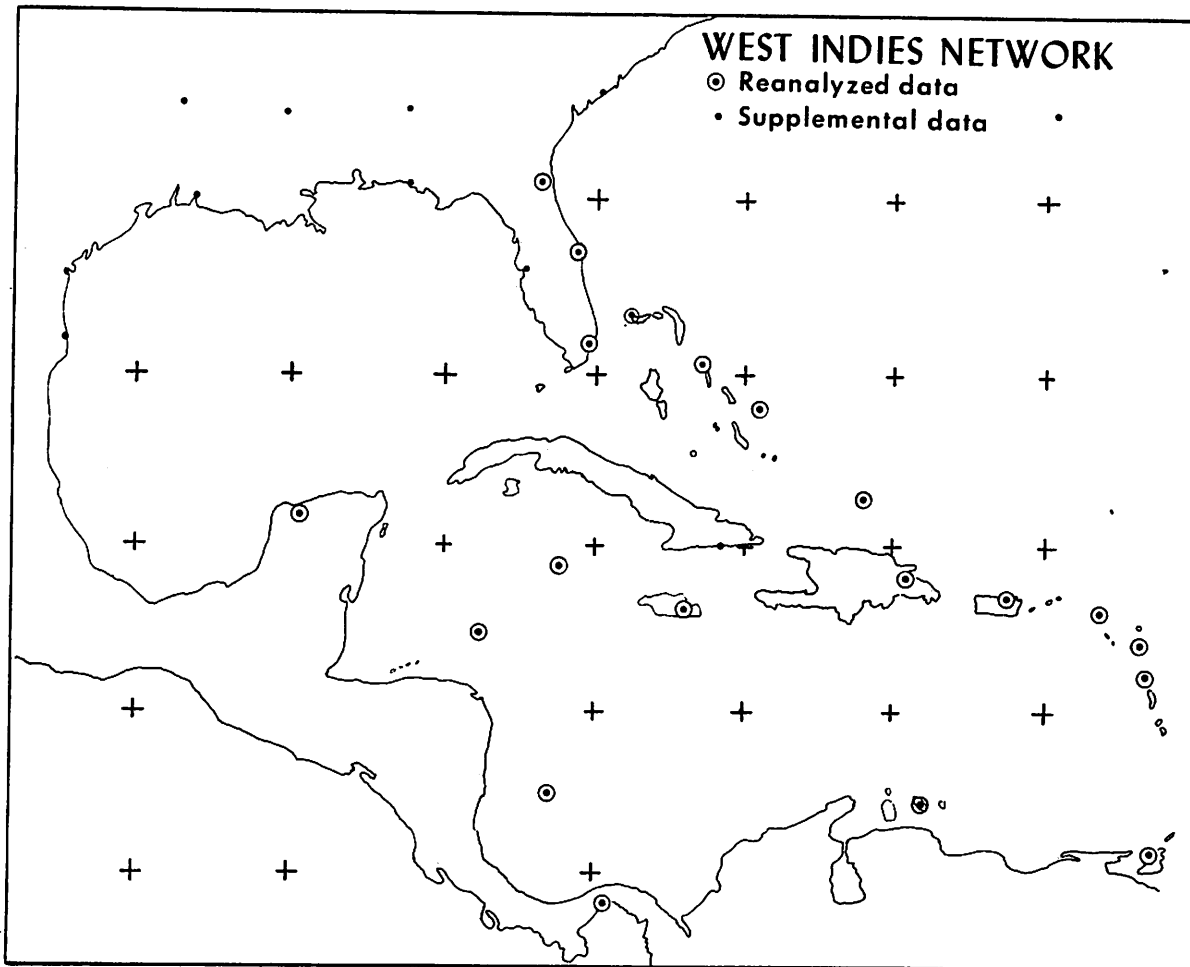


Figure 2. - The West Indies network. Rawinsonde data from stations which are encircled were completely re-evaluated.

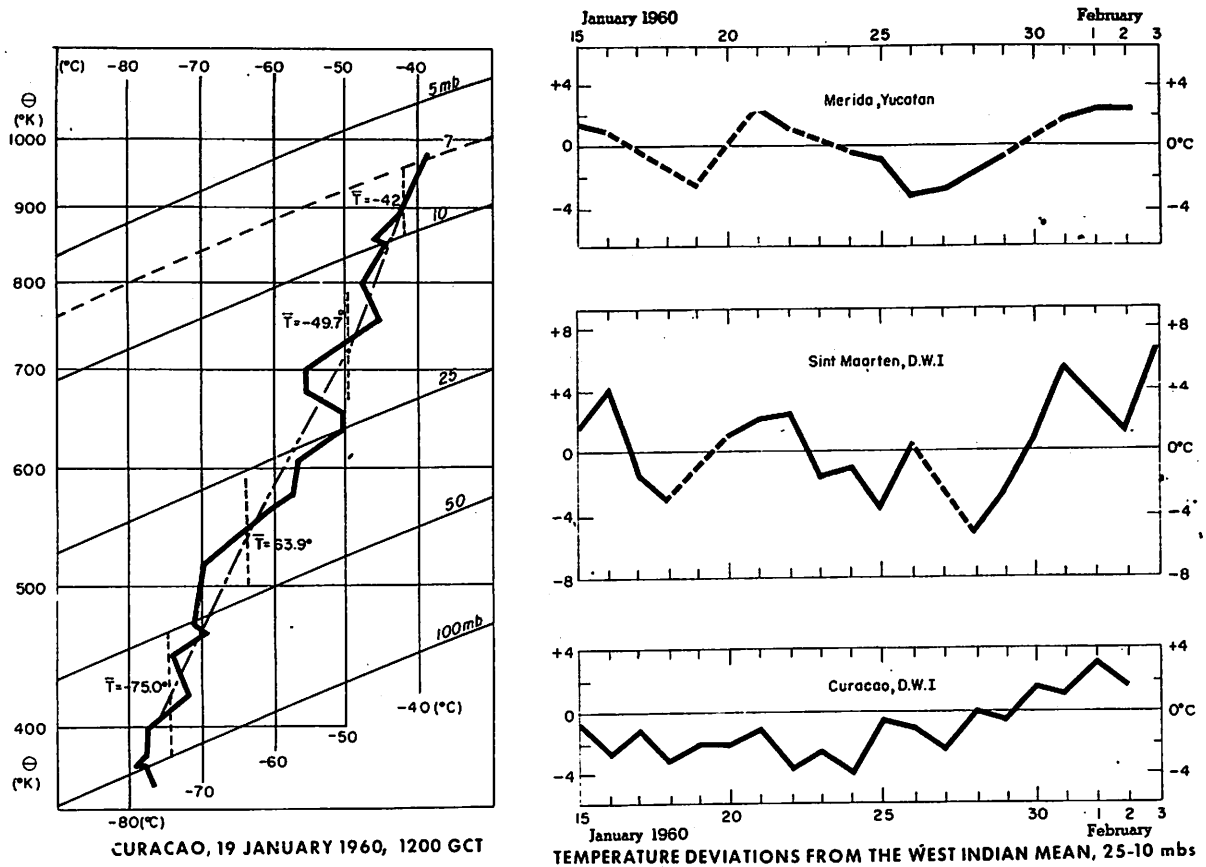


Figure 3. - Procedures for re-evaluation of radiosonde data. Layer mean temperatures for each station were computed as shown. The analysis of isotherm patterns for each layer was guided in first approximation by the pattern of wind shear vectors. Areal continuity of temperature change patterns was used to detect sounding errors.

layer by averaging the layer mean temperatures from all stations for this 20-day period. Then a time graph of layer mean temperatures was constructed for each station and each layer. Examples of these time graphs and a typical sounding from Curacao, DWI, are shown in figure 3. These time graphs helped in identifying temperature variations with synoptic scale continuity, and in separating those without. They also helped in locating systematic errors. One station reported values consistently 2° - 3° colder than any nearby stations during the passage of prominent maxima and minima. Synoptic-scale temperature variations were clearly evident and could be followed from station to station with encouraging continuity as the temperature pattern moved poleward across the area. Some instances of balloon flotation and of instrument malfunction stood out prominently as departures from the area temperature trend. However, there were only twelve such obvious cases among all the data examined.

From maps of layer mean temperature and wind shear, isotherms were constructed to fit the computed mean temperatures with the patterns, being guided in first approximation by the shear vectors. This assumed that the geostrophic thermal wind is a useful approximation of isotherm orientation.

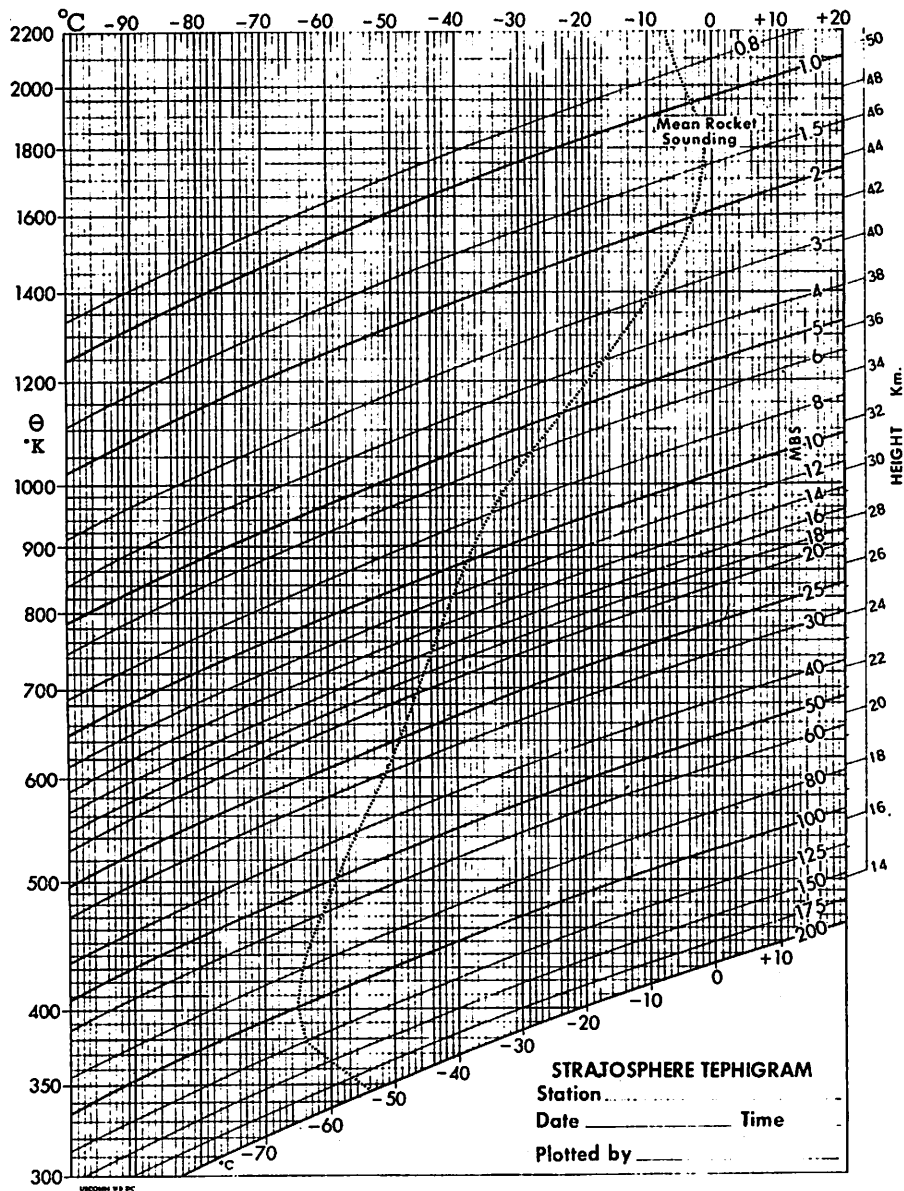


Figure 4. - Tephigram used in analyzing the West Indies data of January 1960.

Where the temperature gradient and pattern were forced to depart considerably from that implied by the shear vector; the time graph of mean temperatures for the stations affected was consulted to determine whether the departure was associated with synoptic-scale continuity, or had to be ascribed to other causes. In the latter case both the wind and temperature observations in question were either set aside for separate re-analysis or discarded. Generally, it was not necessary to set aside more than one or two such observations in any one layer analysis.

Height contours for the 200-mb. surface were computed by differential analysis in two steps, from 1,000 to 500 and 500 to 200 mb. To this contour field was added consecutively the thickness of each layer, derived from layer mean temperatures, to obtain contours for the 100, 50, 25, 10, and 7-mb. surfaces.

All analyses used in this study were based upon observations made at 1200 GMT. This corresponds to 8:00 a.m. local time for stations in the eastern portion of the area and 6:00 a. m. for stations in the extreme western portion. Hence the sun was irradiating the lower mesosphere from a large zenith angle during the period of observation. Intermediate soundings were plotted to determine the magnitude of diurnal variations, and were used also as guides in extrapolating shorter soundings, made at 1200 GMT, to the nearest level of analysis. At the tropopause the 0000 GMT soundings were 3° to 5° C. colder than those at 1200 GMT. At 10 mb. the difference averaged slightly more than 4° C.

The selection of specific layers and pressure surfaces for analysis was based mainly upon changes in prevailing wind with altitude. The pressure surfaces adopted were:

<u>p (mb.)</u>	<u>Approx. Height (km.)</u>
200	12
100	16
50	21
25	25
10	31
7	33

Enough information was available above the 7-mb. surface to indicate that disturbances which affected the layer 25 to 7 mb. remained prominent at least as high as 4 mb. However, at this altitude insufficient data were available for useful synoptic-scale analyses.

Contour fields for each of the above surfaces were constructed from a grid of pressure height data derived in the manner described above. Similarly, the isotherms were constructed from temperatures derived for the same grid. Point values were obtained by interpolation between the mean temperature at the point in question for the layer immediately above and below each pressure surface, except at 7 mb. Here it was necessary to extrapolate from the values at 10 mb. and for the layer 10 to 7 mb.

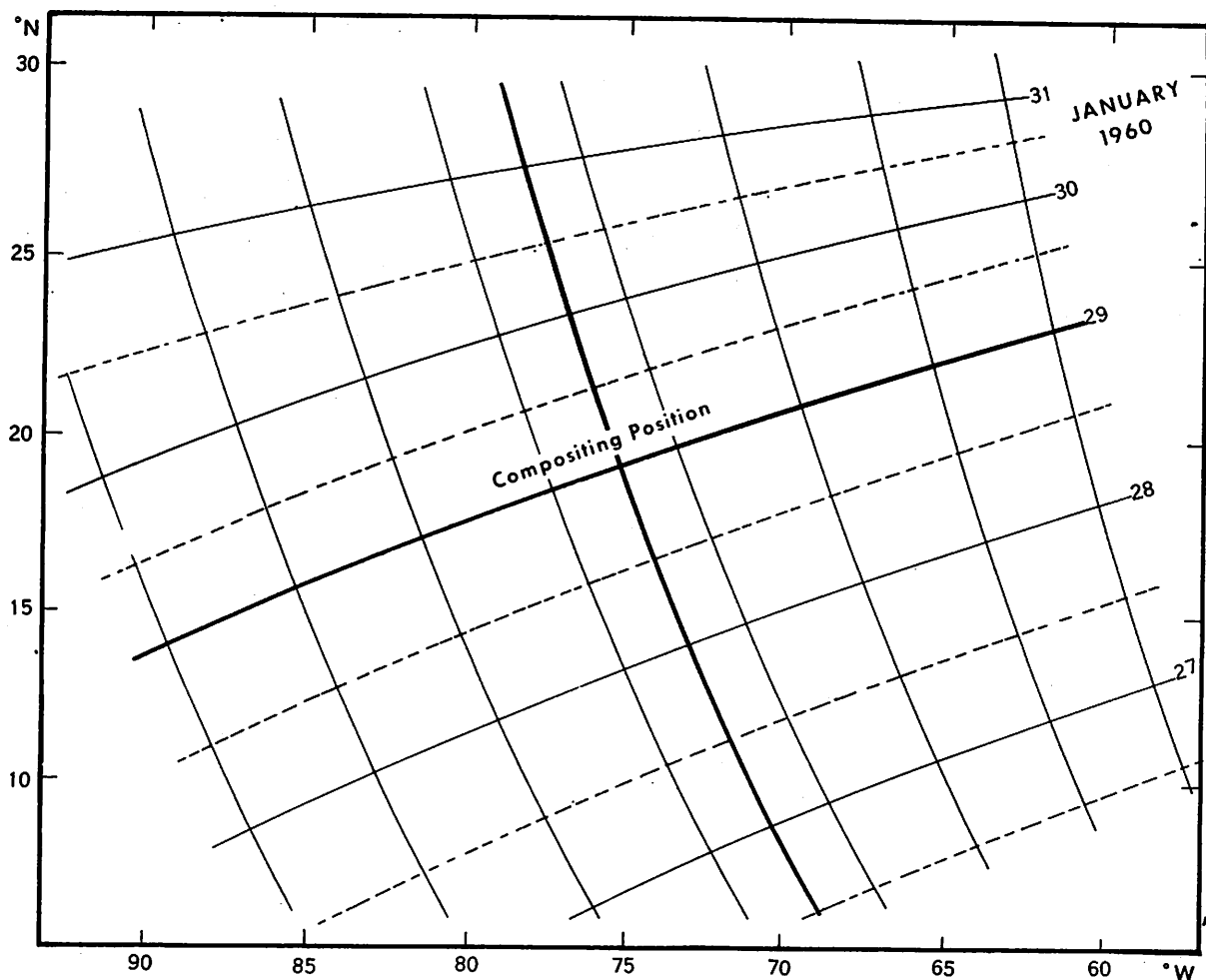


Figure 5. - Grid for compositing data at 10 mb. for the period January 27-31, 1960. Data for the 27th, 28th, 30th, and 31st were compositing around the 1200 GMT position for January 29.

Compositing Methods

In view of the nearly steady circulation of the shear line system, and in order to maximize the information available for analysis, it was decided to composite the data obtained during the time the shear line was crossing the Caribbean area, January 27 to 31, around the shear line position near 20° N. on January 29. Orthogonal grids were used to project the data. The one shown in figure 5 was used for compositing data at 10 mb. It has a family of abscissae with time scale spacing, constructed parallel to the shear line at its consecutive positions on the five days mentioned, and a family of ordinates orthogonal to the abscissae. Observed winds were displaced along their respective ordinates as many grid units as necessary to return the shear line from its position at time of observation to that which it occupied at the compositing hour (1200 GMT, January 29). In this displacement, the angle between the wind direction and its reference abscissa was conserved. Temperatures and pressure surface heights were read on each day at each grid point, then re-located to the composite position in the same manner as the winds. Aggregate

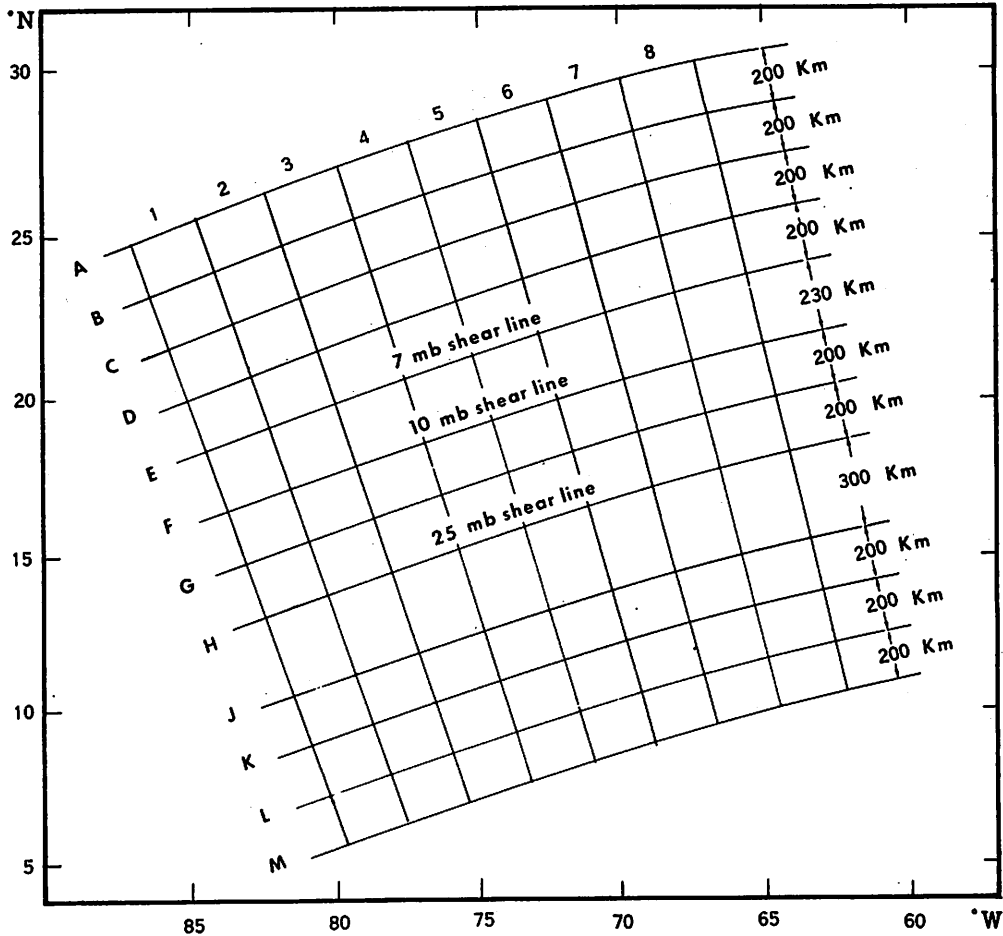


Figure 6. - Computational grid used in summarizing composited data for lines parallel to the shear line.

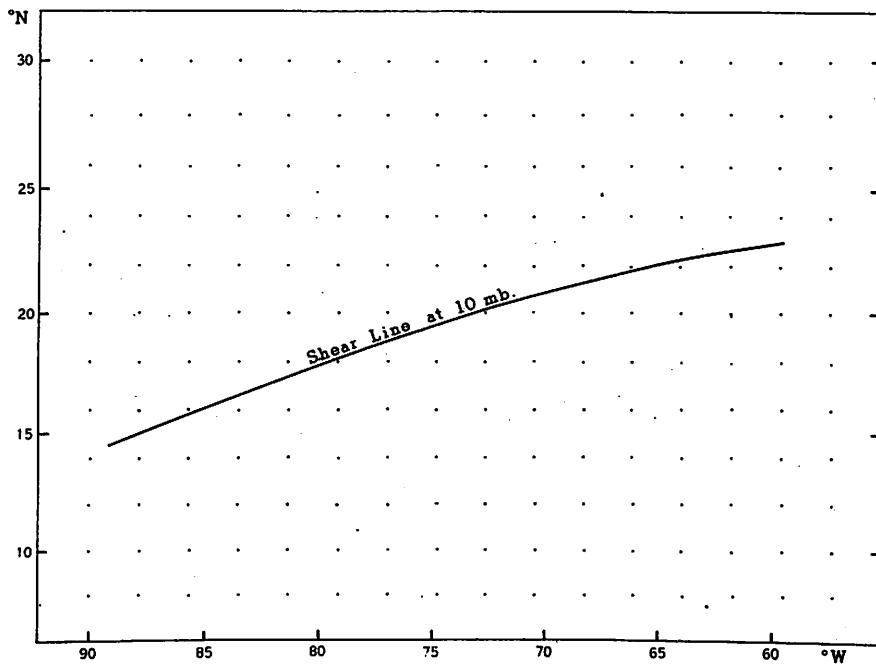


Figure 7. - Computational grid used in summarizing composited data for lines parallel to the latitude circles.

values of temperature and heights composited at each grid point were then averaged to obtain the temperature and height field for the composite system.

Two kinds of computational grids were used for summarizing the composited data and for dynamical analyses. These are shown in figures 6 and 7, one oriented with respect to the shear line, the other with respect to latitude circles. The latter grid was used primarily for computing poleward transports of heat and momentum.

On both of these grids, and in the analyses presented here, the distance scale relative to the system has been indicated in latitude and longitude primarily as an aid in judging distances. However, the compositing processes have spread the data over a somewhat larger area than was actually accessible on any one day.

CHAPTER 3. CIRCULATION IN THE LOWER MESOSPHERE DURING JANUARY 1960

General Characteristics

Balloon soundings from the West Indies during January 1960 revealed a high, cold tropopause between 70 and 80 mb. surmounted by a deep layer in which temperature increased steadily with height. The mean sounding for the area - a simple average of all station data during the period - is presented in figure 8. The polar mean sounding for the same period, also shown in figure 8, represents averages of data from five North American polar stations, all of which had at least five observations during this period. In the polar regions the lower mesosphere was characteristically warmer than that of the West Indies up to about 35 mb. Above this level the polar sounding was colder. There was no evidence of a deep layer temperature inversion such as that observed in the West Indies. In the West Indies, temperature above the tropopause increased with height at a rate which corresponded closely to that of the rocket atmosphere (Rocket Panel [31]). The latter is based mainly upon data obtained during early rocket firings at White Sands, N. Mex.

Figure 9 shows the mean temperature anomalies in a meridional plane for the West Indies during the 20-day period of investigation. These anomalies represent deviations of mean temperature along latitude circles from the average of all West Indian station data for the period. Temperatures increased with latitude to about 25° N. The total temperature difference at 10 mb. from 10° N. to the temperature peak at 25° N., was approximately 5° C. The meridional temperature gradient was at a minimum in the layer 50-25 mb., and circulations there were variable and much weaker than in layers above and below.

Figure 10, a vertical cross section for the 80th meridian, shows the larger-scale zonal circulation setting for the West Indian disturbance. In the southern West Indies the layer above 25 km. was dominated by easterlies which increased with height. The few soundings which reached the 40-km. level indicated that maximum easterlies extended poleward to the 35th parallel. Farther north the entire layer was dominated by westerlies culminating in the polar night jet stream located about 50° N. with maximum winds at 10 mb. This is somewhat higher and farther south than usual (e. g., Krishnamurti [14]). In the upper troposphere the dominant feature was the intense subtropical jet stream centered near 30° N. The polar jet stream during this period was either displaced far south or was so weak that the mean tropospheric flow reflected only a single west wind maximum near the normal position of the subtropical jet stream.

Superimposed upon this characteristic setting were systematic day-to-day variations of wind and temperature. Figure 11, a cross section for Kingston, Jamaica, shows the sequence of wind and temperature variation during the 20-day period. The event of primary concern began on January 23. Colder air began to appear first in the upper levels, then progressively at lower levels. Then at each successive level there followed a rapid transition to warmer conditions. The latter transition was accompanied by a shift from dominant east winds to strong west or southwest winds. The most pronounced change occurred above 30 km. and diminished rapidly toward lower elevations. The influence

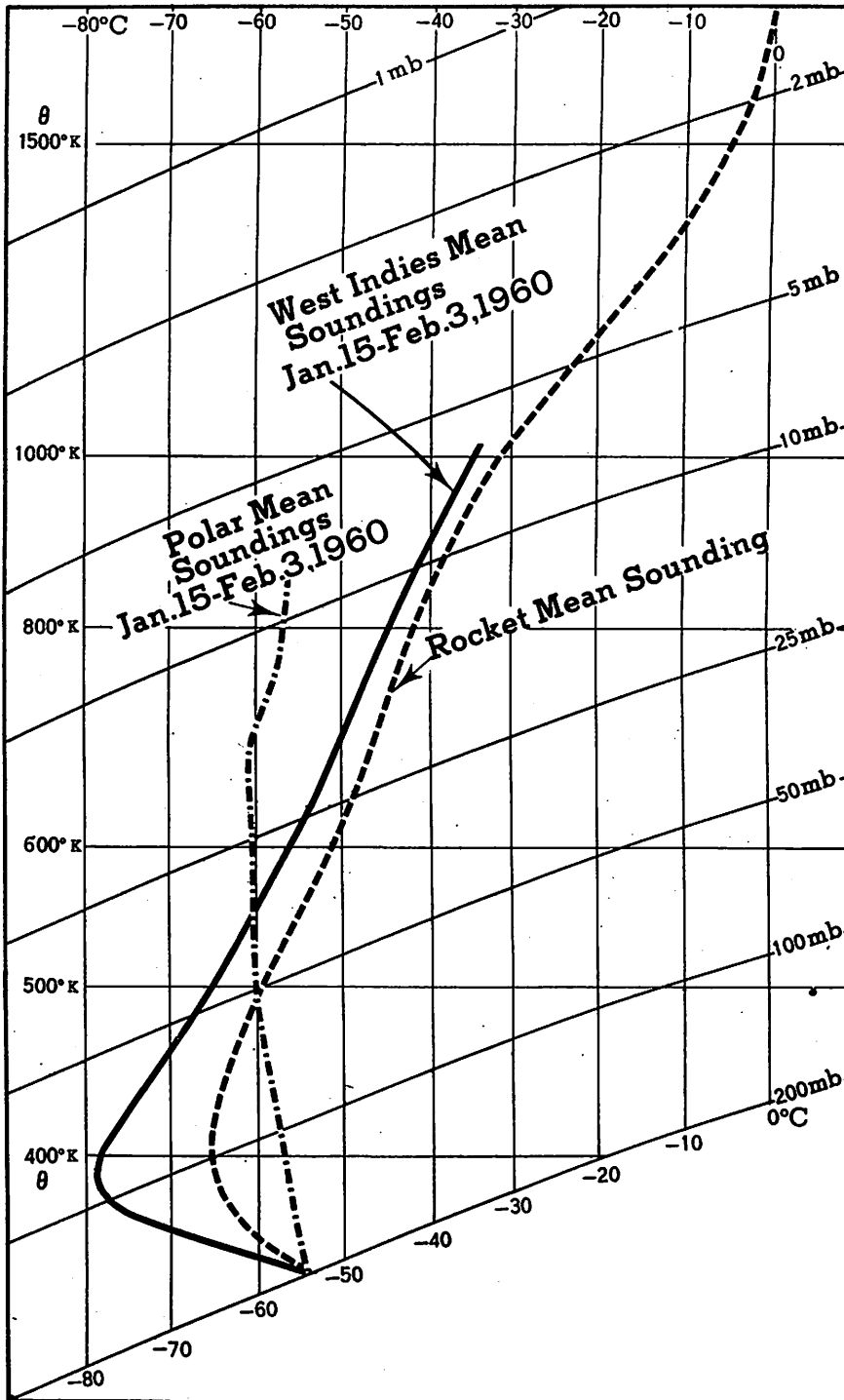


Figure 8. - West Indies mean sounding for the period January 15 to February 3, 1960. This is compared with the sounding for the rocket mean atmosphere (Rocket Panel [39]), and with the mean sounding for five North American polar stations for the same period.

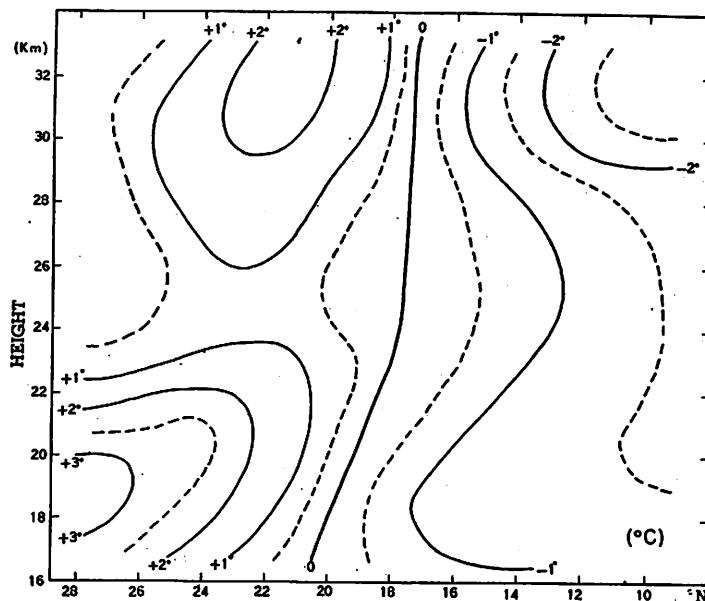


Figure 9. - Mean temperature anomalies in a meridional plane for the West Indies, January 15 to February 3, 1960.

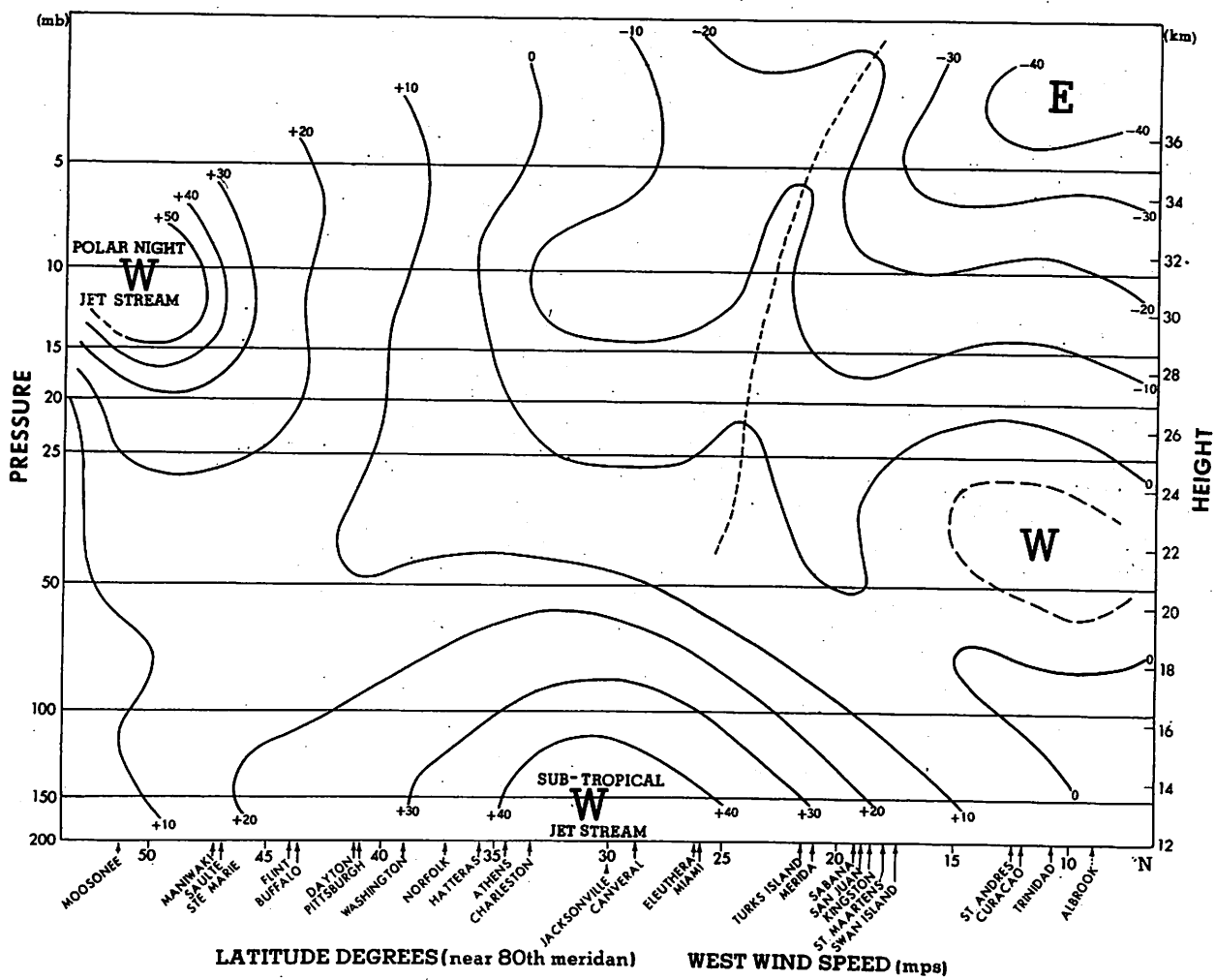


Figure 10. - Mean zonal winds for the 80th meridian, January 15 to Feb. 3, 1960.

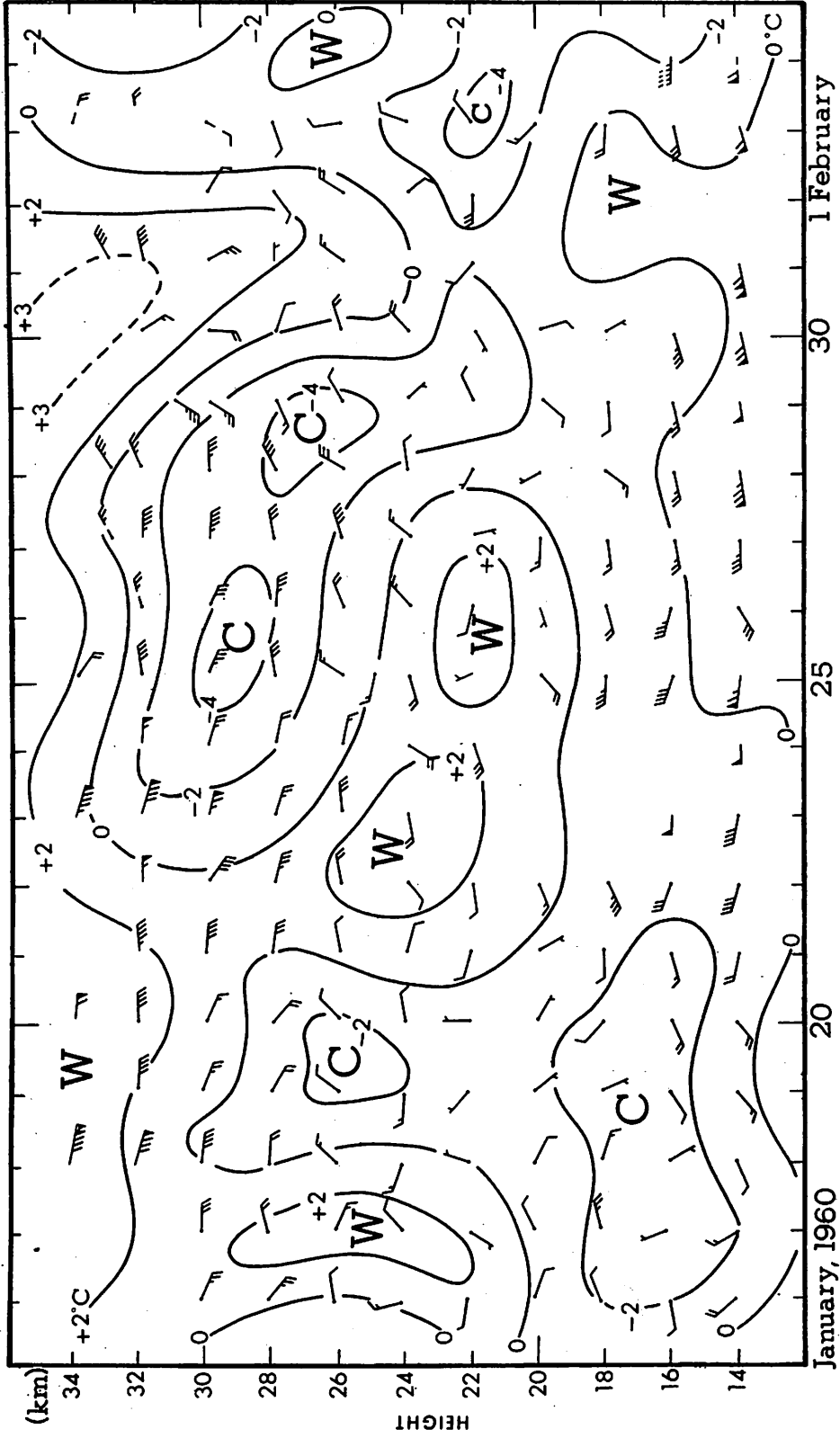


Figure 11. - Wind (knots) and temperature anomalies (°C.) in a z, t plane at Kingston, Jamaica, January 15 to February 3, 1960.

of this disturbance on winds at Kingston was relatively short-lived and strong easterlies returned within less than 48 hours.

Characteristics of the Shear Line

The most prominent of the shear line disturbances which affected the West Indies in January 1960 made its appearance at the southern boundary of the area on January 26, and moved poleward into the Florida-Bahama region by the 31st. Figure 12, a cross section through the shear line (along an n, z plane), shows the composite mean temperature anomalies relative to the shearing surface. It is noteworthy that the disturbance, basically a cold core system, required a reversal of the mean meridional temperature gradient as it moved across the West Indies (compare, e. g., fig. 9). Figure 13 shows the mean relative wind components normal to the shear line, and figure 14 the quasi-zonal wind components parallel to the shear line.

The shearing surface, as shown in figures 12 to 14, represented a boundary between relative cold air on the poleward side and warm air equatorward. Isotherms, especially at 7 and 10 mb., were closely spaced in the cold air near the shear line, a distribution resembling that of a warm frontal system. Coldest temperatures were observed about 300 km. (poleward), and warmest temperatures 600 to 700 km. (equatorward) from the shear line. The extreme difference in temperature between the warm and cold sectors of the system ranged from about 8°C. at the 7-mb. surface to 3.5°C. at the 25-mb. surface.

Figure 14 shows the pronounced discontinuity in zonal wind components which occurred at the shearing surface where strong easterlies in the cold sector shifted to westerlies in the warm sector. The westerlies indicated in the cross section for Kingston extended only about 700 km. equatorward from the shear line. Farther south strong easterlies were present. This relatively small latitudinal extent of the westerlies is a factor which complicates the task of routinely identifying similar disturbances, since sounding balloons in common operational use today do not reach the 10-mb. level regularly.

The relative wind components, figure 13, are normal to the moving shear line, and may be defined as $v_{nr} = (\mathbf{V} - \mathbf{c}) \cdot \mathbf{n}$, where \mathbf{c} is the shear line speed of movement normal to itself and \mathbf{n} a unit normal to the shear line directed poleward. Above 28 km., v_{nr} components were less than 1 m.p.s. and were directed poleward. However, at lower levels they opposed the poleward movement of the shear line. During the period in which data were composited, the average value of \mathbf{c} was about 6 m.p.s. Therefore the shear line system traveled at a speed only slightly less (about 0.5 m.p.s.) than the mean wind normal to the shearing surface in those layers where the shear was most pronounced. The retarding influence of the equatorward components at lower levels did not affect the translation of the upper portion of the system, but during the last 3 days of the compositing period some deceleration of the shear line at 25 mb. was observed.

The slope of the shearing surface averaged about 1:75 (1.3 percent) diminishing with height from more than 1:50 (2.0 percent) below the 25-mb. surface to about 1:100 (1.0 percent) above the 7-mb. surface. Margules slope formula was used to compute the slope of the shearing surface. A distance

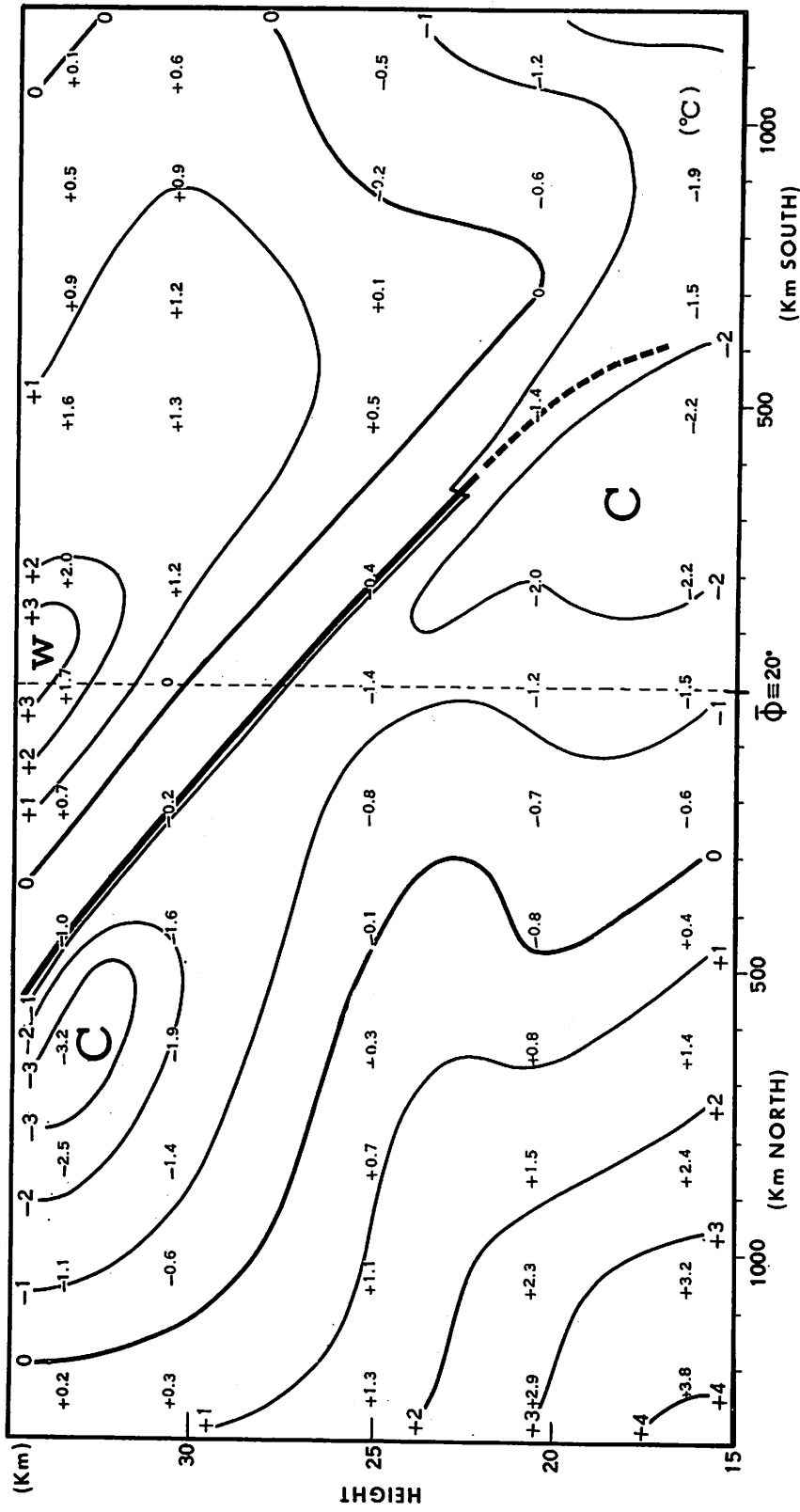


Figure 12. - Composite mean temperature anomalies ($^{\circ}\text{C}$.) in an n, z plane (normal to the shear line).

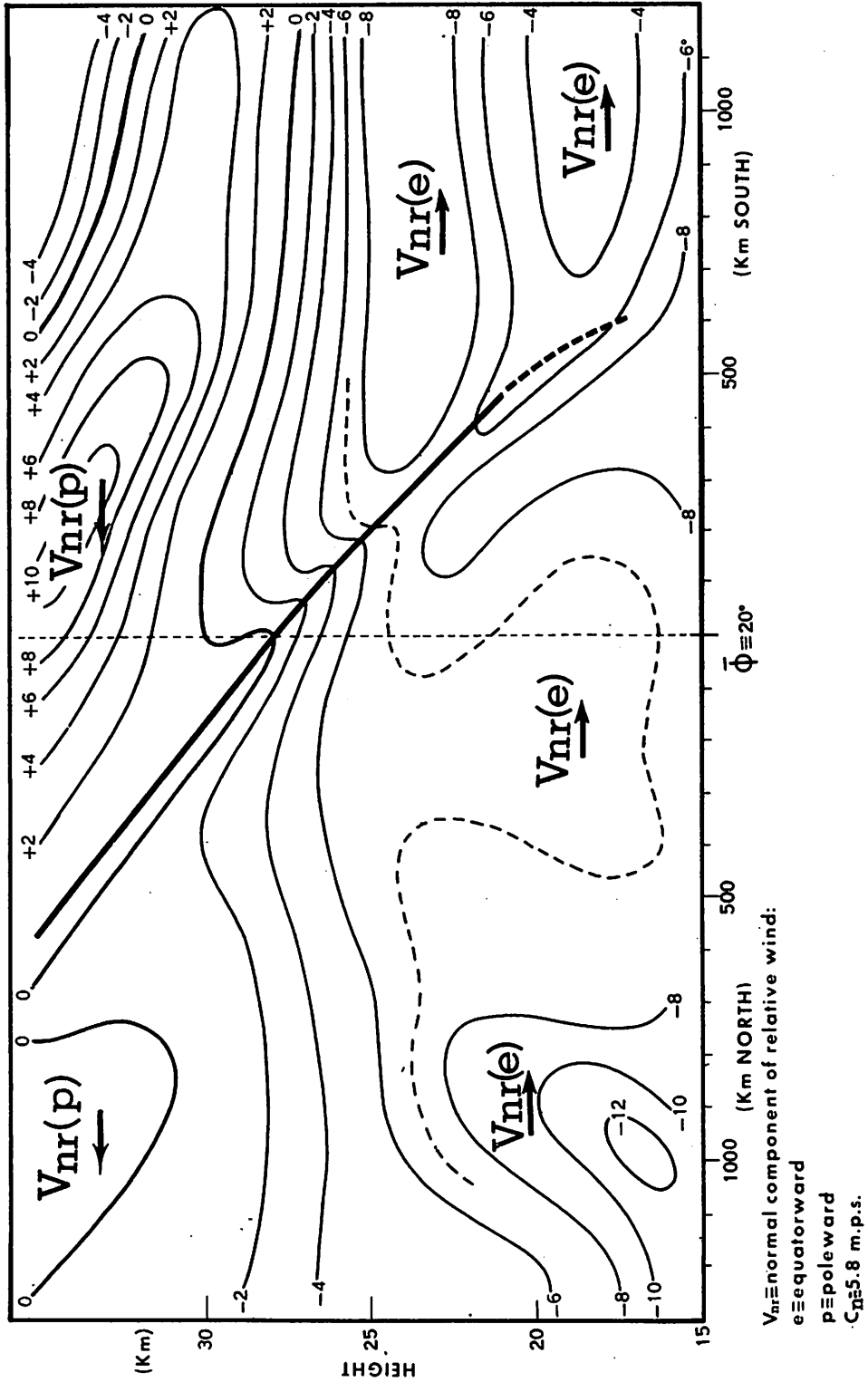


Figure 13. - Mean relative wind components (m.p.s.) normal to the shear line in an n, z plane.

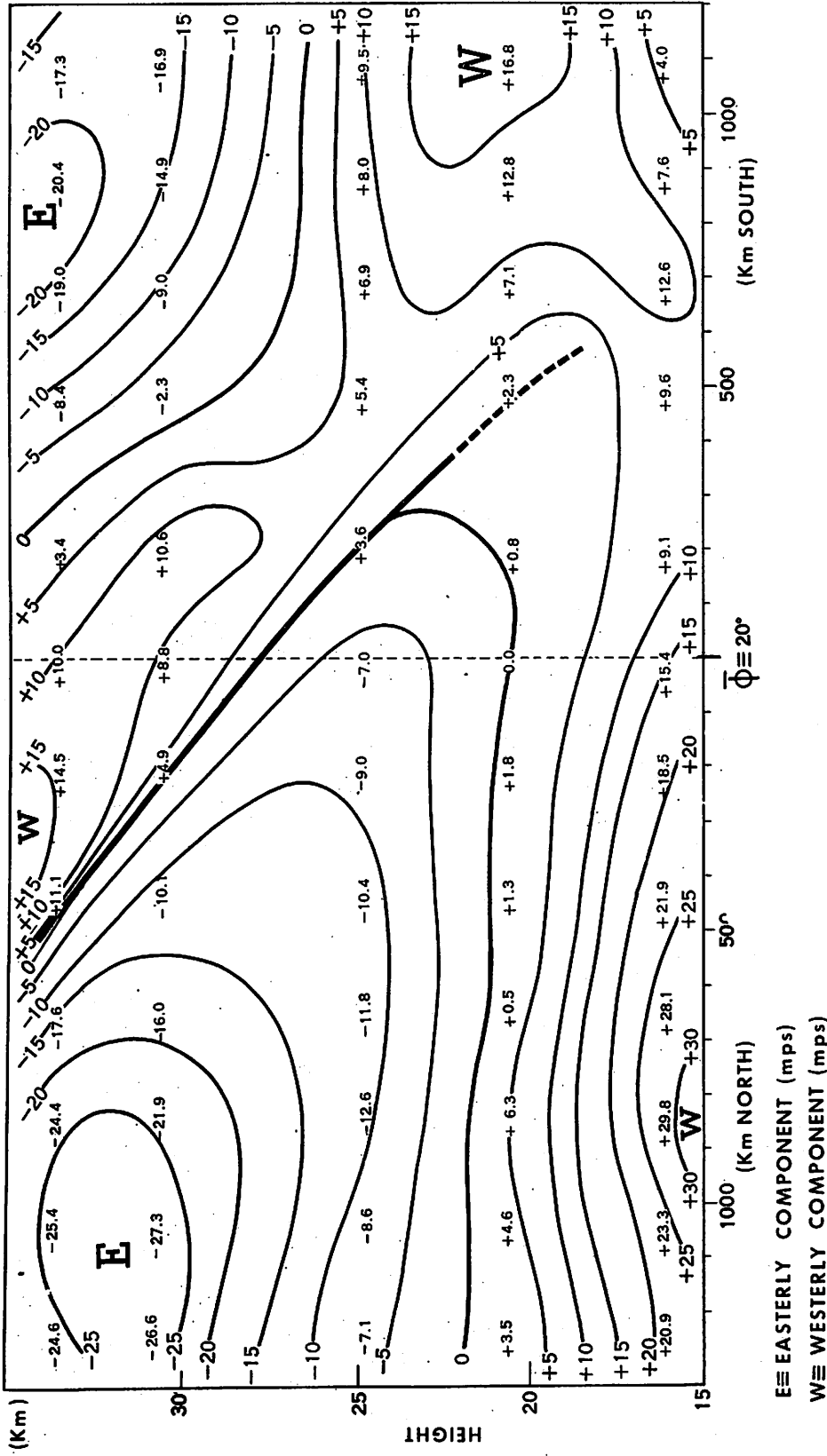


Figure 14. - Wind components (m.p.s.) parallel to the shear line in an n, z plane.

Δx normal to the shear line was selected corresponding to the mean separation of the axes of maximum and minimum temperature in the system. The results were in reasonable agreement with the observed slopes.

Figures 15 to 20 describe the horizontal circulation of the shear line at 7, 10, and 25 mb. Streamlines and contours associate the shear line with a pronounced trough open to the west at 7 and at 10 mb. and extending eastward into a region dominated by a crescent-shaped anticyclone. On the daily charts this anticyclone was present initially only to the north of the shear line, but as the line progressed poleward a developing anticyclone south of the line tended to merge with the residual system to the north.

The horizontal shear across the system diminished downward through the nominal ozone center of mass (25 km.) and was barely detectable at 50 mb. The isotherm pattern, especially the cold center, however, seemed to be conserved through a deeper layer, maintaining its shape and location relative to the shearing surface almost to the tropopause. However, the composite mean temperature anomaly at lower levels was reduced to about 1°C.

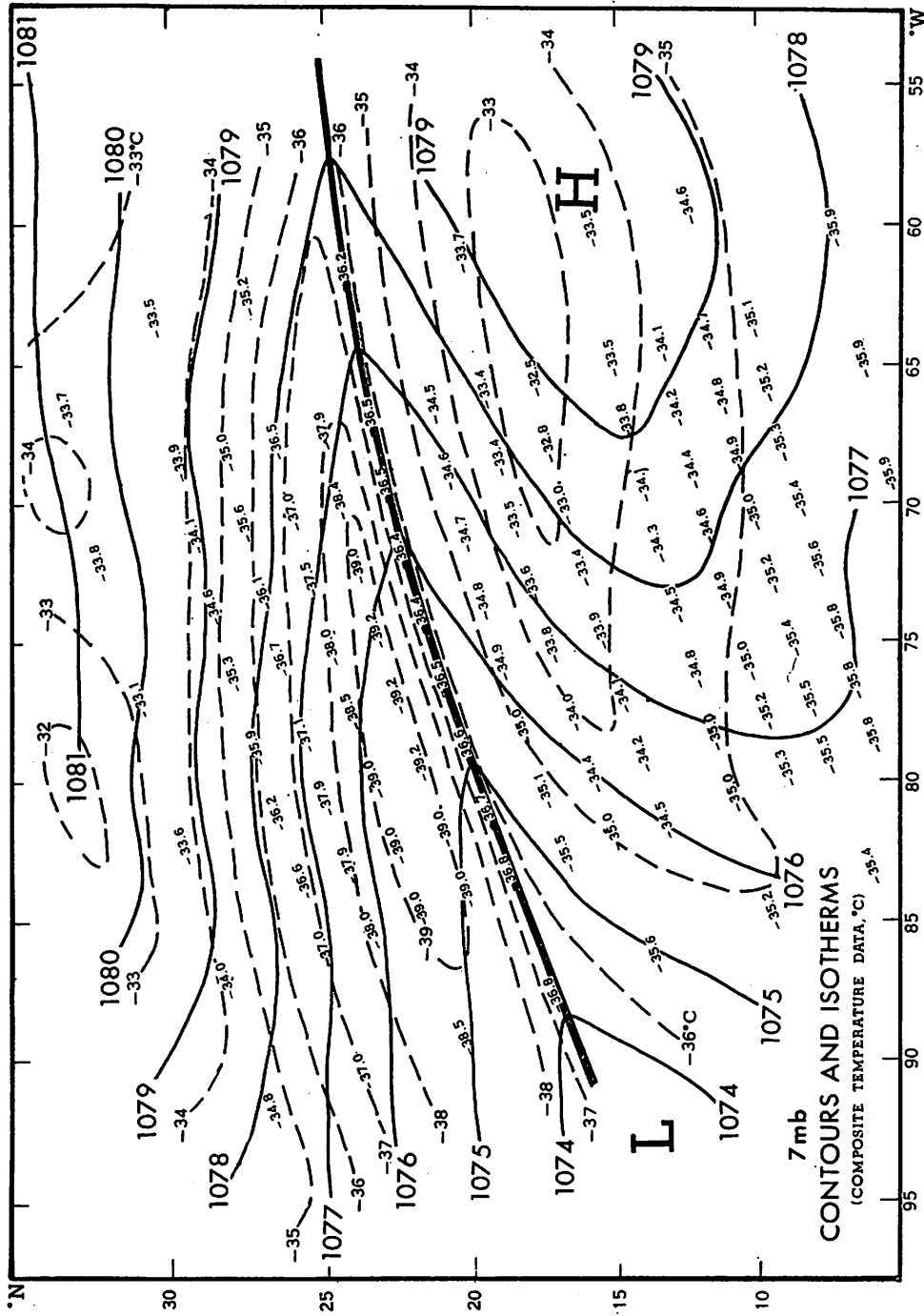


Figure 15. - Contours (hundreds of feet) and isotherms (°C.) for composited data at 7 mb. for January 29, 1960.

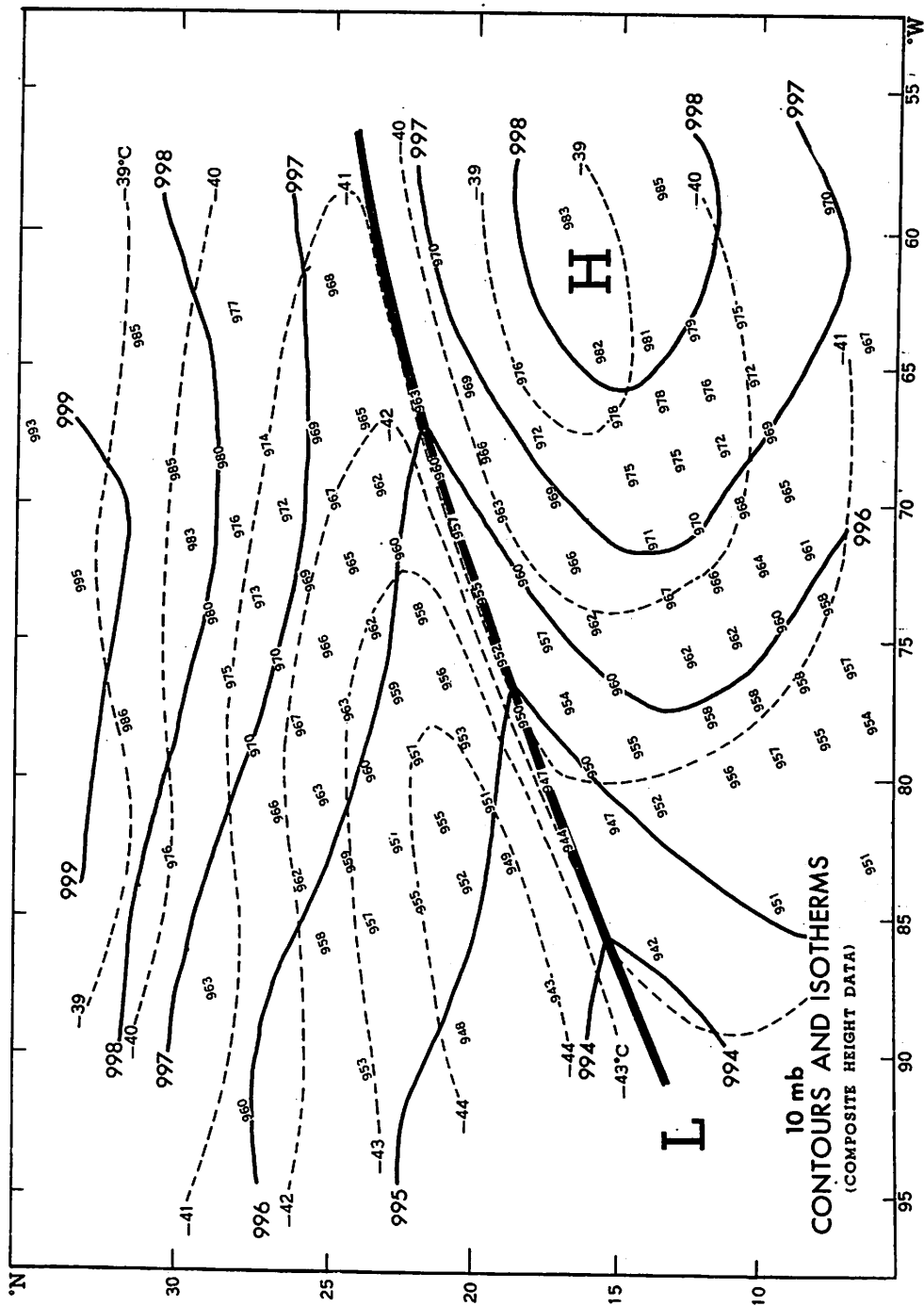


Figure 16. - Contours (hundreds of feet) and isotherms ($^{\circ}\text{C}.$) for compositd data at 10 mb, for January 29, 1960.

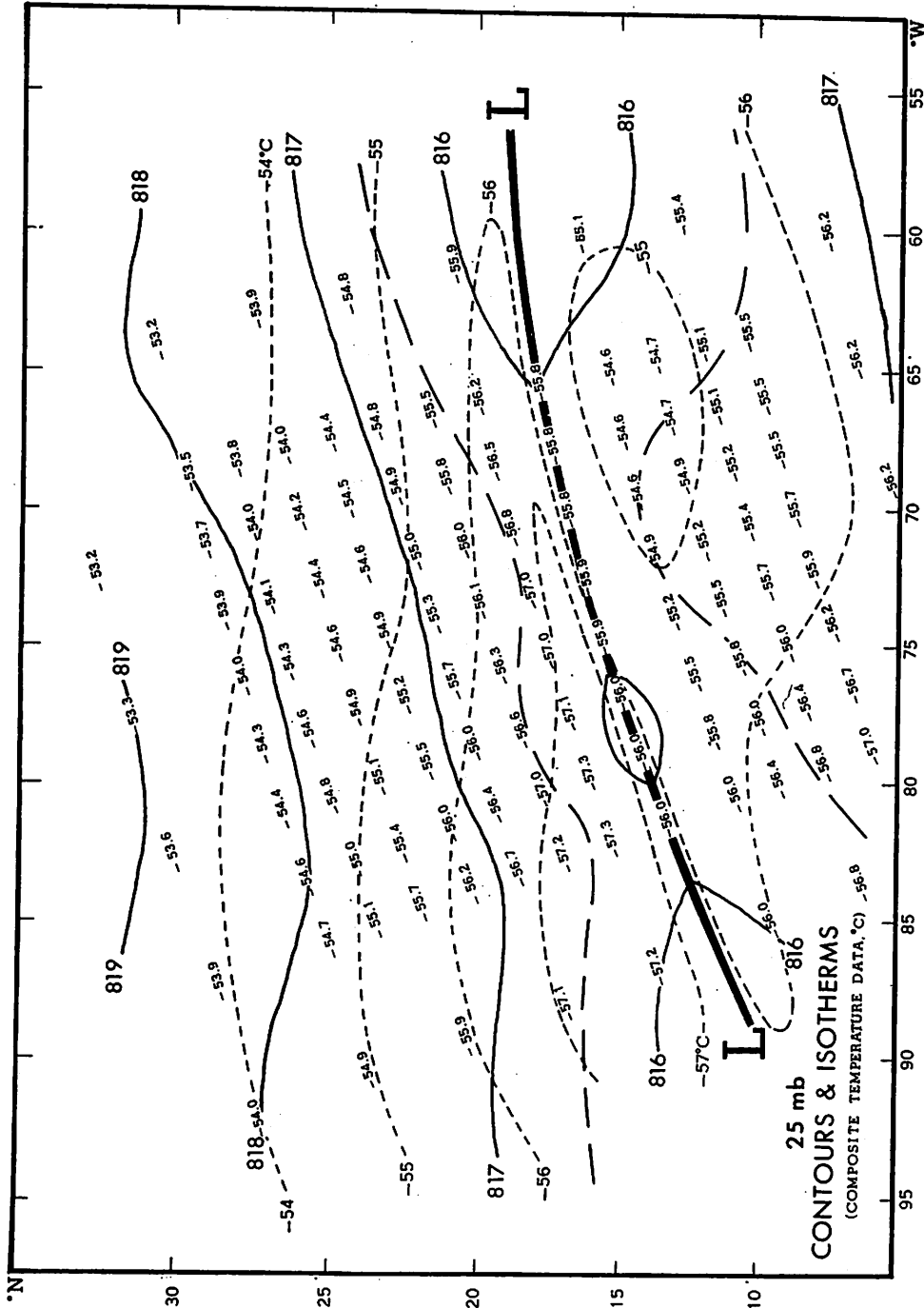


Figure 17. - Contours (hundreds of feet) and isotherms ($^{\circ}\text{C}$.) for compositied data at 25 mb. for January 29, 1960.

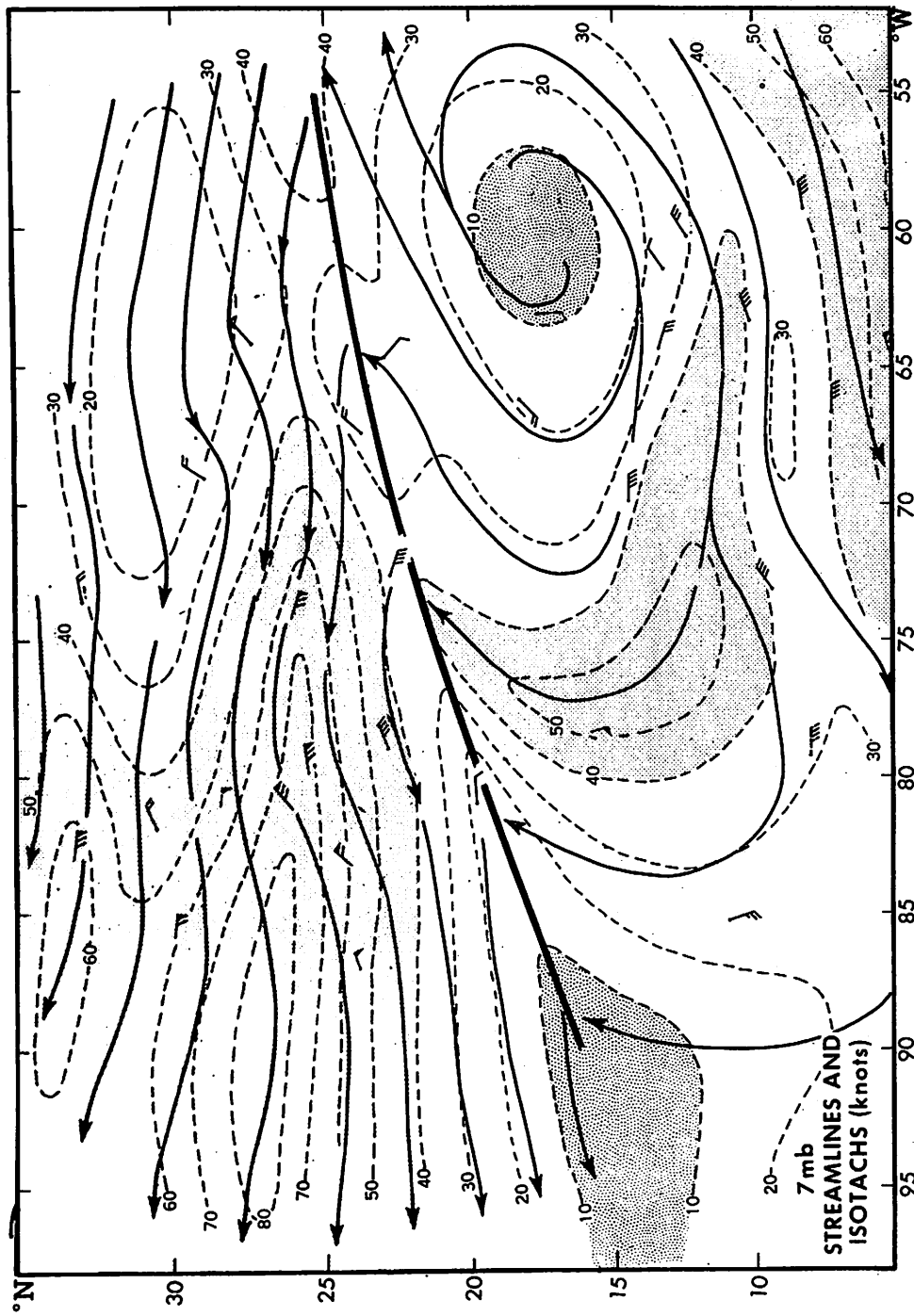


Figure 18. - Streamlines and isotachs (knots) for composited data at 7 mb. for January 29, 1960.

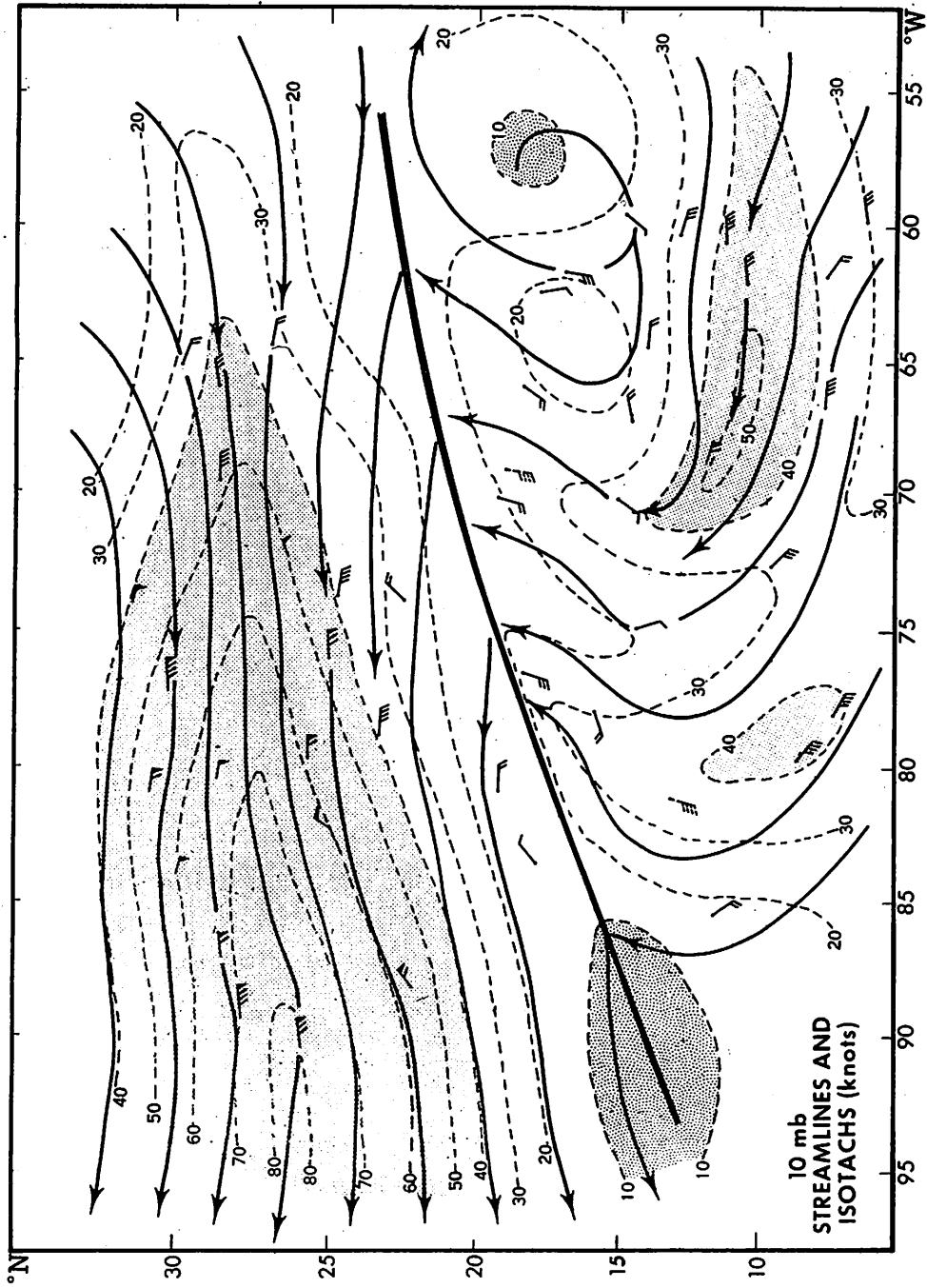


Figure 19. - Streamlines and isotachs (knots) for composited data at 10 mb. for January 29, 1960.

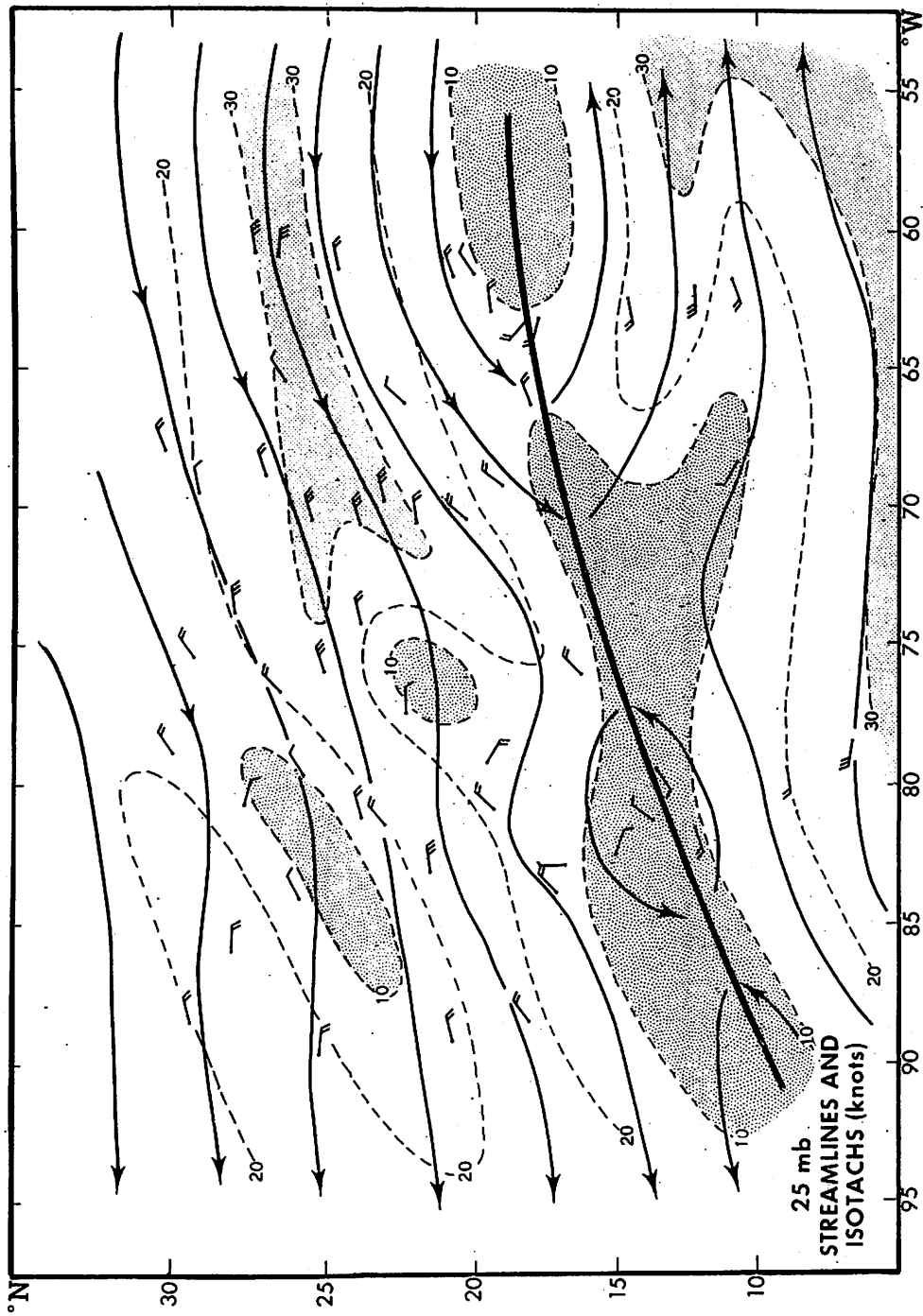


Figure 20. - Streamlines and isotachs (knots) for composited data at 25 mb. for January 29, 1960.

CHAPTER 4. DYNAMICS OF THE SHEAR LINE

The data for the shear line system, analyzed in the manner described above, provide an unprecedented opportunity to examine the laws governing circulation in the high atmosphere, to determine the extent to which motion is accelerative, and to inquire whether the frictionless equations of motion provide a useful representation of the circulation. Field analyses and particle trajectories have both been employed in this investigation. The latter were used first as a means of deriving information to complete the field analyses, and later to analyze the relative contribution of the several forces affecting the motion of a particle as it moved through the disturbance.

Trajectories

In a steady state system relative streamlines are also trajectories with respect to the moving system. From this hypothesis and knowledge of the dis-

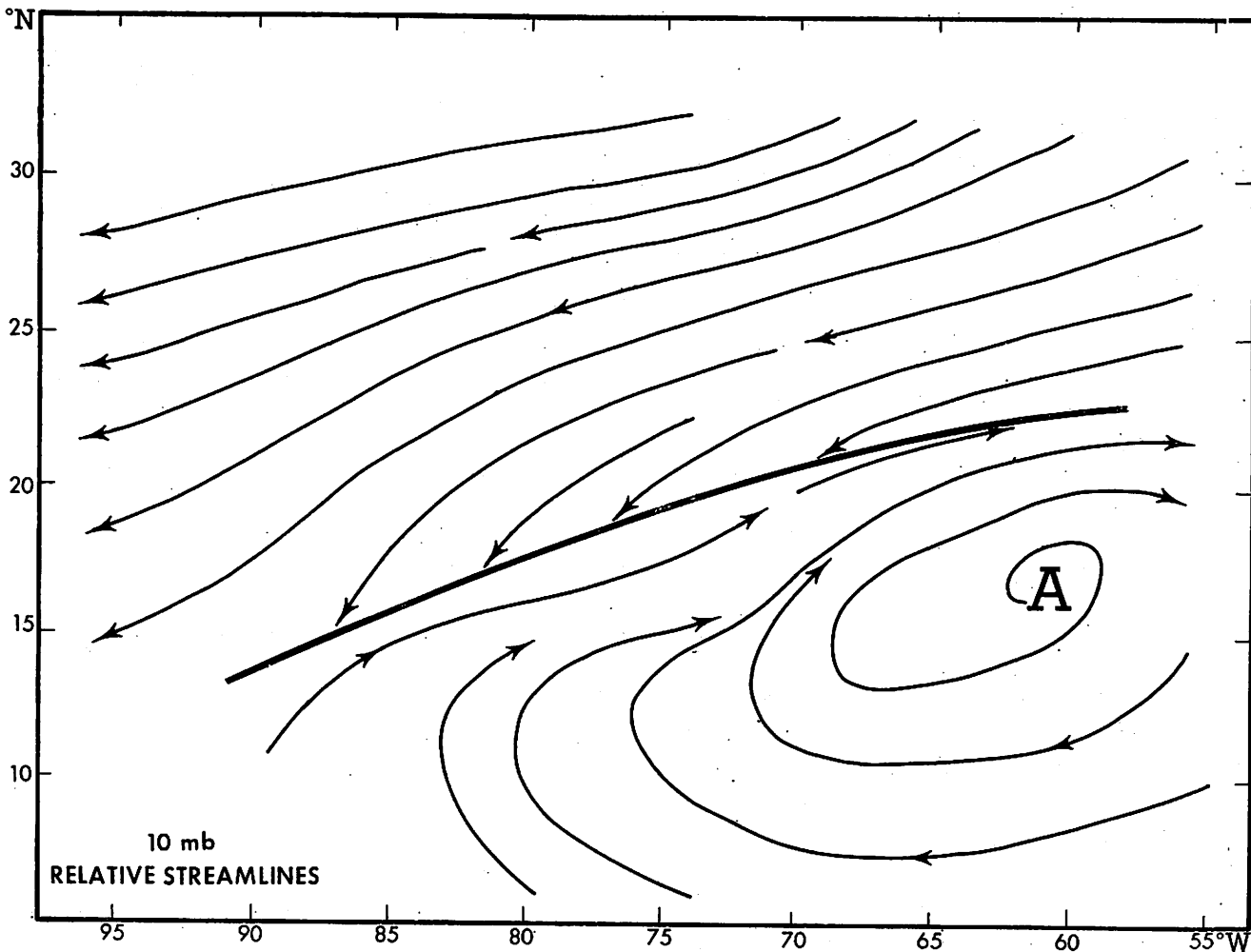


Figure 21. - Streamlines relative to the moving shear line system at 10 mb. for January 29, 1960. This was derived from relative winds which were obtained by subtracting vectorially the shear line movement, 12 knots, from the analyzed wind velocity at each grid point in figure 7.

placement of the shear line, the horizontal components of trajectories relative to the ground were computed for consecutive 6-hour periods. First, relative streamlines were constructed from figures 18, 19, and 20. The shear line movement was subtracted vectorially from the analyzed wind vector at each grid point in figure 7 to obtain relative winds at these points. Streamlines for 10 mb. based on these relative wind values are shown in figure 21. This indicates that air which entered the system in the warm sector was never able to overtake the shear line as it moved poleward, although that which entered the cold sector did ultimately reach the vicinity of the shearing surface where it could sink, rise rapidly, or cross over into the warm air. Here it would have moved eastward slowly, remaining close to the shear line.

Trajectories relative to the ground were computed from figure 22 in the classical manner described by Petterssen [25]. In this case streamline charts for consecutive 6-hour periods were obtained, using the steady state assumption, by displacing the circulation (fig. 19) successively a distance equivalent to the 6-hour movement of the shear line. From these the local turning of the wind was obtained and the trajectories constructed as suggested by Petterssen. The trajectory computations were carried out in 6-hour steps.

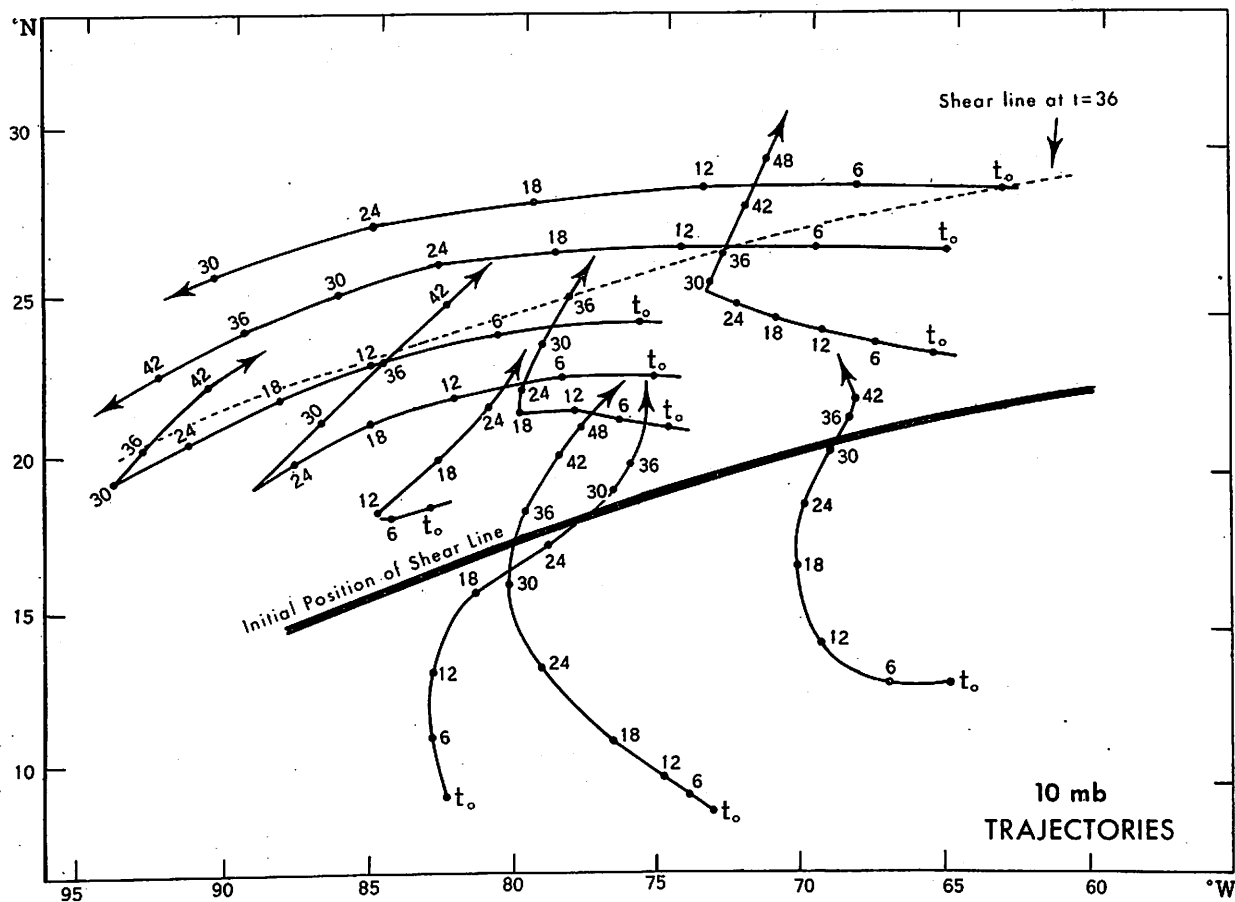


Figure 22. - Earth-oriented trajectories of particles at 10 mb. as the shear line moved poleward. Each trajectory has its origin in time at 1200 GMT, January 29, 1960.

Figure 22 represents a family of trajectories computed for the 10-mb. surface. Each trajectory has its origin at the compositing hour when the shear line lay across the central West Indies. These trajectories do not account for vertical motions which may be present. However, the importance of vertical motion under the constraints of thermal stability in this case can be assumed to be minimal, a conclusion which will be verified by computations presented later. From a balloon operational point of view, recalling the original requirement of Skyhook 60, a balloon released north of the shear line would have moved far

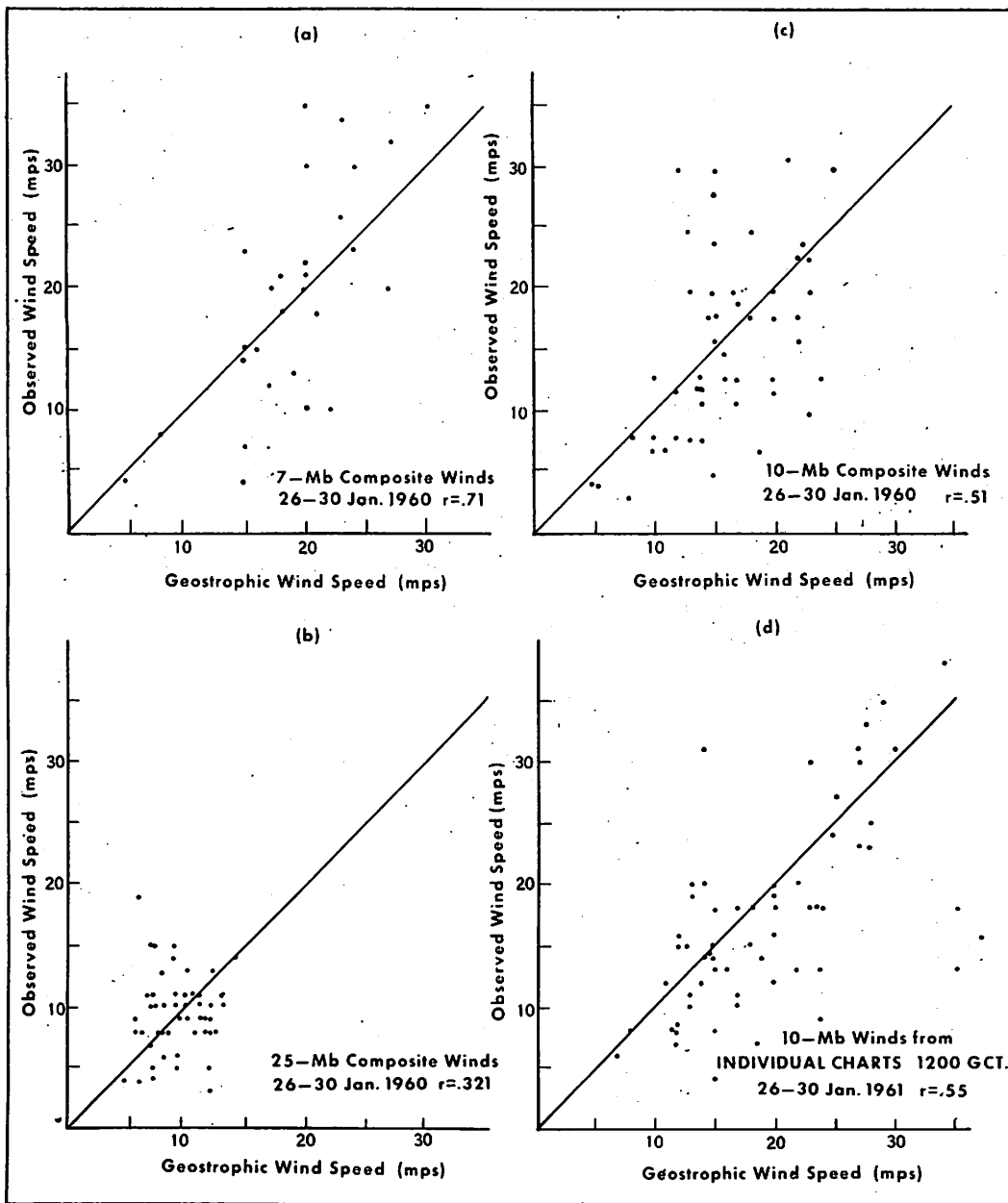


Figure 23. - Scatter diagrams of geostrophic versus observed wind speeds for (a) 7-mb. composite data, (b) 10-mb. composite data, (c) 25-mb. composite data, (d) 10-mb. daily analyses.

west before being overtaken by the shear line and even then would have returned to its initial meridian only after moving to much higher latitudes. A balloon released south of the shear line would never have overtaken the shear line but, after initially moving north or northwestward, would have proceeded steadily on a northeastward course.

Balance of Forces

In view of the large thermal stability present, the balance of forces analysis has neglected contributions due to vertical motion, and used the horizontal equations of motion in the form

$$\frac{du}{dt} = fv - \frac{\partial \Phi}{\partial x} + F_x \quad (1)$$

$$\frac{dv}{dt} = -fu - \frac{\partial \Phi}{\partial y} + F_y \quad (2)$$

or in a natural system of curvilinear coordinates (s, n, p)

$$\frac{dV}{dt} = -\frac{\partial \Phi}{\partial s} + F_s \quad (3)$$

$$fV + \frac{V^2}{R} = \frac{\partial \Phi}{\partial n} - F_n \quad (4)$$

where R, the radius of curvature of the trajectory, is positive in the cyclonic sense. From each pair of these equations a term involving the parameter $\left(\frac{\tan \phi}{a}\right)$ has been omitted since its contribution at low latitudes and at the wind speeds of this system is of second order.

If motion is frictionless and accelerations are negligible, (1) and (2) reduce to the simple equations of geostrophic motion. Figure 23 contains several scatter diagrams showing the observed versus geostrophic wind speeds at 7, 10, and 25 mb. for the composited data, and at 10 mb. for the five individual daily charts. The scatter in each instance is quite large. Evidently, if the data and the analyses are not faulty, the geostrophic approximation is not adequate to describe circulation in this disturbance. First let us consider some of the possible sources of error. Numerous random errors in computing the height of winds could account for the scatter. However, if such errors were numerous neither the daily analyses nor the composited data would exhibit as good continuity of isotach patterns as was observed. Alternatively the compositing process could readily generate systematic errors of several kinds. However, if this were a primary source, the scatter should be appreciably less for daily analyses than for analyses of composite data. But this is not so. Finally one may consider whether the deviations are distributed randomly or systematically. Figure 24 provides some evidence supporting the latter. This analysis shows the ratio of the Coriolis force to the pressure gradient force, measured at each point of wind observation. In general the observed winds appeared to be sub-geostrophic in the warm sector and super-geostrophic in

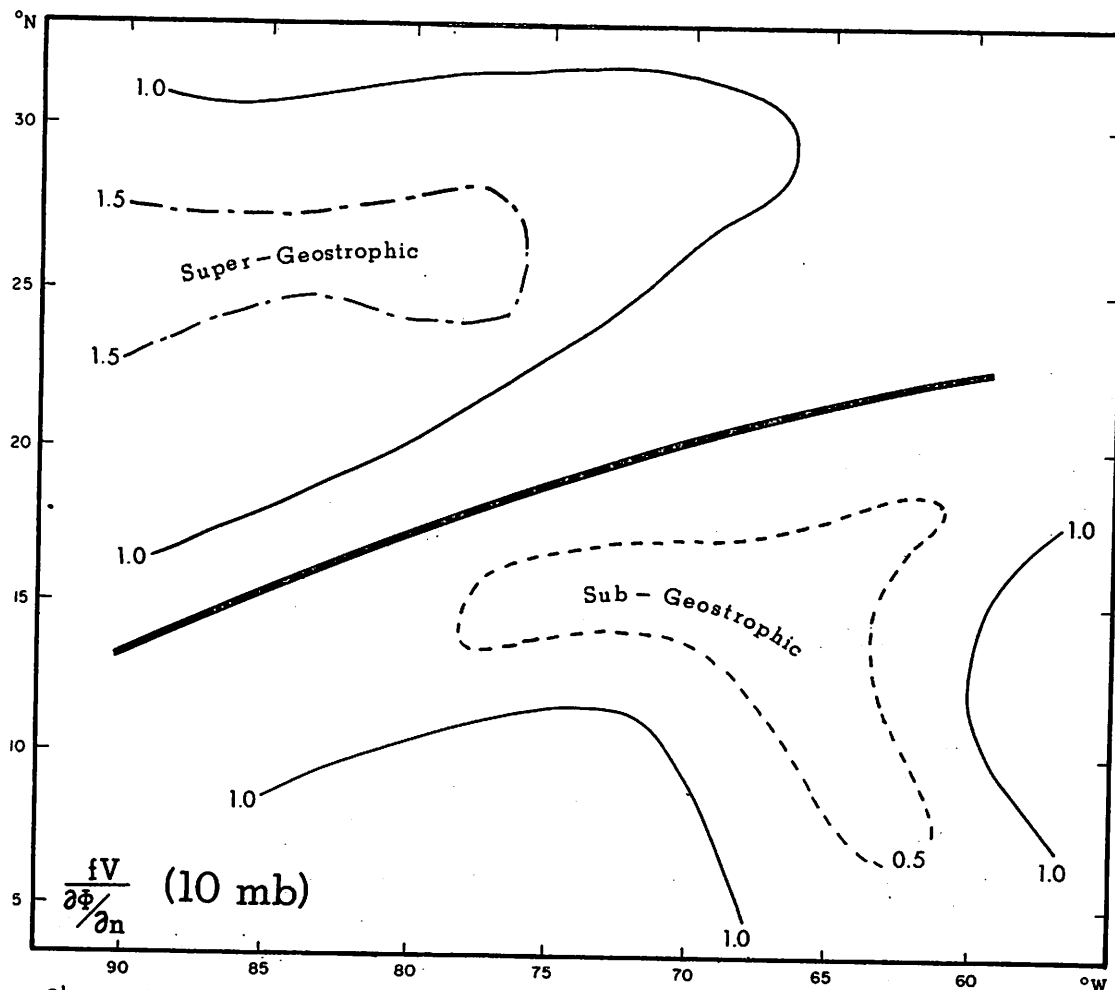


Figure 24. - Areal distribution at 10 mb. of the deviation of observed winds from geostrophic values. The deviation is expressed here as the ratio of the observed Coriolis force to the pressure gradient force normal to the wind.

the cold sector, although the individual values did not describe a completely uniform gradient pattern. The areal distribution of the deviations, however, may be considered as reflecting either the basic character of circulation, or some systematic bias in the development of pressure height data. The uncertainty as to which it is can best be alleviated, by the results from computations which are to follow, and which will support the conclusion that the circulation is systematically accelerative and cannot be described satisfactorily by the geostrophic approximation.

Viscosity

Little is known about frictional forces in the lower mesosphere, at least in the upper reaches of the ozone layer. In order to examine its magnitude we may replace the last term in equations (1) to (4) by the more explicit expression for acceleration due to frictional stresses

$$F \equiv \nu \nabla^2 \mathbf{V} \quad (5)$$

where $\nu \equiv \mu / \rho$ is known as the kinematic coefficient of eddy viscosity, and

μ is the dynamic coefficient. Experience has shown that the vertical shearing stresses are normally much greater than the horizontal stresses, although horizontal and vertical coefficients are not identical or necessarily of the same order of magnitude. In the lower mesosphere it is probably reasonable to assume that the only significant reduction in kinetic energy by friction results from vertical stresses. Therefore equation (3) may be written

$$\frac{dV}{dt} = - \frac{\partial \Phi}{\partial s} + \nu \frac{\partial^2 (\mathbf{V} \cdot \hat{s})}{\partial z^2} \quad (6)$$

where \hat{s} is a unit vector along a streamline. Lettau [16], and more recently Haurwitz [12], have proposed a maximum value of ν for the mesosphere of about $10^7 \text{ cm}^2 \text{ sec}^{-1}$. This is approximately three orders of magnitude greater than the value commonly assigned to circulations in the troposphere. On the other hand, recent statistical studies by Feely and Spar [10] tracing the spread of atomic debris in the lower stratosphere, suggest values ranging from 10^3 to $10^4 \text{ cm}^2 \text{ sec}^{-1}$ for the vertical eddy diffusion coefficient and $10^9 \text{ cm}^2 \text{ sec}^{-1}$ for the meridional coefficient. The West Indies data used in the present study provide an interesting opportunity to compute values for at least the vertical coefficient using synoptic scale analyses.

Equation (6) may be integrated along the path of a particle,

$$(V_t - V_o) \equiv \Delta V_t = \nu \int \frac{\partial^2 V}{\partial z^2} dt - \int \frac{\partial \Phi}{\partial s} dt$$

so that

$$\nu = \frac{\Delta V_t + \int \frac{\partial \Phi}{\partial s} dt}{\int \frac{\partial^2 V}{\partial z^2} dt} \quad (7)$$

Here, the subscripts (t) and (o) are the final and initial times for which the particle motion is followed. Figure 25 shows a family of 18 trajectories at 10 mb. for which ν has been computed. The 12-hour movements were selected to provide a representative coverage of motions through the system and to enable computations to be made at locations where $\partial \Phi / \partial s$ and $\partial^2 V / \partial z^2$ vary almost linearly. Values of $\partial^2 V / \partial z^2$ were computed for all available individual wind soundings. From these, a field analysis of this quantity was made and point values obtained for use in this computation. Examples of the vertical shear for the 10-mb. surface are shown in figure 28. The values of ν and of the several terms of (7) for each of the 18 trajectories are shown in table 1.

The average value of ν obtained in this manner is $7 \times 10^5 \text{ cm}^2 \text{ sec}^{-1}$. This is surprisingly large in terms of the empirical conclusions of Feely and Spar, though not unreasonably so from the heuristic arguments of Lettau and Haurwitz.

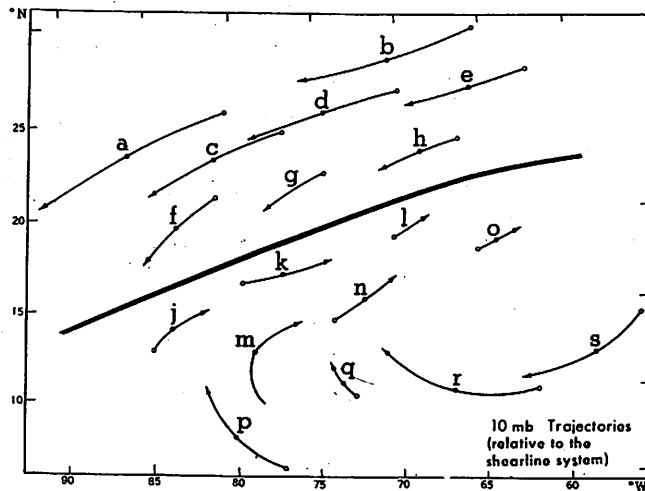


Figure 25. - Twelve-hour trajectories relative to the moving shear line system used in computing eddy viscosity coefficient values for the 10-mb. surface.

Table 1. - Computation of the eddy coefficient of viscosity ν for a family of 10-mb. trajectories (see fig. 25), and comparison of the computed ageostrophic component of the wind, using the mean value of ν , with the observed value.

Trajectory (See fig. 25)	C_t mps	C_s mps	ΔC_t 10^2 cm sec ⁻¹	$\int \frac{\partial^2 \zeta}{\partial s^2} dt$ 10^2 cm sec ⁻¹	$\int \frac{\partial^2 c}{\partial s^2} dt$ 10^{-4} cm ⁻¹	ν 10^8 cm ² sec ⁻¹	V dd vv deg mps	V_g dd vv deg mps	V dd vv deg mps	u_z (obsvd) mps centered	u_z (comp) mps for $\bar{\nu} = 6 \times 10^8$
a	23	30	-7	-12.1	-25.4	7.6	07 30	12 09	05 13	-8	-2
b	30	22	+8	-10.5	-3.4	7.4	08 24	09 05	07 17	-6	-3
c	20	20	0	-8.0	-9.9	8.0	08 22	11 11	06 13	-7	-5
d	23	23	0	-6.4	-7.7	8.0	09 23	11 13	07 13	-5	0
e	20	18	+2	-4.8	-18.5	1.5	10 17	09 13	12 05	+3	+2
f	8	11	-3	-5.4	-8.6	9.8	07 10	10 14	32 05	-5	+3
g	9	11	-2	-0.1	-3.9	5.3	10 10	10 12	28 02	0	+3
h	11	13	-2	-3.2	-15.0	3.6	10 12	10 13	28 01	0	+2
j	13	11	+2	-4.8	-5.6	5.0	20 12	21 21	04 07	-6	-8
k	8	15	-7	-7.4	+0.9	4.0	22 12	22 23	04 11	-9	-3
l	6	6	0	-10.6	-12.9	8.2	20 12	23 22	07 12	-4	0
m	12	18	-6	-3.2	-10.5	8.8	17 18	18 17	08 02	0	+1
n	17	12	+5	+1.0	+9.3	6.4	22 15	21 19	35 06	-6	+1
o	12	8	+4	-11.8	-8.2	9.5	21 10	24 20	28 11	-2	0
p	17	19	-2	-4.8	-31.2	2.2	13 19	13 16	13 03	+2	+4
q	13	16	-3	0	-4.3	7.0	14 15	13 22	28 08	-1	+2
r	17	20	-3	-3.5	-13.8	4.7	11 24	12 27	35 06	-6	-1
s	22	14	+8	-9.6	-21.4	0.6	10 18	07 22	19 07	+7	+8

At this point one needs to consider again whether the values of ν computed here may be strongly influenced by subjective aspects of the analysis. To begin with, the trajectories used in the computation represent the entire area of analysis. Hence, if the results are influenced by bias in analysis, the computed values should reflect a systematic variation from one portion of the system to another. However, while the values range over nearly an order of magnitude, reflecting general deficiencies in the data and the analyses, the variations are randomly distributed.

A useful check on the internal consistency of the analysis and of the above computation can be made by using this value to compute ageostrophic meridional components of the wind, then comparing the results with observed point values. If the ageostrophic meridional component is expressed $v_a = (v - v_g)$ then (1) may be rewritten

$$\frac{du}{dt} = fv_a + \nu \frac{\partial^2 u}{\partial z^2} \quad (8)$$

Integrating with respect to time along the path of the particle

$$\overline{v_a} = \frac{1}{ft} \left[\Delta u_t - \nu \int \frac{\partial^2 u}{\partial z^2} dt \right] \quad (9)$$

Table 1 shows that $v_{a(c)}$ (computed values) and $v_{a(o)}$ (observed values) are comparable in magnitude, although both are small and differ from one another even in sign in several instances. This is due in part to the fact the computed values represent integrations for the entire trajectory.

From these computations one is led toward the conclusion that in the lower mesosphere frictional forces play a more important role in disturbed circulation than in the troposphere, and that both the frictionless equations of motion and the geostrophic approximation are inadequate to describe the circulation. While the usefulness of coefficient of eddy viscosity values derived here must be judged in light of the limited scope and frailties of the analysis, this represents the first opportunity which has presented itself to derive such information from field analyses of synoptic observations, and is subject to fewer uncertainties than values derived from most other approaches heretofore available.

Vertical Motion

The pronounced thermal stability of the lower mesosphere acts as a powerful constraint upon vertical motion. However, to understand the release of energy and the processes which drive the circulations of the shear line there is a need for some estimate of the pattern, the sign, and the order of magnitude of vertical motions. For circular-symmetric or closed systems vertical motions can sometimes be derived directly from horizontal motions at several

levels using Stokes stream functions. In the present case we deal with an open system in which the flow is predominantly zonal, with a substantial amount of shear both horizontally and vertically. Since mass balance cannot be established reliably in such open areas as this, mass circulation computed from horizontal motions is not a satisfactory means of deriving vertical motions. One must therefore look to thermodynamic tools to obtain this information.

The first law of thermodynamics may be expressed

$$\delta H = c_p dT - \alpha dp \quad (10)$$

From this the change in temperature of an air parcel moving through the shear line system is

$$\frac{dT}{dt} = \frac{1}{c_p} \frac{\delta H}{\delta t} + \frac{\alpha}{c_p} \omega \quad (11)$$

where $\omega \equiv \frac{dp}{dt}$. This may be expanded as follows

$$\frac{\delta T}{\delta t} + V_r \frac{\partial T}{\partial s} + \omega \frac{\partial T}{\partial p} = \frac{1}{c_p} \frac{\delta H}{\delta t} + \frac{\alpha}{c_p} \omega \quad (12)$$

Here, a natural system of coordinates with axes n, s, p is used (pressure the vertical coordinate) where n is positive to the right of motion. Since this deals with a moving system, V_r is the wind speed along a relative streamline in which $V_r = V - c$. For a steady circulation (11) reduces to

$$\omega \left(\frac{dT}{dp} - \frac{\partial T}{\partial p} \right) = V_r \frac{\partial T}{\partial s} - \frac{1}{c_p} \frac{\delta H}{\delta t} \quad (13)$$

It may be noted from (11) that for adiabatic motion $\frac{dT}{dp} \equiv \Gamma_a$ is the adiabatic rate of cooling as a parcel moves vertically along a pressure coordinate. If we then follow a parcel as it passes through the system, its vertical displacement is given by

$$\omega = \frac{V_r \frac{\partial T}{\partial s} - \frac{1}{c_p} \frac{\delta H}{\delta t}}{\Gamma_a - \Gamma'} \quad (14)$$

Here $\Gamma' \equiv \frac{\partial T}{\partial p}$ is the change in layer temperature along the vertical pressure axis.

In the layer 25 to 7 mb., the denominator of (14) is large (at 10 mb. approximately 10°C. per mb.) and the percentage variation throughout the shear line system, except at the shearing surface itself, is small. Hence the gradients of vertical motion in the system are almost uniquely reflected

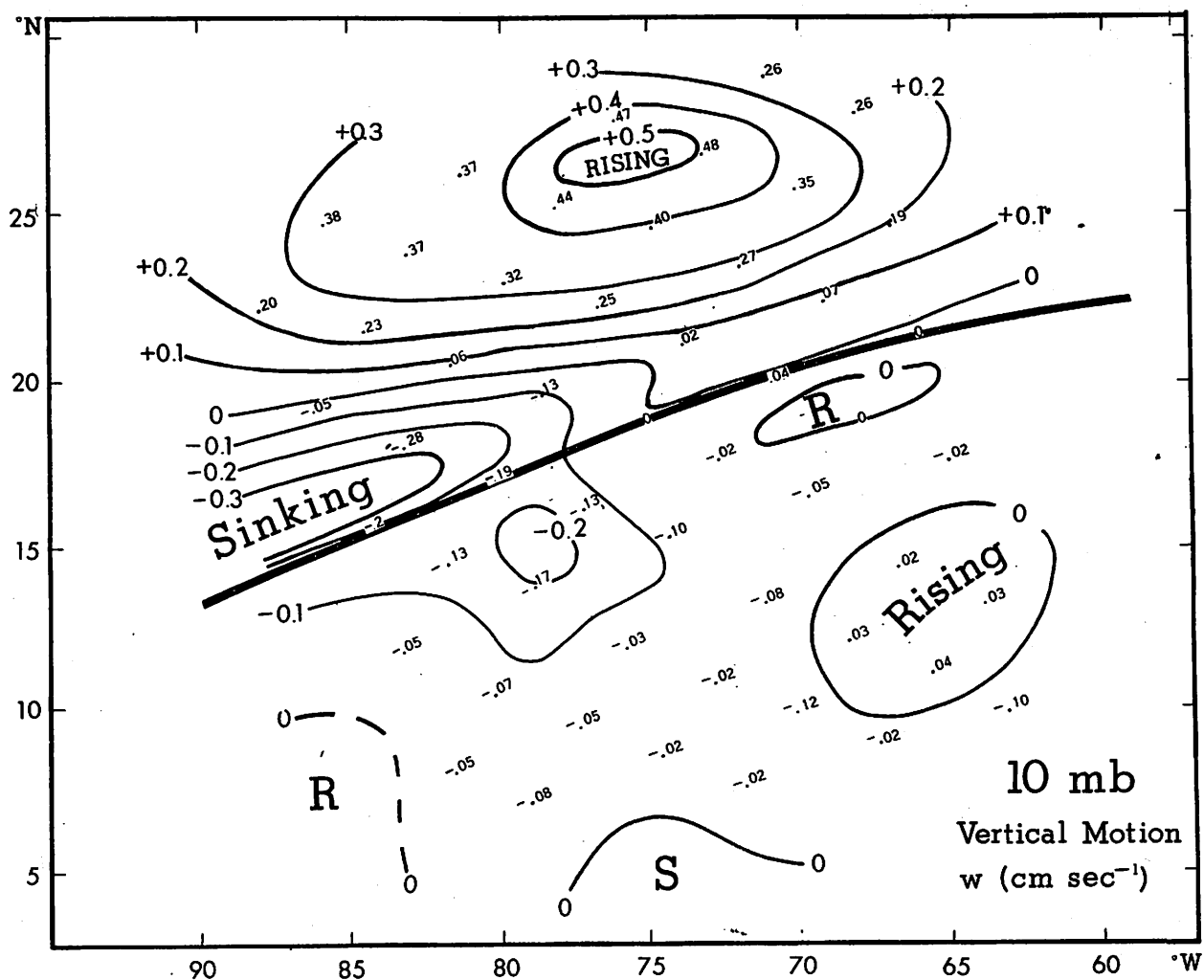


Figure 26. - Vertical motions computed for the 10-mb. surface based on the assumption that motion is adiabatic.

by the isotherm distribution along the particle trajectory if diabatic influences are not considered. If there is net radiational cooling of the parcel, the vertical motion indicated by adiabatic processes must be augmented by a downward component. If there is net warming, the motion is augmented by a net upward component.

As a first approximation, let it be assumed that diabatic processes may be neglected for 12-hour periods during which the change in temperature and the mean wind speed are measured along a family of trajectories encompassing the shear line at 25, 10, and 7 mb. It is appropriate to recall here that the trajectories used in these computations are relative to a moving steady state system. They are based solely upon the instantaneous wind field and hence do not reflect diurnal variations as implied by the selection of a 12-hour segment for computations.

The vertical motion at 10 mb. thus computed is presented in figure 26.

Here ω values have been converted to geometric units of w by using the following approximation.

$$\omega \equiv \frac{dp}{dt} = \frac{\partial p}{\partial t} + \mathbf{V} \cdot \nabla p + w \frac{\partial p}{\partial z} \approx -wpg \quad (15)$$

For steady circulations this is exact, providing the motion is geostrophic. While in this case there is appreciable ageostrophic motion, it turns out that the magnitude is of second order in the transformation of ω to w .

The largest vertical motions occur in the cool sector where a large center of rising air is located about 900 km. north of the line. In this sector there is also an area of sinking near the shear line. The warm sector had no definite centers of vertical motion and computed values were little larger than the probable errors of analysis.

The distribution of vertical motions in the n, z plane is presented in figure 27, a vertical cross section normal to the shear line. Here the relative wind components, v_{nr} , at 25, 10, and 7 mb. have been averaged at various distances from the shear line, then composed vectorially with the mean vertical wind at that distance. In accomplishing this the magnitude of the vertical wind has been augmented by the same multiplying factor as used for the vertical coordinate of the cross section. From these vectors, mean streamlines for the system were constructed. Also included is the field of temperature anomalies from the area mean values.

Figure 27 implies that the shearing surface was a region of sinking motion. In this regard, subsidence near the shear line may have been more pronounced than computed values indicate. Limitations of the computing procedure in the vicinity of the shear line, in addition to the fact that the compositing process tends to underestimate gradients, could have resulted in smaller estimates of subsidence than actually existed.

It should be noted that individual particles which moved through this system were able to participate in only a small portion of the vertical motion identified by the streamlines. In fact, as shown later, they could have moved through the entire system with no more than 300 ft. change in elevation.

Effect of Radiation. Let us now consider the effect which radiation could have had on vertical motions in this system. All of the sounding data used in this study were from balloon releases at 1200 GMT. This corresponds to approximately 8:00 a.m. local standard time in the eastern portion of the West Indies and 6:00 a.m. in the extreme western part. In late January the sun rises about 6:30 a.m. local standard time, and begins irradiating the ozone layer a few minutes earlier. Sounding balloons normally rise about 1 km. every 3 minutes; therefore temperature measurements in the ozone layer were made 60 to 90 minutes after release time. Hence the shear line system (25-35 km.) would have been irradiated by the sun from 1 to 3 hours at the time observations were recorded. Ozone absorbs radiation mainly in the ultra-violet region, especially in the Hartley bands (2600 Å) but also absorbs weakly in both the visible and infrared spectra. However, the effectiveness of ozone as a radiator is not well known. Wexler [35] computed the diurnal variation of temperature in the ozone layer to be of the order of degrees

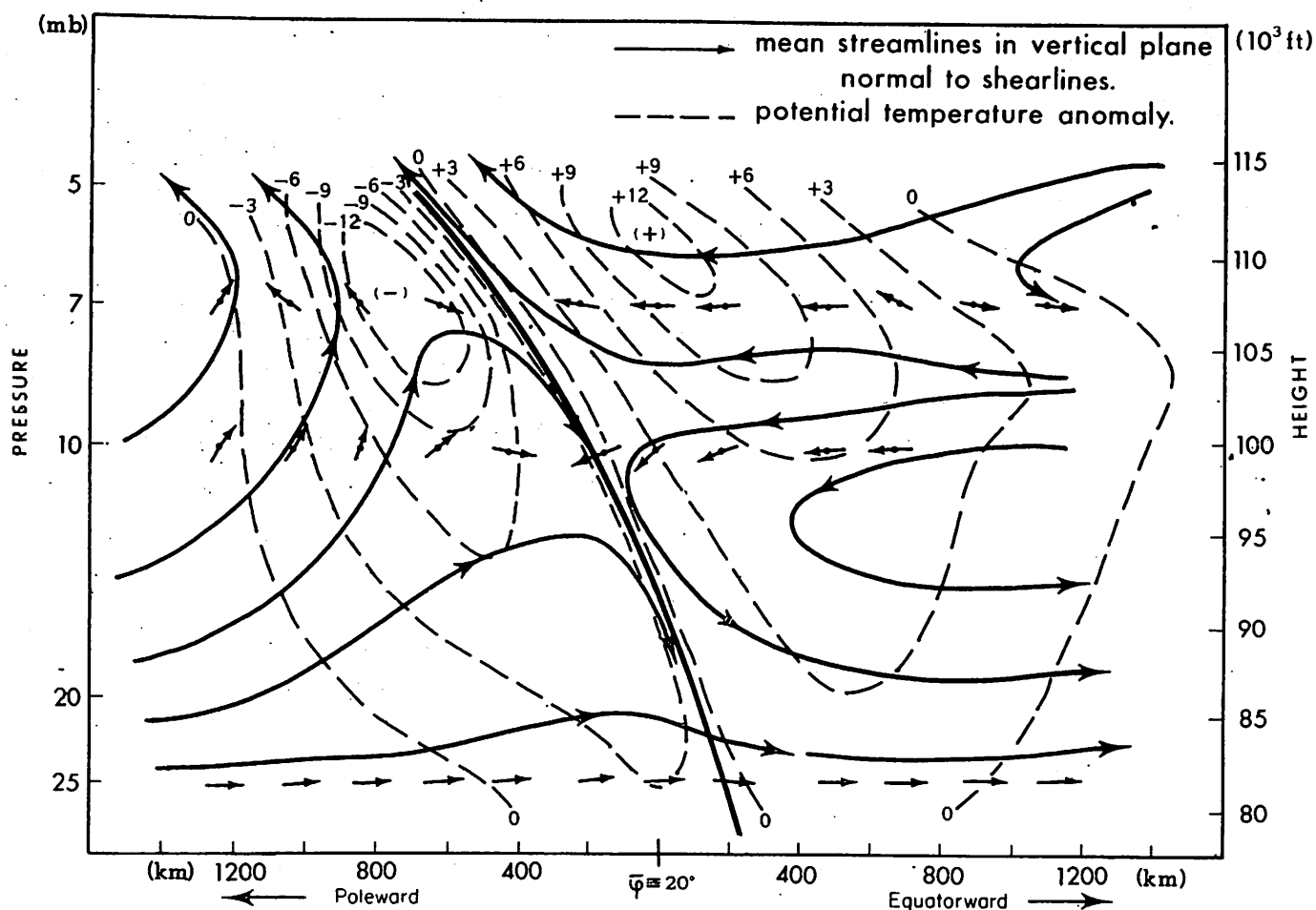


Figure 27. - Streamlines of mean circulation in a vertical plane normal to the shearing surface. The broken lines represent mean potential temperature anomalies ($^{\circ}\text{K}$).

per day which agrees with observations. Recently, new and direct means of studying the effect of radiation on temperatures in the ozone layer have been developed. Radiometersonde instruments, designed to measure net outgoing radiation, were used in the series of balloon soundings at some of the West Indies network stations in October and November 1960. The instrument used was one developed by Suomi and Kuhn [32]. In many instances the observations extended well into the ozone layer.

Table 2 shows the net radiation flux divergence in the layer 5 to 25 mb. at five West Indies stations obtained with these instruments during this period. In virtually every instance there is net cooling, the average of all observations for the period being + 0.012 langley's per minute per 10-mb. layer. At this rate the layer would cool approximately 3.5°C . in a 12-hour period. This agrees with the observed temperature changes between the morning and evening soundings at 10 mb. during January 1960. In applying these results it should be noted, however, that the radiometersondes had to be flown at 0000 GMT (about dusk) to avoid problems of separating out the effect of insolation,

Table 2. - Radiation flux divergence in the upper ozone layer (5-25 mb.).

Date (1960)	Langley's per minute (10-mb. layer)				
	Miami	San Juan	St. Maartin	Grand Cayman	Curaçao
Oct. 17	0.050		-0.005		
19	.013				
20	.015				
21			.022		
22	.001				
24					
27		0.017			
28		.033			
29		.009			
Nov. 1					0.001
5					.007
7				0.003	.007
10		.019			.010
11		.007			
12		.009			
15		.007			
16		.013			
18		.010			
20					.005
Station Average	0.020	0.014	0.009	0.003	0.006
Mean value: 0.012 langley's per minute per 10-mb. layer					

whereas the soundings used in the shear line analysis were made at 1200 GMT (near sunrise). Obviously there are important differences between radiative conditions at these two times of day. The radiometer sonde data were obtained when most of the observing stations had just experienced dusk, a time when the flux divergence from the ozone layer was probably near its maximum value. The shear line data, on the other hand, were obtained shortly after sunrise when the ozone layer might be expected to be as nearly in radiative equilibrium as any time during the 24-hour period. To the extent that the temperature distribution observed at 1200 GMT was a representative mean for the day, and radiative equilibrium prevailed most of the time, figure 27 is a useful expression of vertical circulations in the shear line system. However, during any period in which the layer cooled at the rate indicated in table 2 ($0.012 \text{ ly. min.}^{-1}$), a net downward component of almost 5 cm. sec.^{-1} would have been

superimposed upon the vertical motion otherwise computed. This is an order of magnitude greater than the largest w values in figure 27. Therefore, in view of the uncertain influence of radiation upon the system, it is possible that figure 27 may be useful mainly in delineating horizontal gradients of vertical motion.

Particle Dynamics

The foregoing discussion on the dynamics of the shear line system can be placed in perspective by considering the individual experience of a particle during its transit of the shear line system. Figure 28 presents two trajectories, one through the cold sector, the other through the warm sector at 10 mb. and shows graphically the changes which particles would encounter.

In the warm sector a particle would have required at least 4 days to cross the analyzed portion of the system, while one in the cold sector would have completed its transit in less than half that time. In the cold sector a particle moving at constant pressure would have encountered progressively colder temperatures the first 30 hours, then warmer conditions as it approached the shear line. Hence if the motion was adiabatic the particle first rose and cooled to conform with its new environs, then sank as it reached warmer air near the shear line. In this transit the vertical displacement would have been about 300 ft. In the warm sector, similarly, the particle would have sunk approximately 160 ft. Along these trajectories, acceleration of particles was due primarily to an imbalance between tangential pressure gradient forces and frictional stresses. If the sum of frictional forces is considered to be the residue, expressed as the difference between the observed acceleration and the tangential pressure gradient forces, the next to last set of panels in figure 28 shows this residue and its relation to the wind speed and pressure gradient forces. Since vertical shearing stresses apparently provided the major contribution to friction in this layer, the variation of $\partial^2 V / \partial z^2$ along each trajectory is also shown. Variations observed in shearing stresses follow the residue trace satisfactorily except near each starting point. It is astonishing to note that in both sectors there was continuous deceleration as particles moved toward lower pressure. In this layer, evidently, frictional forces were of the same general magnitude as pressure gradient forces along the trajectory. The panel on the upper right of figure 28 shows typical examples of the pronounced curvature of the vertical wind profile and its variation through the system. Such curvatures support the evidence that vertical stresses contribute substantially to particle acceleration.

Finally, along both these trajectories, the flow was in geostrophic balance only momentarily as a parcel moved from relatively large super-geostrophic to sub-geostrophic values and vice versa. Friction in the layer was sufficiently large and variable that geostrophic balance could not be maintained. Here again the evidence is that neither the frictionless equations of motion nor the geostrophic approximation is adequate to describe circulation in the lower mesosphere.

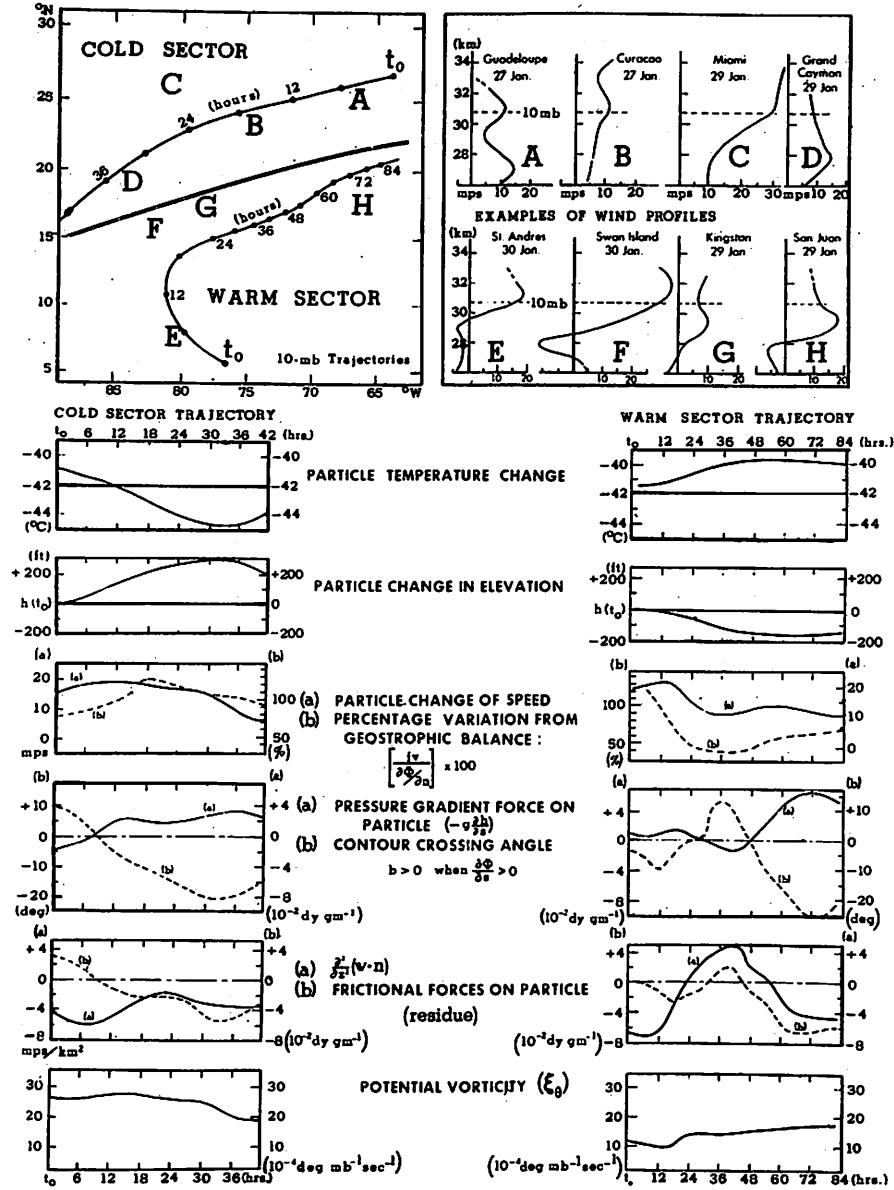


Figure 28. - The nature of motions and forces acting on particles which move through the shear line system.

Conservation of Potential Vorticity

The shear line system embodies a mechanism for concentrating vorticity, and affords an opportunity to compare the distributions of vorticity here with those commonly observed in the troposphere, and to consider whether potential vorticity is effectively conserved.

If motion can be assumed to be adiabatic, the potential vorticity may be expressed in the form

$$\xi_{\theta} = Q \frac{\partial \theta}{\partial p} \quad (16)$$

where ξ_{θ} is potential vorticity in $\text{deg. mb.}^{-1} \text{sec.}^{-1}$, and $Q \equiv f + \zeta$. Absolute vorticities were computed from circulations at 25, 10, and 7 mb. Because of the small horizontal range of temperature, there was little difference in slope of pressure and isentropic surfaces, and for all practical purposes re-

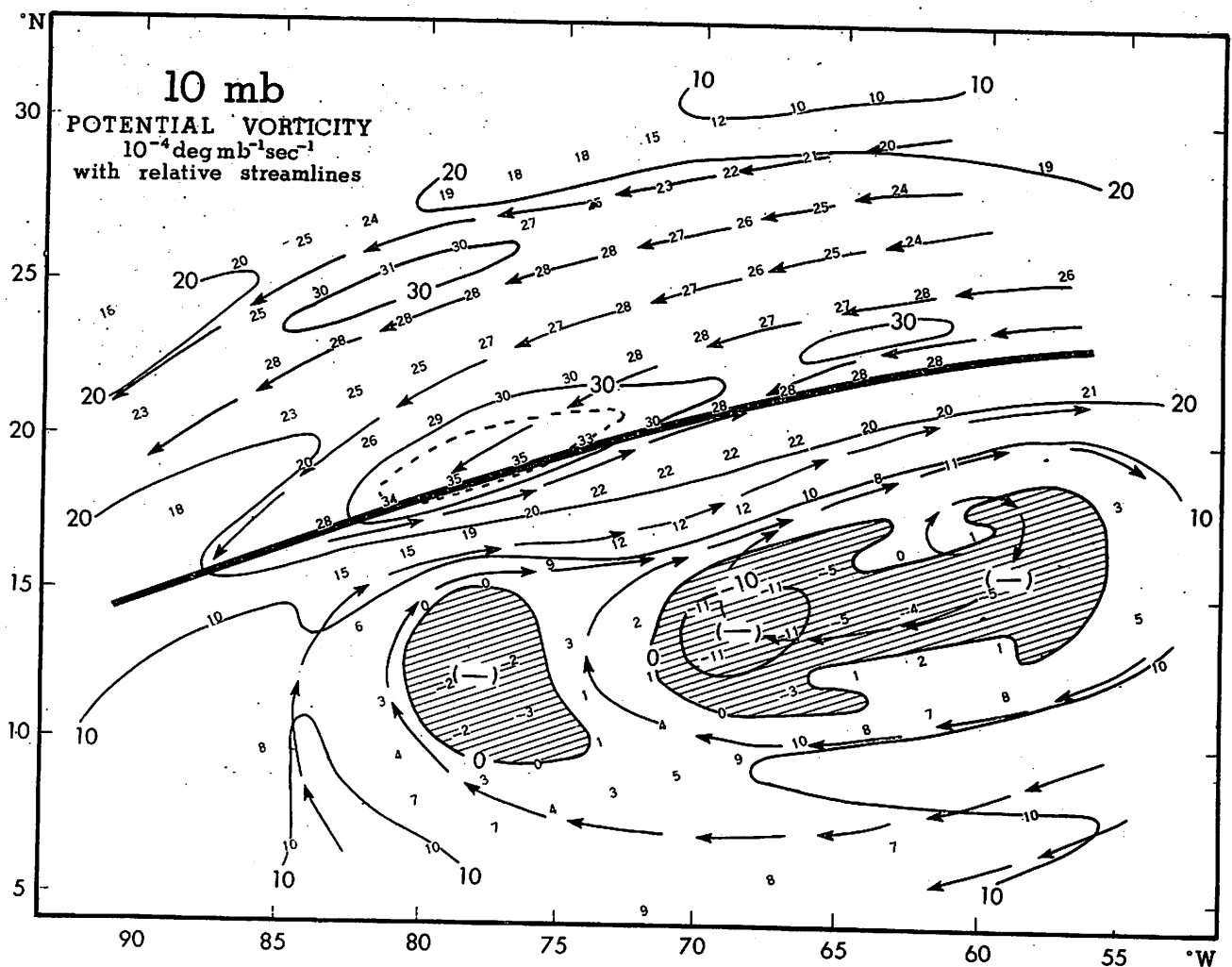


Figure 29. - Potential vorticity at 10 mb., January 29, 1960. Compare with the distribution in the n, z , plane (fig. 30). Relative streamlines imply that the potential vorticity of air parcels approaching the shear line is not well conserved, especially in the cold sector.

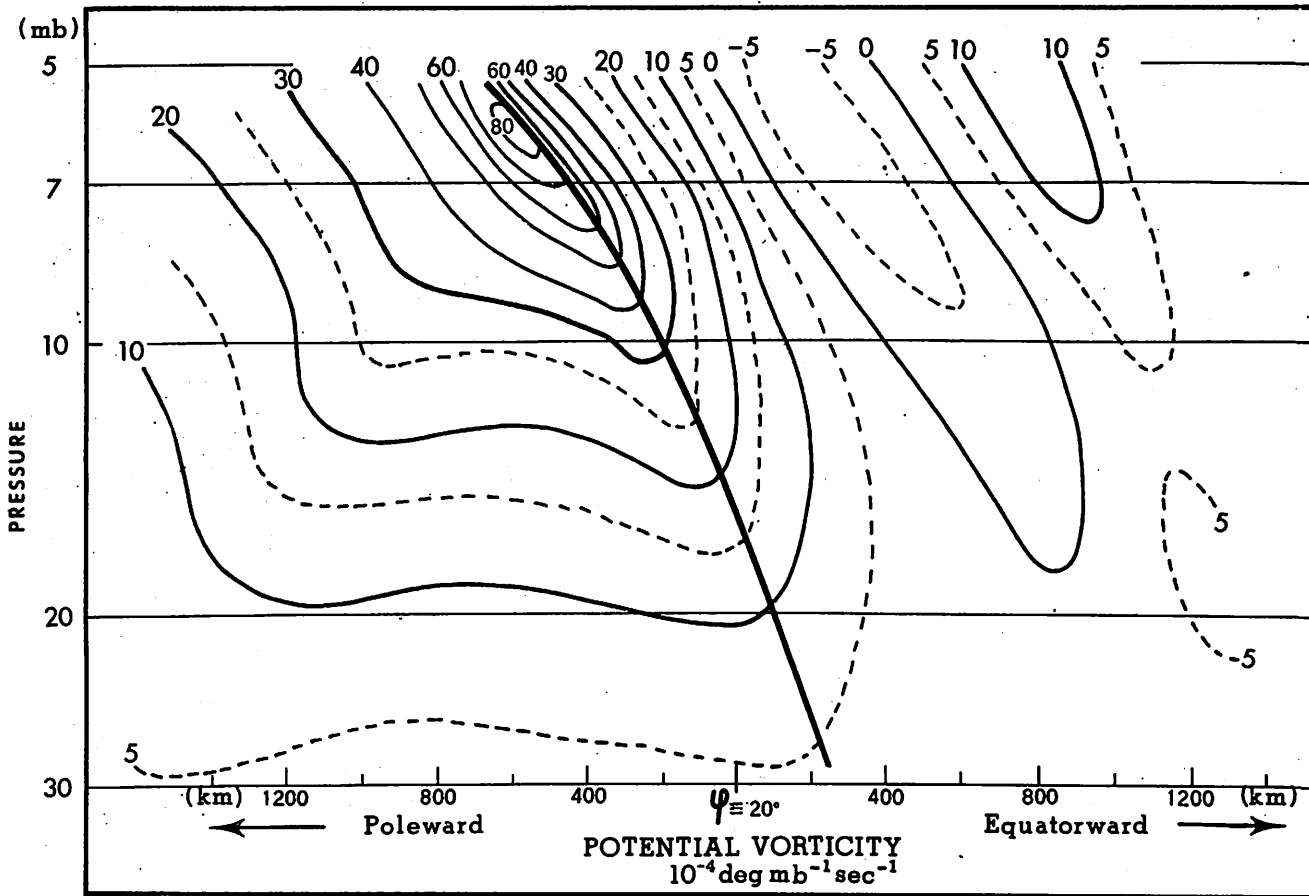


Figure 30. - Mean potential vorticity for the shear line system, shown in the n, z , plane. Compare with Fig. 29.

relative vorticity computed for one was equivalent to that of the other. The absolute vorticities computed for these surfaces were assumed to be representative for layers in which $\delta\theta \cong 200^\circ\text{K}$. This represented pressure differences ranging from less than 5 mb. in the top layer to about 16 mb. in the lowest layer. Because of the great stability of the meso-incline, there is generally less than 10 percent variation in $\partial\theta/\partial p$ values for the temperature range encountered. In sharp contrast to conditions in the troposphere, where no comparable stability exists, the distribution of potential vorticity is well approximated by that of absolute vorticity.

Figure 29 shows the distribution of potential vorticity at 10 mb., and figure 30 the mean vertical distribution in a plane normal to the shearing surface. The concentration of vorticity near the shearing surface compares favorably with that of the polar night jet stream reported by Krishnamurti [14], and is an order of magnitude greater than that of a well developed subtropical jet stream.

Figure 31 compares profiles of mean ξ_θ normal to the shear line at 7 mb. with a similar profile across a subtropical jet stream at 200 mb. The similarity is striking. However, in neither of these cases is it evident how the peak values were accumulated.

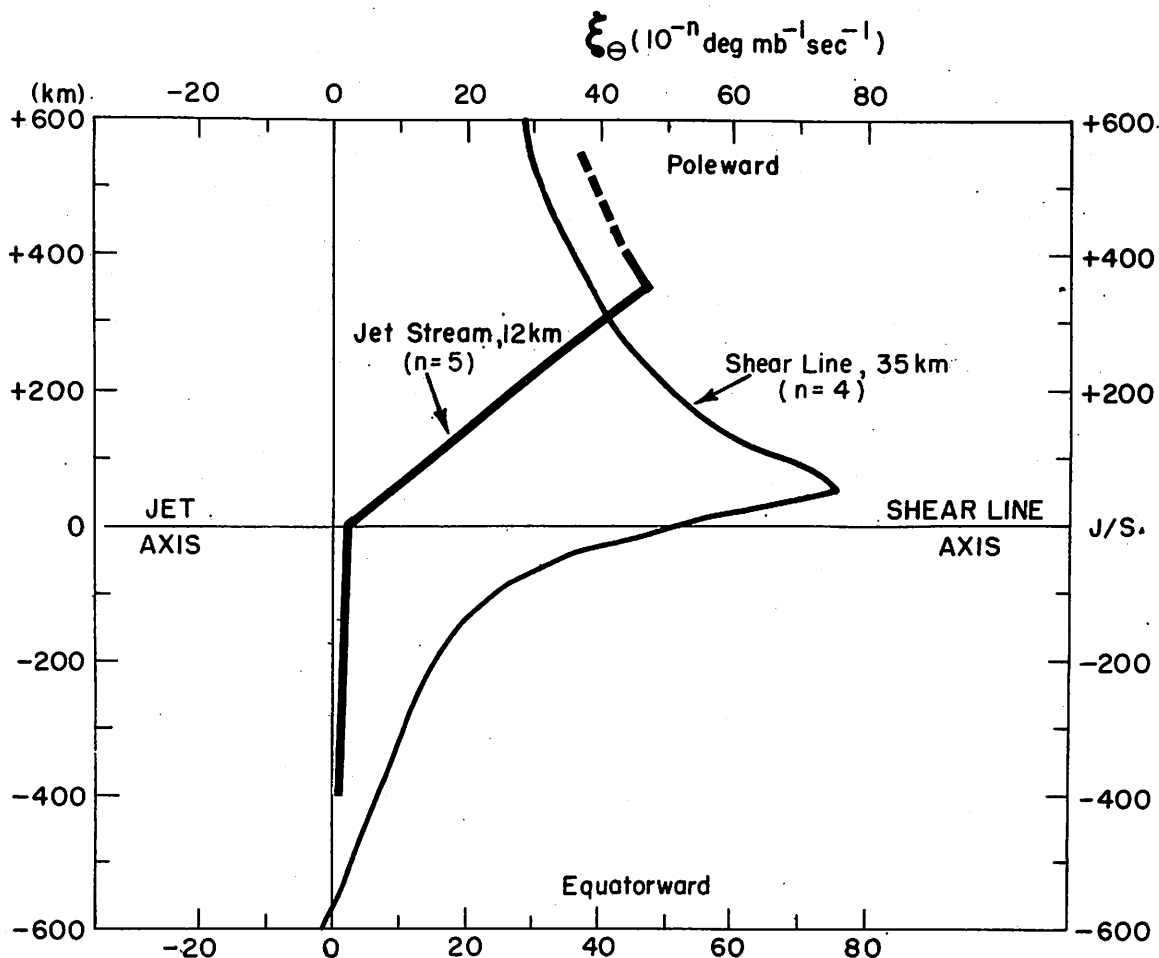


Figure 31. - Mean profiles of potential vorticity (1) normal to the shear line at the 7-mb. level, and (2) normal to a subtropical jet stream at the 200-mb. level. While the profiles are similar, the absolute values of ξ_{θ} for the jet stream are an order of magnitude less than those of the shear line.

Returning to figures 29 and 30, the area of negative potential vorticity is particularly interesting and curious. It appears at all three levels of analysis, and negative maximum values in the vertical plane occur along an axis which has the same slope as the shearing surface. If the negative values could be attributed to individual faulty wind observations, the negative maxima would have tended to be vertically aligned. Moreover, a careful re-examination of the analyses indicated that subjective elements in the analysis could not be reasonably adjusted to eliminate the negative values.

If these extreme values, both positive and negative, are acknowledged to be real then what can be said concerning processes which generate or aggregate such values and what conclusions can be reached regarding conservation of potential vorticity here? Figure 29 shows the relative streamlines for 10 mb. in relation to the patterns of ξ_{θ} . Since these streamlines represent mass circulation through the system, the constancy of ξ_{θ} values along a streamline

is a measure of how well potential vorticity is conserved. Clearly a parcel moving along these streamlines must experience appreciable change in potential vorticity especially as it approaches the shear line. Moreover, it is difficult to conceive that either of the remarkable peak values of ξ_θ could have developed through processes which conserve potential vorticity. Rather, they suggest that non-conservative factors may have been singularly important in the circulations of this system.

The possibility must therefore be considered that motion may not be adiabatic and that potential vorticity is generated or dissipated in situ either by eddy diffusion of heat downward through the stable meso-incline, by frictional torques, or by processes which cause tilting of the vortex tubes. In order to investigate the contribution due to eddy diffusion of heat, the expression for potential vorticity must be formulated differently. The equation of continuity may be expressed.

$$\frac{d}{dt} (\ln \rho) = - \nabla_H \cdot \mathbf{V} - \frac{\partial w}{\partial z} = - (\nabla_\theta \cdot \mathbf{V} - \nabla_\theta^z \cdot \frac{\partial \mathbf{V}}{\partial \theta} \frac{\partial \theta}{\partial z} + \frac{\partial w}{\partial \theta} \frac{\partial \theta}{\partial z}) \quad (17)$$

If we write

$$w = \left. \frac{dz}{dt} = \frac{\partial z}{\partial t} \right]_\theta + \mathbf{v}_\theta \cdot \nabla_\theta z + \dot{\theta} \frac{\partial z}{\partial \theta}$$

then differentiate with respect to θ .

$$\begin{aligned} \frac{\partial w}{\partial \theta} &= \frac{\partial}{\partial t} \left(\frac{\partial z}{\partial \theta} \right) + \frac{\partial \mathbf{v}_\theta}{\partial \theta} \cdot \nabla_\theta z + \mathbf{v}_\theta \cdot \nabla \frac{\partial z}{\partial \theta} + \frac{\partial \dot{\theta}}{\partial \theta} \frac{\partial z}{\partial \theta} + \dot{\theta} \frac{\partial}{\partial \theta} \frac{\partial z}{\partial \theta} \\ &= \left(\frac{\partial}{\partial t} + \mathbf{V} \cdot \nabla_\theta + \dot{\theta} \frac{\partial}{\partial \theta} \right) \frac{\partial z}{\partial \theta} + \frac{\partial \mathbf{v}_\theta}{\partial \theta} \cdot \nabla_\theta z + \frac{\partial \dot{\theta}}{\partial \theta} \left(\frac{\partial z}{\partial \theta} \right) \end{aligned} \quad (18)$$

Substituting for $\frac{\partial w}{\partial \theta}$ in (17)

$$\begin{aligned} \frac{d}{dt} (\ln \rho) &= - \nabla_\theta \cdot \mathbf{V} - \frac{\partial \dot{\theta}}{\partial \theta} - \frac{\partial \theta}{\partial z} \left(\frac{\partial}{\partial t} + \mathbf{V} \cdot \nabla_\theta + \dot{\theta} \frac{\partial}{\partial \theta} \right) \frac{\partial z}{\partial \theta} \\ &= - \left[\nabla_\theta \cdot \mathbf{V} + \frac{\partial \dot{\theta}}{\partial \theta} + \frac{d}{dt} \ln \frac{\partial z}{\partial \theta} \right] \end{aligned} \quad (19)$$

which may be rewritten

$$\frac{d}{dt} (\ln \rho \frac{\partial z}{\partial \theta}) = - \nabla_\theta \cdot \mathbf{V} - \frac{\partial \dot{\theta}}{\partial \theta} \quad (20)$$

Using the vorticity theorem in the form

$$\frac{d}{dt} (\ln Q) = - \nabla_\theta \cdot \mathbf{V} \quad (21)$$

then substituting for the divergence term in (20)

$$\frac{d}{dt} \left(\ln \rho \frac{\delta z}{\delta \theta} \right) = \frac{d}{dt} (\ln Q) - \frac{\partial \dot{\theta}}{\partial \theta} \quad (22)$$

and after substituting from the hydrostatic equation

$$\frac{d}{dt} \ln \left(Q g \frac{\partial \theta}{\partial p} \right) = \frac{\partial \dot{\theta}}{\partial \theta} \quad \text{or} \quad \frac{d}{dt} \ln \xi_{\theta} = \frac{\partial \dot{\theta}}{\partial \theta} \quad (23)$$

where $\xi_{\theta} \equiv Qg \frac{\partial \theta}{\partial p}$. If the term $\frac{\partial \dot{\theta}}{\partial \theta}$, known as the heating function, is neglected, (22) reverts immediately to (16) where the acceleration of gravity is generally considered constant and incorporated into the dimensions of ξ_{θ} . If, conversely, $\frac{\partial \dot{\theta}}{\partial \theta}$ may not be neglected, its role in circulations of the system may be considered as follows

$$\frac{\partial}{\partial \theta} \left(\frac{d\theta}{dt} \right) = \frac{\partial}{\partial \theta} \left(\frac{\partial \theta}{\partial t} + \mathbf{V} \cdot \nabla \theta + \omega \frac{\partial \theta}{\partial p} \right) \quad (24)$$

where pressure is the vertical coordinate and $\omega \equiv \frac{dp}{dt}$. For steady state, and for approximately horizontal θ surfaces

$$0 \cong \frac{\partial \theta}{\partial t} = \mathbf{V} \cdot \nabla \theta$$

so that (24) becomes

$$\frac{\partial}{\partial \theta} \left(\frac{d\theta}{dt} \right) = \frac{\partial}{\partial \theta} \left(\omega \frac{\partial \theta}{\partial p} \right) \quad (25)$$

Now (23) can be rewritten

$$\frac{d}{dt} (\ln \xi_{\theta}) = \frac{\partial}{\partial \theta} \left(\omega \frac{\partial \theta}{\partial p} \right) \quad (26)$$

Integrating

$$\delta (\ln \xi_{\theta})_{\Delta t} = \int_{t_1}^{t_2} \frac{\partial}{\partial \theta} \left(\omega \frac{\partial \theta}{\partial p} \right) \delta t$$

or

$$\frac{\xi_{\theta}(t_2) - \xi_{\theta}(t_1)}{\xi_{\theta}} = \int_{t_1}^{t_2} \frac{\partial}{\partial \theta} \left(\omega \frac{\partial \theta}{\partial p} \right) \delta t \quad (27)$$

This is the percentage change in potential vorticity of a parcel moving along a trajectory from time t_1 to t_2 . Mean values of $\omega \frac{\partial \theta}{\partial p}$ were computed at equal intervals from the shear line at 25, 10, and 7 mb. These were then plotted in a vertical cross section normal to the shearing surface with θ as the vertical coordinate. The result is shown in figure 32. The order of magnitude of $\frac{\partial}{\partial \theta} \left(\omega \frac{\partial \theta}{\partial p} \right)$ in the cross section is $10^{-6} \text{ sec.}^{-1}$, representing about 10 percent change in ξ_{θ} per day. Since air requires several days to move through the shear line system, the heating function may play an important role in the generation of extreme positive values of potential vorticity.

The heating function, however, cannot account for the negative maximum which appears on the equatorward side of the shear line. Negative potential vorticities are sometimes interpreted to be conserved properties of an air mass which has crossed the equator. However, such remarkable conservation as this over a period of 5 days or more is difficult to envisage, especially when potential vorticity is not conserved for as much as one day in the cold sector near the shear line.

Alternatively, the vorticity of parcels moving through the system may be altered by tilting of the vortex tubes. This would require a horizontal gradient of vertical motion. In the warm sector there is essentially no distinguishable pattern of vertical motion; hence, any contribution to vorticity change from the tilting effect would be negligible.

Finally, the contribution due to frictional torques needs to be considered. The change in relative vorticity due to viscous stresses is

$$\frac{d\zeta}{dt} = -\nu \nabla^2 \zeta \quad (28)$$

If one assumes a value for ν of $10^6 \text{ cm.}^2 \text{ sec.}^{-1}$, computations at 10 mb. show that the potential vorticity in the warm sector may be reduced by as much as 10^{-4} vorticity units per day. This is of sufficient magnitude to account for at least a part of the negative values observed.

Table 3. - Extreme values of potential and absolute vorticity in the shear line system.

Pressure Surface (mb.)	$Q \equiv f + \zeta_{max}$ $10^{-4} \text{ sec.}^{-1}$	$\xi_{\theta} = Q \frac{\partial \theta}{\partial p}$ $10^{-4} \text{ mb. deg.}^{-1} \text{ sec.}^{-1}$
7	1.8	76.0
10	1.0	34.0
25	0.2	6.4

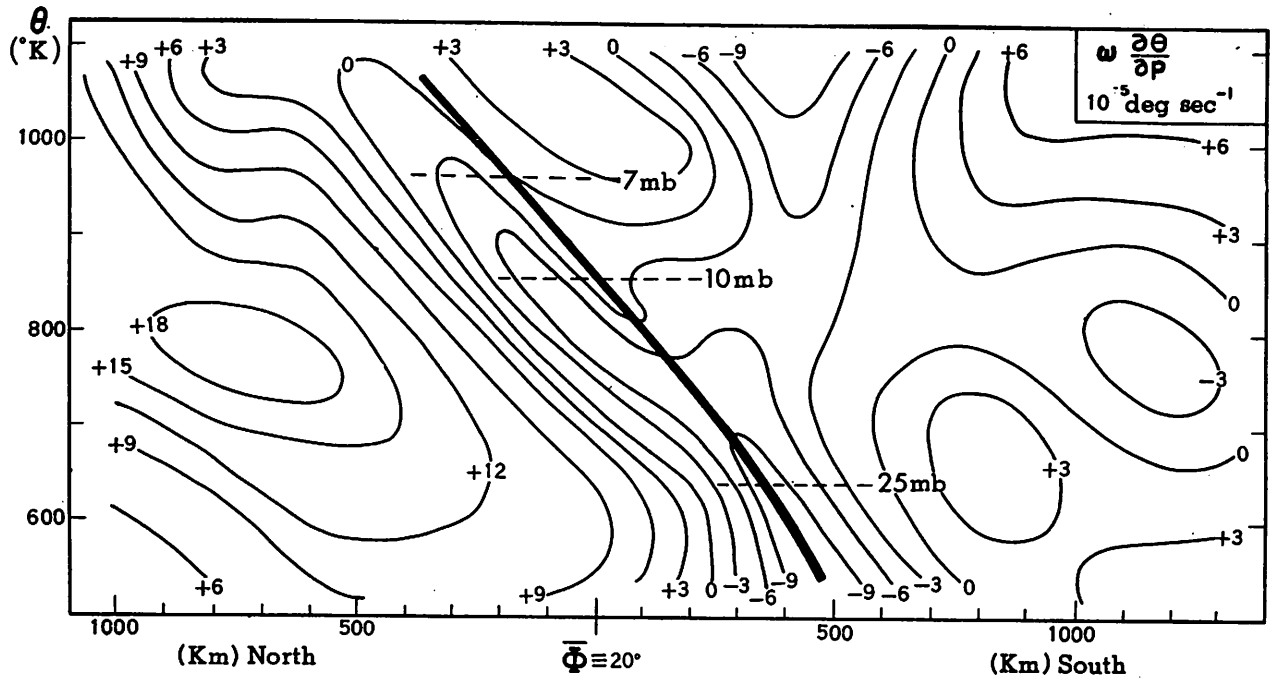


Figure 32. - Mean values of the heating function $\frac{\partial}{\partial \theta} (\omega \frac{\partial \theta}{\partial p})$ in a plane normal to the shearing surface. The distribution of this quantity determines percentage change in potential vorticity which air parcels may experience due to vertical diffusion of heat.

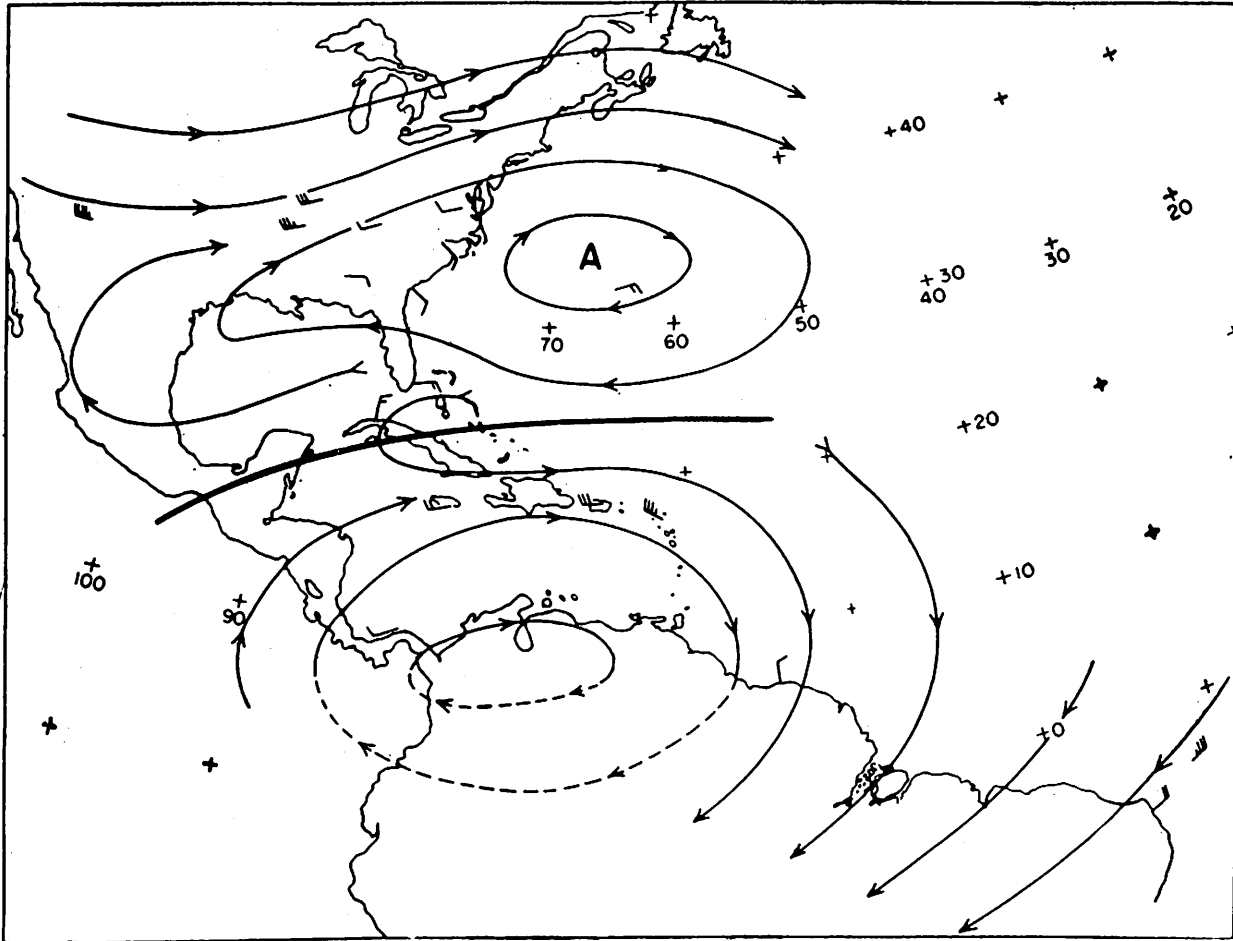


Figure 33. - An equatorial shear line of the troposphere, September 1945 (from [28]). Streamlines are for the 200-mb. surface.

Comparison With Equatorial Shear Lines of the Troposphere

Several references have been made to the similarity of the disturbance reported here to shear lines in the troposphere. Figure 33 is a good example of a troposphere shear line discussed by Riehl [28, 29].

In the West Indies area, shear lines such as that in figure 33 are relatively common. They slope poleward; there is prominent upward motion on the poleward side, and subsidence on the equatorward side. Also, they are similar to the mesosphere system in that air north of the shearing surface has negative temperature anomalies and that on the south positive anomalies. While the shear diminishes downward, and sometimes cannot be distinguished in surface circulations, the system carries distinct weather patterns with it. As mentioned earlier, extensive areas of cloudiness extend poleward from the shear line, and near the surface position winds are sometimes squally with heavy rain. South of the line the weather is fair and convection is suppressed.

Riehl points out that the energy for driving the system and for lifting

the air to produce negative temperature anomalies in the upper troposphere must come from some unspecified outside source. The shear lines are similar in this respect also.

Aside from these obvious resemblances, the dynamical and thermodynamical settings of the two shear lines are quite different. In the lower mesosphere the circulation is embedded in a deep temperature inversion which suppresses vertical motion, while in the upper troposphere the lapse rate is close to, and slightly less than, the moist adiabatic. In both systems vertical motion produces temperature changes which are in the same sense. However, a given amount of cooling requires an order of magnitude less vertical motion in the lower mesosphere than in the troposphere.

In the troposphere, surface friction enters as a prominent factor in circulation, whereas the system in the mesosphere has no comparable factor which enters uniformly. On the other hand, vertical shearing stresses in the troposphere exert relatively little influence on synoptic-scale circulations, the coefficient of eddy viscosity being generally less than $10^4 \text{ cm}^2 \text{ sec}^{-1}$. In the mesosphere, however, this coefficient appears to be nearly two orders of magnitude greater, as discussed. Moreover, in a disturbance involving a sloping surface such as the shear line, the curvature of the wind speed profile in the vertical is not only pronounced but varies with distance from the shearing surface. Hence, while friction may play a significant role and the motion may be accelerative in both cases, its importance is appreciably greater in the mesosphere.

Finally, circulation in the lower mesosphere is essentially non-divergent, whereas in the troposphere the deep and varying layers of convection, together with other non-conservative influences, impose a prominent divergent component of motion.

CHAPTER 5. RELEASE OF ENERGY

Figure 27 provides a qualitative means of estimating the release of potential energy in the shear line system. However, more quantitative information concerning the release of energy in this system is needed, first to learn whether the primary source of energy is within the system itself, or is imported from the environment. Secondly, in view of the large coefficient of eddy viscosity obtained in earlier computations, it will be useful to compute the dissipation of kinetic energy as a residue from the algebraic difference between the net generation of kinetic energy in the volume and its boundaries, and the net export to the environment.

For purposes of computation the shear line system will have boundaries defined in figure 34 and will include the layer 25 to 5 mb. The change in kinetic energy of this system may be expressed

$$\frac{\delta}{\delta t} \int_V K dV = - \int_V \mathbf{V}_s \cdot \nabla_H p \delta V - \int_s \rho \frac{v_s^2}{2} v_{nr} \delta s \delta z + \int_V \mathbf{V}_s \cdot \frac{\partial \tau}{\partial z} \delta V \quad (29)$$

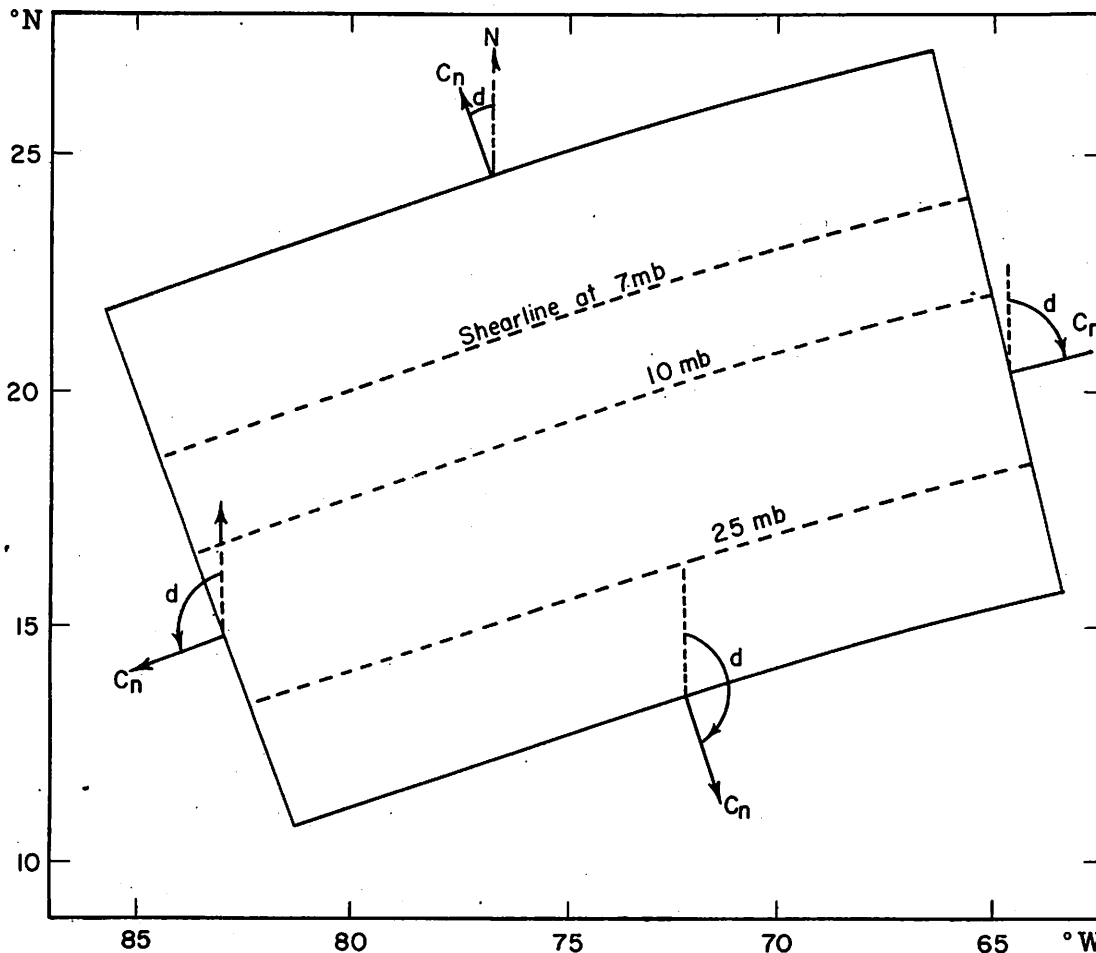


Figure 34. - Portion of the shear line system used in kinetic energy computations.

where v_{nr} is the component of relative wind normal to the boundaries (positive outward), \mathbf{V}_s is the vector wind, and τ is the shearing stress at some height z . The first term on the right represents the work done by pressure forces of the system, the second the export of kinetic energy to the environment, and the third the net contribution of frictional stresses in reducing kinetic energy. The first term may be expressed as the sum of kinetic energy production by pressure forces within the volume and by normal pressure at the boundary. While these two ordinarily are computed individually, this computation has been made in one step here since point values of pressure gradient and of wind in the interior were considered more reliable than the boundary values. Similarly the third term on the right, ordinarily expressed as the sum of frictional dissipation inside the volume and of the energy transferred by tangential stresses at the boundary, has been treated here as the net reduction of kinetic energy in the system due to viscous stresses. For a steady circulation (29) may be restated

$$[\text{net generation}] - [\text{export}] - \int_V \mathbf{V}_s \cdot \nabla p \delta V - \int_s \rho K \mathbf{V}_r \cdot \mathbf{n} \delta s \delta z = D \quad (30)$$

where D is the net reduction of kinetic energy by frictional forces, \mathbf{V}_s and \mathbf{V}_r are three-dimensional winds, \mathbf{V}_r being the wind relative to the moving system, and \mathbf{n} a unit vector normal to the boundaries, positive outward. If (30) is expressed as the sum of contributions from the symmetrical and asymmetrical parts (sometimes referred to as mean and eddy components) of the circulation, and Cartesian wind components v_n and v_s , normal and parallel to the shear line, are used, (30) becomes

$$D = -A \int_{p=5}^{p=25} \left[\bar{v}_s \left(\frac{\partial z}{\partial s} \frac{p}{\delta s} \right) + \bar{v}_n \left(\frac{\partial z}{\partial n} \frac{p}{\delta n} \right) \right] \delta p - A \int_{p=5}^{p=25} \left[v'_s \left(\frac{\partial z}{\partial s} \frac{p}{\delta s} \right)' + v'_n \left(\frac{\partial z}{\partial n} \frac{p}{\delta n} \right)' \right] \delta p - \frac{s}{g} \int_{p=5}^{p=25} \bar{K}_s \bar{v}_{nr} \delta p$$

(a) (b) (c)

$$- \frac{s}{g} \int_{p=5}^{p=25} \bar{K}'_s v'_{nr} \delta p - \frac{1}{g} \int (\bar{K}'_b \bar{\omega}'_b - \bar{K}'_t \bar{\omega}'_t) \delta A - \frac{1}{g} \int (\bar{K}'_b \bar{\omega}'_b - \bar{K}'_t \bar{\omega}'_t) \delta A \quad (31)$$

(d) (e) (f)

Here A is the horizontal area of the system, δs and δn are elements parallel and normal to the shear line, positive in the direction of increasing longitude and latitude, respectively, and subscripts b and t refer to base and top of the volume. Each term of (31) can be computed from the basic analyses, although the third term on the right cannot be adjusted for mass balance and is therefore less meaningful than the other terms. Since vertical transport of kinetic energy is relatively large at 7 mb., the computation was made for an upper boundary at 5 mb. rather than carrying the integration through the layer 30 to 0 mb. as before.

Table 4. - Kinetic energy statement for the shear line volume in 10^7 ergs sec.⁻¹. Here P represents net generation; E export through the vertical boundaries; e export through the base and top of the layer; and D net loss due to viscous stresses. The bar and prime quantities represent the contributions from the symmetrical and asymmetrical parts of the circulation respectively.

layer/level (mb.)	$\int_V \bar{P} \delta V$	$\int_V P' \delta V$	$\int_S \bar{E} \delta s$	$\int_S E' \delta s$	$\int_S \bar{e}_b \delta s$	$\int_S e'_b \delta s$	D (residue)
10-5	+56	+33	-6	+4	-0.24	-0.69	92
15-10	+50	-1	-20	+3	-0.14	+0.06	66
20-15	+33	-7	-12	+1	-0.06	+0.18	38
25-20	+20	-10	-5	-4	-0.02	+0.21	19
25-5	+159	+15	-43	+4	-0.46	-0.24	215

Table 4 shows the results of these computations. Here we are confronted with the astonishing fact that large net generation of kinetic energy within the volume was accompanied by net import of kinetic energy through the boundaries! If this result is valid, a very large reduction in kinetic energy by turbulent eddies was required to maintain a steady state. It is interesting to note that if the kinetic energy lost had gone entirely into heating the volume, it would have raised the temperature approximately 0.25°C. per day. Of greater importance, however, is the magnitude of the viscosity coefficient required for such dissipation. The last term of (29) may be rewritten

$$\nu A \int_V \cdot \frac{\partial^2 V}{\partial z^2} \frac{\delta p}{g} \quad (32)$$

where A is the horizontal area of the system. From examination of individual soundings, values of $V \cdot \frac{\partial^2 V}{\partial z^2}$ at 10 mb. were found to lie in the range (-5 to -90) $\times 10^{-6}$ sec.⁻². If a mean value is used and equation (32) is equated to the computed residue in table 4, ν turns out to be of the order 10^6 cm.² sec.⁻¹, which is consistent with values of ν computed in the preceding sections.

Both the production and export of kinetic energy are supported primarily by the mean terms, or symmetric parts of the circulation, net contributions from the asymmetric parts being nearly an order of magnitude smaller. While the export terms have not been adjusted for mass balance, it is evident by inspection that this term has the correct sign in table 4 and must be comparatively large. Evidently kinetic energy is not transported in important amounts through the horizontal boundaries of the system. Finally, while the generation mean term is positive throughout and increases with height, the asymmetric

part of the circulation contributes to generation only in the layer above 10 mb. In the deep layer below, it acts to reduce kinetic energy.

From these computations the shear line emerges as a disturbance which draws its energy primarily from the mass circulation through the system, but because its circulations comprise a voracious sink of kinetic energy, it must depend upon imports from the environment to maintain the level of circulation energy.

CHAPTER 6. TRANSPORT OF HEAT

If the shear line plays a significant role in circulations and in heat balance of the stratosphere, it is because of diffusion of matter or the transport of heat and of momentum poleward. To investigate this it is useful to hypothesize that the West Indies shear line is simply one section or component of a system which encircles the hemisphere, all of which participates in these transports. Due to shortage of data elsewhere there is no objective way to determine whether other regions participate in poleward surges of this kind. However, there is less reason to suspect that this shear line is unique to the West Indies than to regard it as part of a hemispheric system. Moreover, data sequences for the same period from Hawaii and other Pacific island stations examined by the present author show evidence of variations in wind and temperature similar to those of the West Indies.

In any event, the computations which follow are intended to serve mainly as a means of estimating the potential contribution of a hemispheric system of shear lines transporting heat and momentum poleward.

If the heat content of air per unit mass is

$$H = c_p T + gz + Lq \quad (33)$$

the flux of heat from the volume designated in figure 34 is represented by

$$- \frac{1}{g} \int_s H c_n \delta s \delta p$$

where c_n is an exterior normal to the boundary. Now if α is the angle between a poleward unit vector and c_n , where $0^\circ < \alpha < 180^\circ$, then poleward transport of heat from the system is given by

$$\mathcal{F}(H)_p = - \frac{1}{g} \int_s H c_n \cos \alpha \delta s \delta p \quad (34)$$

If this is expressed as the sum of transports by the symmetric and asymmetric parts (mean and eddy components) of the circulation, (34) becomes

$$\mathcal{F}(H)_p = - \frac{1}{g} \int_s \overline{H c_n \cos \alpha} \delta s \delta p - \frac{1}{g} \int_s \overline{H' (c_n \cos \alpha)'} \delta s \delta p \quad (35)$$

The value of the first term on the right depends upon circulation adjustments to satisfy mass balance. Since this could not be accomplished in this case, the computation will be confined to the second term, the transport by the asymmetric part of the circulation. The integration carried out for the layer 30 to 0 mb. and the area indicated in figure 34 gives the results in table 5.

Table 5. - Poleward transport of heat by the shear line in the layer 30 to 0 mb. The single system involves the area indicated in figure 34. This envisages a family of shear lines girdling the earth, each participating in transports equivalent to that of the single system.

Layer (mb.)	$\mathcal{F}(H)_p = -\frac{1}{g} \int_s \overline{H'(c_n \cos \alpha)'} \delta s \delta p$	
	single system	global system
10-0	3.5 ($\times 10^9$ kj. sec. ⁻¹)	35.0 ($\times 10^9$ kj. sec. ⁻¹)
20-10	1.55 "	15.5 "
30-20	-0.30 "	-3.0 "
30-0	4.75 ($\times 10^9$ kj. sec. ⁻¹)	47.5 ($\times 10^9$ kj. sec. ⁻¹)

If the hemispheric system comprises a family of shear lines each with transports equivalent to that of the single system, the total heat available for warming the polar cap would amount to about 4.8×10^{10} kj. sec.⁻¹. If it is assumed further that the heat is distributed uniformly over the area north of 60°N. and in the layer 30 to 0 mb., the temperature there would increase 0.4°C. per day, other factors equal. This is about half the rate at which that sector should be expected to cool by radiation (e. g. Ohring [21]).

It is possible that the choice of boundaries for the computation of heat flux may have been poor. In order to examine this, a computation was made of eddy transport across a series of lines parallel to the shear line. This transport (poleward) is given by

$$\mathcal{F}(H)_p^* = -\frac{1}{g} \int_s \overline{H'(c_n^* \cos \alpha)'} \delta s \delta p \quad (36)$$

where c_n^* is the poleward component normal to the line and α the angle between c_n^* and its meridian. Figure 35 shows the resulting profile. The continuous profile here was obtained from computations of transport by the asymmetric circulation across each of nine lines, parallel to the shear line, distributed uniformly on the poleward and equatorward sides at the 10-mb. surface. Since this represents the integrated transport through the layer 30 to 0 mb., the position of the shear line at 7, 10, and 25 mb. has been inserted for reference purposes. The distances poleward and equatorward along the profile are with reference to the position of the shear line at 10 mb. Maximum transports occurred at some distance to either side of the shearing surface.

These computations show that the asymmetric circulations transport significant but not spectacular amounts of heat poleward. If the system indeed

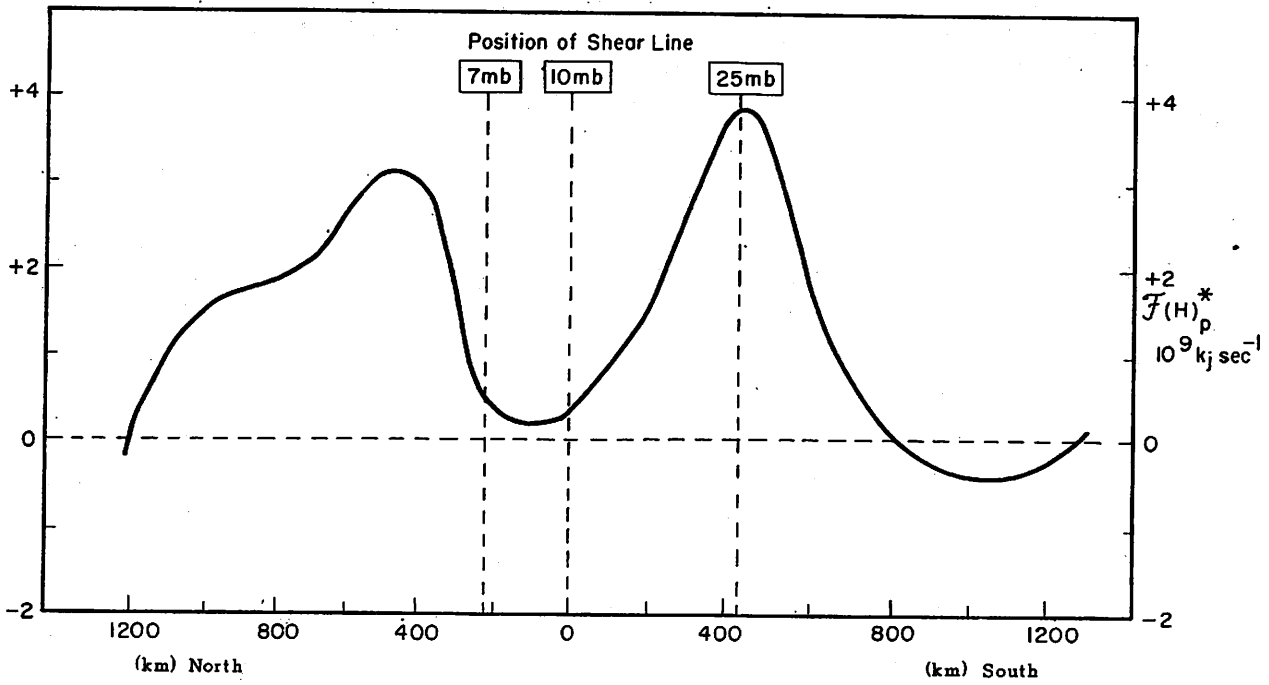


Figure 35. - Poleward transport of heat by the shear line system along an n, z plane.

girdles the hemisphere and frequently transports such quantities of heat to the polar cap, the system may play a significant role in the heat budget of the stratosphere and the lower mesosphere. However, the extent of such contributions must await more copious information from other regions and for other times of the year.

CHAPTER 7. TRANSPORT OF ANGULAR MOMENTUM

The absolute angular momentum of a ring of air at latitude θ , with mass m , is

$$M = [ua \cos \theta + (a^2 \cos^2 \theta) \Omega] m \quad (37)$$

and the poleward transport is

$$\bar{M}\bar{v} = (\bar{u}\bar{v} \cos \theta + a^2 \Omega \bar{v} \cos^2 \theta) m \quad (38)$$

where u and v are again the zonal and meridional wind components respectively. Here the mass m may be specified as

$$m = 2\pi a \cos \theta \cdot \bar{\rho} \delta z$$

Transport of Relative Angular Momentum

Since the data sample does not permit an assessment of transports beyond the West Indies, this computation must confine itself to the relative momentum and to transports by the asymmetric part of the circulation. It is probably realistic to consider that half of the ring transports relative angular momentum in the manner of the regional system. If we designate this participation by the coefficient $\mu \equiv 0.5$, the net poleward transport of relative angular momentum across a latitude circle θ by asymmetric circulations is

$$\mathcal{F}(M)_{\text{asym.}} = 2\pi\mu \frac{a^2}{g} \int_{p_2}^{p_1} \overline{u'v'} \cos^2 \theta \delta p \quad (39)$$

Figure 36(a) shows the area for which the computations of momentum were made and the data points used. The position of the 10-mb. shear line is also indicated on the diagram. Integration was carried out through the layer 30 to 0 mb. and along individual latitude circles at 2-degree intervals. The results indicate that the magnitude of poleward transport for a hemispheric system (where $\mu \equiv 0.5$) was of the order of 10^{24} gm. cm.² sec.⁻². The variation of this transport across the system is shown in figure 36(b). The maximum transport coincided with the most active portion of the shearing surface (30-34 km.), but a secondary maximum appeared in the southern portion of the warm sector where winds had turned back to easterly again.

The magnitude of this transport is substantial if the system does extend around the hemisphere. By comparison, Krishnamurti [15] in studying the subtropical jet stream of winter found values of 15×10^{25} gm. cm.² sec.⁻² associated with standing wave patterns. His integration was carried out for a total mass approximately 30 times that used in the present computation. It is not unreasonable, therefore, to conjecture that the shear line system may

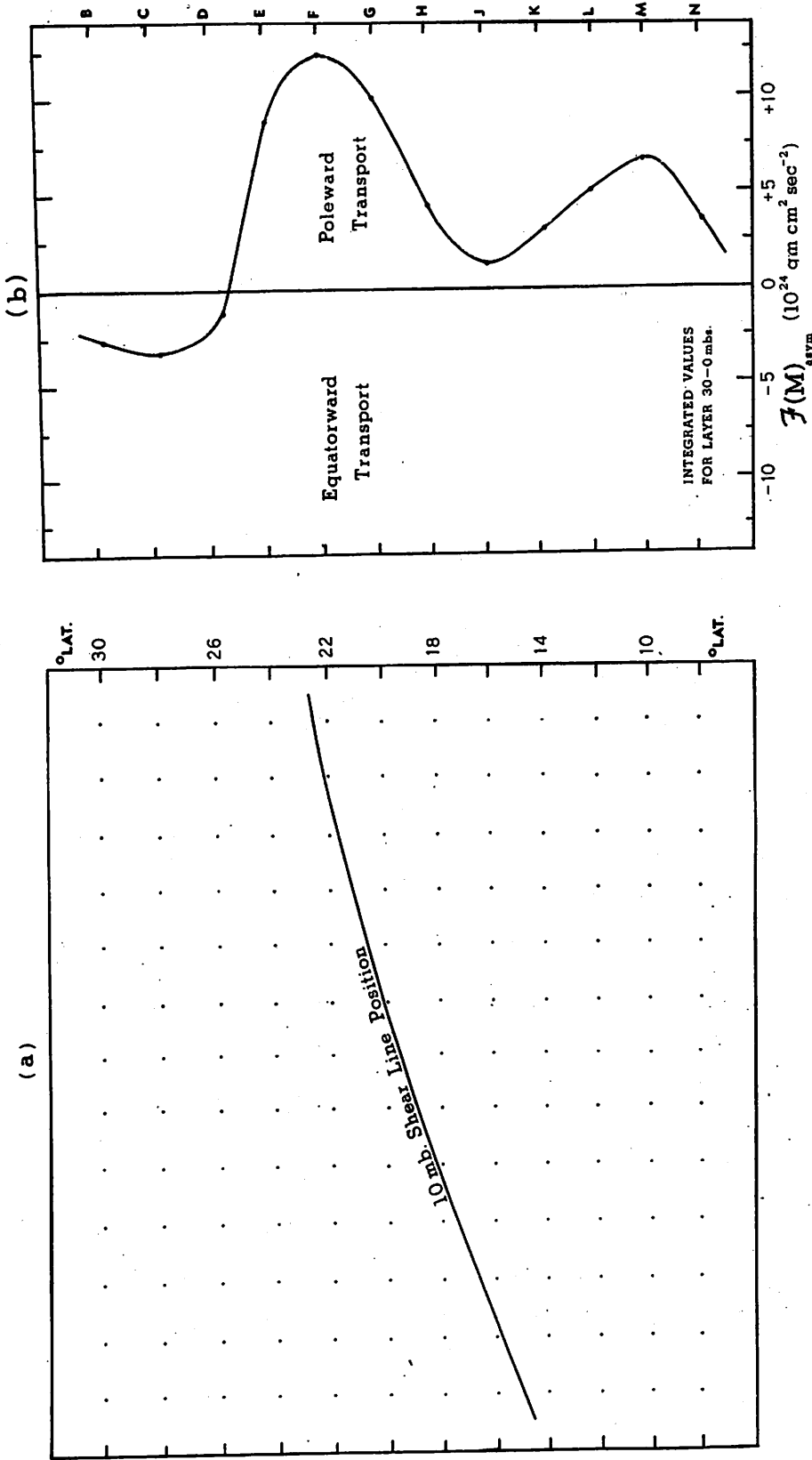


Figure 36. - Poleward transport of angular momentum by the shear line system.

contribute materially to regional development of the polar night jet stream or other vigorous westerly circulations of winter in the lower mesosphere. Lacking information from other meridians, or some means of assessing transports due to the symmetric part of the circulation, conclusions about the net influence of the system on circulations at higher latitudes must necessarily be limited.

CHAPTER 8. SUMMARY AND CONCLUSIONS

The high-altitude sounding data from the West Indies during 1960 have provided a number of unique or initial opportunities. To begin with, they provided the means of identifying the existence of a unique synoptic-scale disturbance with steady, vigorous circulations in an area where neither theory nor previous observational evidence had suspected its existence. But more important, they provided an opportunity to examine the structure and dynamical character of a disturbance imbedded in a deep layer of pronounced thermal stability, and to compare these characteristics with those of disturbances in the troposphere where the constraints of thermal stability are small or absent.

The West Indies shear line displayed the kinematical and thermodynamical properties of a warm frontal system as it moved steadily poleward with a speed of 12 kt. The mean temperatures during the 20-day period investigated, increased poleward across the West Indies. However, the intrusion of the shear line from the south was accompanied by a reversal of the temperature gradient.

This disturbance in the lower mesosphere has a counterpart in the troposphere in the form of the equatorial shear line. While the similarities between the two disturbances are striking, the two important questions are, first, What is the generating source and is it the same for both? secondly, Are there important differences in the laws which govern circulations in a stable layer and those in unstable media? This study has not shed light on the first question but has illucidated the latter.

By compositing the mesosphere data obtained during the Skyhook 60 operation, it was possible to construct detailed analyses of the high-altitude shear line from which much quantitative information has been derived. Conclusions based upon this information, however, must consider first the reliability of the data and the extent to which subjectivity may have biased the results. In the present case it was possible to develop the contour and isotherm patterns at successive levels in the mesosphere with greater objectivity and skill than might ordinarily be possible. This was due to the fact that the disturbance had pronounced gradients of temperature and wind and maintained a relatively steady circulation while crossing the observing network. One of the strongest evidences of this, and justification for confidence in the analyses, lies in the fact that the compositing process did not materially change the gradients or diffuse the patterns of daily analyses.

Nevertheless, subjective decisions and judgment in the analysis obviously entered in various ways which could influence some of the results. Perhaps the greatest uncertainty is in the contour heights. Because of day-to-day continuity of temperature patterns, however, the uncertainty in this case is considered to be mainly one of gradient and not of pattern. This would influence the computation of frictional stresses, of kinetic energy generation, and the geostrophic deviations. However, it should not change the order of magnitude or the sign of the first two. The weakest link in the chain of computations is that of vertical motion. However, the weakness here lies not in the data or analyses but rather in the fact that computed values, using the adiabatic assumption, are in millimeters per second whereas values

which could result from radiation flux divergence in the system are an order of magnitude larger. Computed values depend mainly upon 12-hour relative trajectories and the isotherm pattern. Within limitations of the analyses these should provide a reliable pattern of vertical motions. However, absolute values might vary by a factor of 2 due to the subjectivity of analysis.

Ultimately, the principal reason for confidence in the analyses is the internal consistency of computational results, especially as regards values of the eddy viscosity coefficient derived independently from computations of kinetic energy, balance of forces, and potential vorticity.

Despite the constraints imposed by thermal stability, the evidence is that horizontal motions were mainly accelerative. Geostrophic balance appeared only momentarily as a parcel moved alternately from sub-geostrophic to super-geostrophic speeds. Evidently this was due to frictional forces much larger than have previously been considered applicable to the lower mesosphere. Computations indicate that the coefficient of eddy viscosity for vertical stresses averages $7.0 \times 10^5 \text{ cm}^2 \text{ sec}^{-1}$, more than two orders of magnitude greater than found by Feely and Spar in studying the meridional transport of debris from nuclear explosions. In the shear line, frictional forces were found to be of the same order of magnitude as tangential pressure gradient forces. In some areas mass points experienced continuous deceleration while moving toward lower pressure. Also, a requirement for substantial dissipation of kinetic energy in the system was noted in connection with a large production of kinetic energy within the system without net export to the environment.

The difference in eddy coefficient values computed in this study and those obtained by Feely and Spar [10] is puzzling and deserves further investigation. Two possible reasons for these conflicting results might be considered. First, in the shear line investigation the influence of horizontal stresses was not considered. In view of the large horizontal coefficients found by Feely and Spar, there may have been some contribution from this source which in combination with the vertical stresses could have influenced the computation of ν for the vertical stresses. On the other hand, however, the computations of Feely and Spar were based upon the observed movement of ionized materials. The movement of ions in air is subject not only to the transport and diffusive properties of air but also to the electrostatic and magnetic fields through which the ions are transported. It has been suggested,¹ therefore, that the results of Feely and Spar may have been influenced by extraneous systematic body forces acting on the ionized material.

The shear line system not only maintains a substantial deformation in the flow, but also generates peak values of potential vorticity which apparently cannot be explained by advection. It has been shown that the so-called heating function $\frac{\partial}{\partial \theta} (\omega \frac{\partial \theta}{\partial p})$, a term ordinarily omitted in formulations of potential vorticity, has an interesting distribution in the shear line system, and may account for potential vorticity variations of as much as 10 to 20 percent per day in the cold sector. While this may assist in generation of maximum (positive) values near the shear line, it cannot account for the area of negative

¹Private communication from Mr. D. Lee Harris, Washington, D. C. April 1962.

values in the warm sector. Moreover, the negative values apparently are not associated with a tilting of the vortex tubes, since horizontal gradients of vertical motion are minimal in the warm sector. However, the evidence suggests that frictional torques are present which are capable of reversing the sign of the potential vorticity for parcels moving through some portions of the warm sector.

Computations of kinetic energy indicate that the circulations of the disturbance are primarily sustained by the action of pressure forces on the mass circulation in the system. If the circulation remains steady then there must be a continuous source replenishing the potential energy converted to drive the circulation. Since systematic sinking apparently occurs along the shearing surface, it is suggested that this disturbance is a device for transporting ozone downward through the meso-incline to the ozone center of mass (about 25 km.). The collection and storage of ozone in this manner would protect it from destruction by ultraviolet radiation, while it absorbs radiation of longer wavelength, thus warming the system and replenishing the supply of potential energy tapped in driving the circulation.

The significance of heat and momentum transport by the shear line on the general circulation has been difficult to evaluate since so little is known as to whether its influence is hemispheric in scope or only regional. Also it has been possible to consider only these transports due to the asymmetric part of circulations. No evidence was found that the shear line is capable of producing spectacular or sudden changes of temperature in the polar stratosphere. However, if the transport of the individual system were continuous around the hemisphere, it could warm the polar cap at the rate of about 0.5°C . per day. This suggests that if such disturbances develop at frequent intervals and migrate steadily poleward, they may cause periodic warming sufficient to account for the bimodal distributions of temperature in the winter stratosphere reported by McClain [19].

The poleward transport of angular momentum by asymmetric circulations was impressive, in fact sufficient to support or to intensify such regional features of winter circulations as the polar night jet stream.

The results of computations presented here do not answer directly the fundamental questions about general circulation and the distribution of ozone discussed in chapter 1. However, they do provide useful information about sources of instability which may have a significant bearing on the general circulation. If, for example, one uses the coefficient of eddy viscosity computed for the shear line system and assumes a mixing length and wind speed of 20 km. and 20 m.p.s. respectively, the Reynolds number for the lower mesosphere turns out to be about 6×10^3 . This value is two to three orders of magnitude less than characteristic values for the troposphere. Viscous stresses in the mesosphere, therefore, may serve as a source of instability in large-scale vigorous circulations, and indeed may have been a factor in the formation of the West Indies shear line.

In any event, the importance of extending investigations of the kind to other low-latitude regions, and of seeking means to obtain sounding data to higher altitudes regularly has been demonstrated.

ACKNOWLEDGMENTS

The author is indebted to Professors Herbert Riehl and Sverre Petterssen for encouragement, counsel, and for stimulating discussion throughout the course of the research; also to Mrs. Helene S. Mayes and Messrs. R. D. Decker and Merlin Ahrens who provided secretarial and other assistance in assembling the manuscript and the diagrams.

REFERENCES

1. J. K. Angell, "Use of Constant Level Balloons in Meteorology," Advances in Geophysics, vol. 8, Academic Press, New York, 1961, pp. 138-219.
2. J. K. Angell and J. Korshover, "The Biennial Wind and Temperature Oscillations of the Equatorial Stratosphere and Their Possible Extension to Higher Latitudes," Monthly Weather Review, vol. 90, No. 4, Apr. 1962, pp. 127-132.
3. A. W. Brewer, "Evidence for a World Circulation Provided by Measurements of Helium and Water Vapour Distribution in the Stratosphere," Quarterly Journal of the Royal Meteorological Society, vol. 75, No. 326, Oct. 1949, pp. 351-363.
4. A. Court, "Antarctic Atmospheric Circulation," Compendium of Meteorology, American Meteorological Society, Boston, 1951, pp. 917-941.
5. R. A. Craig, "The Observations and Photochemistry of Atmospheric Ozone and Their Meteorological Significance," Meteorological Monographs, vol. 1, No. 2, American Meteorological Society, Boston, 1950, 50 pp.
6. G. M. B. Dobson, "Observations of the Amount of Ozone in the Earth's Atmosphere and Its Relation to Other Geophysical Conditions," Part IV, Proceedings of the Royal Society, London, Series A, vol. 129, 1930, pp. 411-433.
7. G. M. B. Dobson, "Meridional Circulation in the Stratosphere," Proceedings of the Royal Society, London, Series A, vol. 236, 1956, pp. 187-193.
8. H.-V. Dütsch, Photochemische Theorie des Atmosphärischen Ozons unter Berücksichtigung von Nichtgleichgewicht-Zuständen und Luftbewegungen, Doctoral thesis, University of Zurich, Leeman and Co., Zurich, 1946, 113 pp.
9. R. A. Ebdon, "Notes on the Wind Flow at 50 mb. in Tropical and Subtropical Regions in January 1957 and January 1958," Quarterly Journal of the Royal Meteorological Society, vol. 86, No. 370, Oct. 1960, pp. 540-542.
10. H. W. Feely and J. Spar, "Tungsten-185 from Nuclear Bomb Tests as a Tracer for Stratospheric Meteorology," Nature, vol. 188, 1960, pp. 1062-1064.
11. B. Haurwitz, "Atmospheric Ozone as a Constituent of the Atmosphere," Bulletin of the American Meteorological Society, vol. 19, No. 10, Dec. 1938, pp. 417-424.

12. B. Haurwitz, "Frictional Effects and the Meridional Circulation in the Mesosphere," Journal of Geophysical Research, vol. 66, No. 8, Aug. 1961, pp. 2380-2391.
13. W. W. Kellogg and G. F. Schilling, "A Proposed Model of the Circulation in the Upper Stratosphere," Journal of Meteorology, vol. 8, No. 4, Aug. 1951, pp. 222-230.
14. T. N. Krishnamurti, "A Vertical Cross Section Through the 'Polar-Night' Jet Stream," Journal of Geophysical Research, vol. 64, No. 11, Nov. 1959, pp. 1835-1844.
15. T. N. Krishnamurti, The Subtropical Jet Stream of Winter, Doctoral Thesis, University of Chicago, 1960.
16. H. Lettau, "Diffusion in the Upper Atmosphere," Compendium of Meteorology, American Meteorological Society, Boston, 1951, pp. 320-333 (see p. 325).
17. W. F. Libby and C. E. Palmer, "Stratospheric Mixing from Radioactive Fallout," Journal of Geophysical Research, vol. 65, No. 10, Oct. 1960, pp. 3307-3317.
18. L. Machta, "Meteorology and Radioactive Fallout," WMO Bulletin, vol. 9, 1960, pp. 64-70.
19. E. P. McClain, "A Contribution to the Climatology of the Arctic Stratosphere," Journal of Applied Meteorology, vol. 1, No. 1, Mar. 1962, pp. 107-117.
20. R. J. Murgatroyd and F. Singleton, "Possible Meridional Circulations in the Stratosphere and Mesosphere," Quarterly Journal of the Royal Meteorological Society, vol. 87, No. 372, Apr. 1961, pp. 125-135.
21. G. Ohring, "The Radiation Budget of the Stratosphere," Journal of Meteorology, vol. 15, No. 5, Oct. 1958, pp. 440-451.
22. E. Palmén, "Über die Temperaturverteilung in der Stratosphäre und Ihren Einfluss auf die Dynamik des Wetters," Meteorologische Zeitschrift, vol. 51, 1934, pp. 17-23.
23. E. Palmén, "Über die dreidimensionale Luftströmung in einer Zyklone und die Ozonverteilung," Procès-Verbaux, International Union of Geodesy and Geophysics, Association of Meteorology, Washington, 1939, pp. 75-76.
24. R. Penndorf, "Beiträge zum Ozonproblem," Veröffentliche, Geophysische Institut, Universität Leipzig, Series 2, vol. 8, 1936, pp. 236-285.
25. S. Petterssen, Weather Analysis and Forecasting, vol. 1, 2nd Edition, McGraw-Hill Book Co., Inc., New York, 1956 (see p. 30).
26. R. J. Reed, "The Effects of Atmospheric Circulation on Ozone Distribution and Variation," Doctoral thesis, Massachusetts Institute of Technology, 1949.
27. R. J. Reed, W. J. Campbell, L. A. Rasmussen, and D. G. Rogers, "Evidence of a Downward-Propagating, Annual Wind Reversal in the Equatorial Stratosphere," Journal of Geophysical Research, vol. 66, No. 3, Mar. 1961, pp. 813-818.

28. H. Riehl, "On the Formation of West Atlantic Hurricanes," Miscellaneous Reports No. 24, Dept. of Meteorology, University of Chicago, 1948, pp. 1-67.
29. H. Riehl, Tropical Meteorology, McGraw-Hill Book Co., Inc., New York, 1951, 392 pp. (See pp. 235-280.)
30. H. Riehl and R. Higgs, "Unrest in the Upper Stratosphere Over the Caribbean Sea During January 1960," Journal of Meteorology, vol. 17, No. 5, Oct. 1960, pp. 555-561.
31. Rocket Panel, Harvard College Observatory, "Pressures, Densities, and Temperatures in the Upper Atmosphere," Physical Review, vol. 88, No. 5, Dec. 1, 1952, pp. 1027-1032.
32. V. E. Suomi and P. M. Kuhn, "An Economical Net Radiometer," Tellus, vol. 10, No. 1, Feb. 1958, pp. 160-163.
33. S. Teweles, L. Rothenberg, and F. G. Finger, "The Circulation at the 100-millibar Constant Pressure Surface over North America and Adjacent Ocean Areas, July 1957 through June 1958," Monthly Weather Review, vol. 88, No. 4, Apr. 1960, pp. 137-150.
34. W. Viezee, "The Mean Circulation of the Equatorial Stratosphere," Final Report, Contract AF19(604)-2134, Institute of Geophysics, University of California, Aug. 1958, 65 pp.
35. H. Wexler, "Annual and Diurnal Temperature Variations in the Upper Atmosphere," Tellus, vol. 2, No. 4, Nov. 1950, pp. 262-274.
36. H. Wexler, "Seasonal and Other Temperature Changes in the Antarctic Atmosphere," Quarterly Journal of the Royal Meteorological Society, vol. 85, No. 365, July 1959, pp. 196-208.
37. H. Wexler and W. B. Moreland, "Winds and Temperatures in the Arctic Stratosphere," Polar Atmosphere Symposium, Part I. Meteorology Section, Pergamon Press, London, 1958, pp. 71-84.
38. O. Wulf, "The Distribution of Atmospheric Ozone," Proceedings, Eighth American Science Congress, vol. 2, 1940, pp. 439-446.